

國立臺灣大學電機資訊學院電信工程學研究所

博士論文

Graduate Institute of Communication Engineering
College of Electrical Engineering and Computer Science
National Taiwan University
Doctoral Dissertation



物聯網資訊採集與群組多播的機制設計

Mechanism Design for IoT

Information Gathering and Multicast Distribution

柯君翰

Chun-Han Ko

指導教授：魏宏宇 博士

Advisor: Hung-Yu Wei, Ph.D.

中華民國 106 年 6 月

June 2017



國立臺灣大學博士學位論文
口試委員會審定書

物聯網資訊採集與群組多播的機制設計
Mechanism Design for IoT Information Gathering and
Multicast Distribution

本論文係柯君翰君（學號：D01942010）在國立臺灣大學電信工程學研究所完成之博士學位論文，於民國一〇六年六月二十九日承下列考試委員審查通過及口試及格，特此證明

口試委員：

魏之辛

(指導教授簽名)

王蒞君

高榮鳴

張時中

逢愛君

洪樂文

傅子仲

所長

吳宗霖

(簽名)

致 謝



能順利完成博士論文，最要感謝的是指導教授「魏宏宇」老師！博士班就學以來，風雨飄搖，每當研究遇到瓶頸之際，老師給予我的指導與建議猶如點亮風雨中屹立不搖的燈塔，使我終能抵達彼岸。彼岸並不是終點，眼前迎來的是更開闊的道路，我會善用學習過程中所學到的一切，期望自己更加成熟以迎接更開闊的未來與挑戰。真的很感謝老師！

在家庭方面，最要感謝親愛的家人，包括爸爸「錫福」、媽媽「碧梅」、姊姊「翠婷」，還有族繁不及備載等人，有你們的支持與體諒，我才能全力完成學業。書念了這麼久，我自覺還是很不會寫作文，時常辭不達意，長話不如短說：謝謝您們，我愛您們！

感謝一同奮戰的同學們，與你們的討論總是獲益良多，我也很懷念一起吃飯、打網球的時光。相信與大家相處的時光在未來一定會是讓我回憶最深的。

最後，必須感謝我的老婆「幸芸」，多虧妳覺得我的口試投影片看起來都不重要，硬是要我刪了好多張投影片……我能把報告時間從 75 分鐘濃縮於一小時以內，以致於順利完成口試，妳絕對是最大功臣，真的很「幸運」有妳。未來還請妳多多指教，我愛妳喔～

中文摘要



物聯網是智能設備、車輛、機器還有其他智能物體等互相聯通而形成的網路。實現複雜物聯網的關鍵因素則在於許多新型通信協定和技術的整合，它們將使物聯網設備能夠進行協作、溝通並作出決策。物聯網設備的互相聯通作用可以簡單的資料流說明：諸如無線感應器的物聯網設備從環境中收集資料，並將資料傳輸到資料伺服器進行信息處理。爾後伺服器會將處理獲得的信息傳輸分送到諸如用戶設備的物聯網設備以實現更好的使用者效用。由於物聯網的快速發展，無處不在的信息收集、處理和分送，均使無線電資源的需求不斷上升，這也使原本就有限的無線電資源更為稀少。此外，無線傳輸通道會隨著時間波動。而能量採集技術雖能實現自我維持運作的物聯網設備，但採集的能量通常是間歇並隨時間變化的。因此，考量到無線電資源的稀少性、無線通道的時間波動和能量的時間變化，如何有效地在空間和時間上分配運用無線電資源將是物聯網中極為重要的一項議題。此外，我們也考慮了物聯網設備的自私特性與物聯網環境的不完整信息。不完整信息意味著網路環境中如無線通道狀況與設備的能量儲存量等信息通常僅為設備本身所知。為了最佳化網路效能，網路設計者將需要設備回饋這些不完整信息。由於整體網路最佳化通常會犧牲部分設備的個別效能，因



此自私的設備可能會通過虛假的信息回饋來操縱網路最佳化結果，以使自己的效能表現變得更好。此時整體網路效能表現將可能不是網路設計者所希望達到的最佳結果。有鑑於此，我們在物聯網中制定了無線電資源分配問題，並以機制設計的概念提出了創新的物聯網資源分配機制。透過理論研究，我們證明設計的資源配置機制將可使物聯網設備回饋真實的信息，並從而實現最佳的均衡資源分配。均衡資源分配實現了數個效率和公平的度量，包括最大系統吞吐量/環境資料保真度，柏拉圖效率，最大公平性，與比例公平性。而透過提出的定價方案，我們證明均由設備付錢給機制。換言之，我們設計的機制將不需要付錢給設備才能確保真實的反饋（預算平衡）。此外，我們也證明所有設備將加入設計的機制以獲得比沒有加入時更高的效用（個別理性）。

關鍵詞：物聯網；能量採集；無線電資源分配；機制設計；賽局理論。



Abstract

The Internet of Things (IoT) is the inter-networking of smart devices, vehicles, machines, and other items. The key factor for enabling this sophisticated paradigm is the integration of novel communication protocols and technologies, which allows IoT devices to cooperate, communicate, and make decisions. The interconnection of IoT devices can be explained in simple data flows: Devices such as wireless sensors gather data from the environment and transmit the data to data servers for information processing. The processed information is then distributed to devices such as user equipments to achieve greater user utility. Due to the rapid development of the IoT, ubiquitous information gathering, processing, and distribution have escalated the demand of radio resources, which makes radio resources even scarcer. In addition, wireless channels are time-fluctuating. Energy harvesting technology enables self-sustainable IoT devices but harvested energy is usually intermittent and time-varying. Therefore, taking into account radio resource scarcity, channel fluctuations, and energy variations, efficient radio resource allocation in space and time is particularly important in the IoT. Moreover, we also consider selfishness of IoT devices and incomplete information of the network environment. Incomplete information means that the network environment, such as channel conditions and energy levels, is only known to devices themselves. To optimize the network performance, feedback of the incomplete information from devices is required. Note that overall network optimization usually sacrifices individual performance of some devices. Selfish devices can manipulate the network optimization result through untruthful feedback if doing so increase their own performance. The network performance may not be optimal. In this regard, we formulate radio resource allocation problems in the IoT and adopt a mechanism

design approach to propose novel IoT resource allocation mechanisms. Our theoretic findings show that the proposed resource allocation mechanisms can induce truthful information feedback from devices so as to achieve optimal equilibrium resource allocation. The equilibrium resource allocation achieves several efficiency and fairness metrics, including maximum system throughput/data fidelity, Pareto efficiency, max-min fairness, proportional fairness. With the proposed pricing schemes, the payment is always made from the devices to the mechanisms. In other words, the mechanisms do not need to pay to ensure truthful feedback (budget balance). Moreover, all devices will join the proposed mechanisms to gain higher utility than without joining (individual rationality).

Keywords: The IoT; energy harvesting; radio resource allocation; mechanism design; game theory.

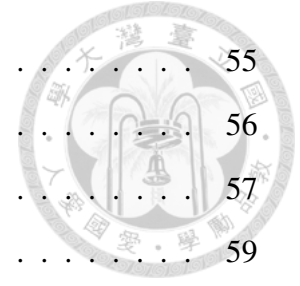


Contents

Doctoral Dissertation Certification by Oral Defense Committee	i
Acknowledgements	ii
Chinese Abstract	iii
Abstract	v
1 Introduction	1
1.1 Selfish Devices and Incomplete Information	2
1.2 Problem Overviews and Contributions	3
1.2.1 Strategy-Proof Resource Allocation Mechanism for Multi-Flow Wireless Multicast (Chapter 2)	3
1.2.2 Wireless Multicast over Time-Varying Channels for Energy-Harvesting Devices (Chapter 3)	4
1.2.3 On Maximizing Data Fidelity in Energy-Harvesting IoT: A Me- chanism Design Approach (Chapter 4)	5
1.3 Mechanism Design	6
1.3.1 Basic Knowledge	6
1.3.2 Equilibrium Concepts	6
1.3.3 Infinite Time Horizon Mechanisms	7
2 Strategy-Proof Resource Allocation Mechanism for Multi-Flow Wireless Mul- ticast	9

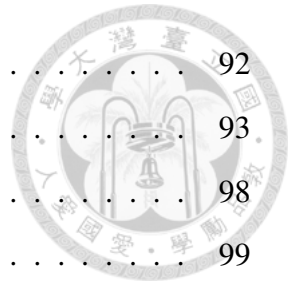


2.1	Introduction	9
2.2	Related Work	12
2.3	Multicast System Model	14
2.3.1	Multicast Flows	14
2.3.2	Lossy Channels and Generalized Erasure Coding	15
2.3.3	UEs' Utility	16
2.4	Resource Allocation Problem and Mechanism Design	17
2.4.1	Pricing and Access Control	19
2.4.2	UE Resource Demands and Group Resource Demands	20
2.4.3	Group Weights	22
2.4.4	Weighted Water-Filling Resource Allocation	23
2.5	Resource Allocation Game	26
2.6	Strategy-Proofness – Truth-Revealing Equilibrium	28
2.7	Desirable Properties of the Equilibrium Resource Allocation	34
2.8	Numerical Simulation Results	38
2.8.1	Numerical Analysis	38
2.8.2	3GPP MBMS Simulation	41
2.9	Summary	42
3	Wireless Multicast over Time-Varying Channels for Energy-Harvesting Devices	44
3.1	Introduction	44
3.2	Related Works	46
3.3	System Model	48
3.3.1	Types of Multicast Flows	49
3.3.2	Energy Arrivals and Markov Energy States	50
3.3.3	Fading Channels and Markov Channel States	51
3.3.4	Joint States and Information Assumptions	52
3.3.5	One-Shot and Long-Term Throughput	52
3.4	Resource Allocation Problem and Mechanism Design	54



3.4.1	Feedback Strategies of the Devices	55
3.4.2	Flow Resource Allocation Policy	56
3.4.3	Bayesian Update of the State Information	57
3.4.4	Device Pricing Policy	59
3.4.5	Ex-Post Utility of the Devices	60
3.5	Resource Allocation Game	60
3.6	Truth-Revealing Equilibrium and Desirable Properties	62
3.7	Value Iteration for the Resource Allocation Policy	66
3.8	Further Discussions	68
3.8.1	Feedback per n Time Slots	68
3.8.2	Markov Data Sources	69
3.9	Numerical Results	69
3.10	Summary	73
4	On Maximizing Data Fidelity in Energy-Harvesting IoT: A Mechanism Design Approach	75
4.1	Introduction	75
4.2	Related Works	77
4.3	System Model	80
4.3.1	Data Statistics and Entropy	81
4.3.2	Energy States and Activation Intervals	82
4.3.3	Information Assumption on the Data Statistics, Energy States, and Activation Intervals	84
4.3.4	Data Fidelity	84
4.4	Node Activation Mechanism	85
4.4.1	Feedback Strategies of the Servers	87
4.4.2	Node Activation Policy and Value Iteration	87
4.4.3	Update of the Energy State Information	89
4.4.4	Server Pricing Policy	90
4.4.5	Utility of the Servers	91

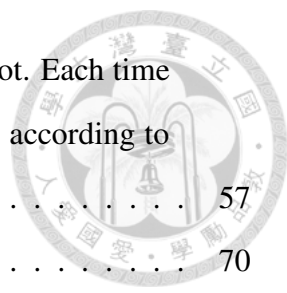
4.5	Node Activation Game and Solution Concept	92
4.6	Truth-Revealing Equilibrium and Desirable Properties	93
4.7	Further Discussions	98
4.7.1	Synchronous Feedback per n Time Slots	99
4.7.2	Asynchronous Group Feedback	100
4.7.3	Stationary, Markov Energy Arrivals and Time-Varying Channels	101
4.8	Numerical Results	103
4.8.1	Parameter Setting	103
4.8.2	Verification of Incentive Compatibility, Budget Balance, and Individual Rationality	103
4.8.3	Impacts of Parameter Change	105
4.8.4	Performance Comparison of Synchronous and Asynchronous Feedback Designs	106
4.9	Summary	107
5	Conclusions	108
A	Proofs for Lemmas 2.1, 2.3, and 2.4	110
A.1	Lemma 2.1	110
A.2	Lemma 2.3	113
A.3	Lemma 2.4	115
	Bibliography	118



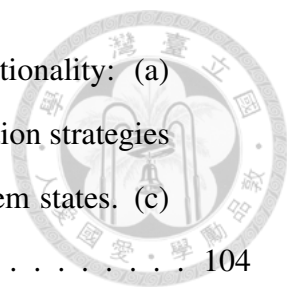


List of Figures

1.1	Illustration of the IoT from the viewpoint of data flows.	2
2.1	System model. The BS provides multiple multicast flows to wireless UEs.	14
2.2	The flow diagram of the proposed resource allocation mechanism.	18
2.3	The UE's utility under different PEP values. (a) Loss-tolerant flow. (b) Loss-sensitive flow.	39
2.4	The UE's utility with respect to the reported PEP. (a) The UE's true resource demand is "greater" than the group resource demand, and the group "fulfills" its group resource demand. (b) "less" and "fulfill". (c) "equal" and "fulfill". (d) "greater" and "not fulfill". (e) "less" and "not fulfill". (f) "equal" and "not fulfill".	40
2.5	Performance comparison among the proposed mechanism, the weighted scheme, and the random scheme: (a) Weighted proportional fairness. (b) Weighted max-min fairness.	41
2.6	PSNR evaluation of the proposed mechanism in LTE MBMS: (a) Average PSNR. (b) Standard deviation of the PSNR.	42
3.1	System model. The BS provides multiple multicast flows to energy harvesting devices. The energy source can be solar power, radio-frequency (RF) energy, etc. Each device accesses only one flow. Device i accessing flow g is denoted by device (i, g)	48
3.2	The block diagram of the proposed resource allocation mechanism. The detailed designs are specified in each subsection.	55



3.3	Illustration of three different information stages in a time slot. Each time slot can be broken into ex-ante, interim, and ex-post stages according to what information is known at different time instants.	57
3.4	The utility of each device in all possible feedback states.	70
3.5	Budget balance and individual rationality: (a) The net payment from the devices to the BS in all system states. (b) The utility of each device in all system states.	71
3.6	Performance comparison in the system throughput: (a) The weighted system throughput of the proposed resource allocation mechanism, and other schemes. (b) The weighted system throughput of the proposed resource allocation mechanism with different values of the discount factor β	72
3.7	Trade-off among the signaling overhead, the system throughput and the time complexity: (a) The weighted system throughput under feedback frequencies from per time slot to per 5 time slots. (b) The number of iterations and the total time complexity under feedback frequencies from per time slot to per 5 time slots.	73
3.8	Throughput performance of each device and the system with/without the proposed weight design.	74
4.1	A model of the energy-harvesting IoT. There are one BS and multiple sensor nodes owned by different servers. Sensor node i owned by server g is denoted by node (i, g) . The nodes can harvest energy from the environment. The BS decides to activate nodes to sense and transmit data back through the BS to their servers. The node activation $a_{i,g}^t = 1$ means that the BS activates node (i, g) in time slot t	80
4.2	The block diagram of the proposed node activation mechanism. The servers and the nodes are required to feedback the data statistics and the energy states, respectively. The BS makes the node activation decision and also charges the servers prices.	86



4.3 Incentive compatibility, budget balance, and individual rationality: (a) The utility of each server under all possible one-shot deviation strategies in time slot 0. (b) The price charged by the BS in all system states. (c) The utility of each server in all system states. 104

4.4 Impacts of the parameter change on the system data fidelity: (a) The discount factor $\beta = 0, 0.4, 0.8, 0.9, 0.95, .099$. (b) The energy capacity $EC_{i,g} = 1, 2$. (c) The spatial kernel $l_x = 0, 5, 10$ and the temporal kernel $l_t = 0, 1, 2$. (d) The number of resource blocks $R = 1, 2, 3, 4, 5, 6$. (e) The number of nodes $|\mathcal{I}_g| = 2, 3, 4$ 105

4.5 Comparison of the synchronous and the asynchronous feedback designs: (a) The system data fidelity. (b) The complexity. 107



List of Tables

2.1	Notation of the multicast system model	17
2.2	Notation of the multicast resource allocation mechanism	26
2.3	Parameter setting	38
5.1	Summary of the significant results	108



Chapter 1

Introduction

The Internet of Things (IoT) is a novel paradigm that is rapidly emerging in modern wireless communications. It is the inter-networking of smart devices, vehicles, machines, and other items. Fig. 1.1 uses simple data flows to show the interconnection of IoT devices. In the IoT, devices such as wireless sensors and radio-frequency identifiers (RFID) first sense and gather data from the environment. The gathered data are then transmitted to data centers or servers for processing and analysis to gain meaningful information. The information is then distributed to devices such as user vehicles and machines to achieve greater user utility. Wireless multicast, a promising technology for common information delivery to multiple devices, can be adopted. The key factor for enabling the sophisticated paradigm of the IoT is the integration of novel communication protocols and technologies, which allows IoT devices to cooperate, communicate, and make decisions [1, 2].

Despite the promising future of the IoT, new design challenges are imposed due to the rapid development of the IoT with a numerous number of devices. In particular, ubiquitous information gathering, processing, and distribution have escalated the demand of radio resources, which makes radio resources even scarcer. Efficient radio resource allocation is especially important in the IoT. In addition, wireless channel conditions are time-fluctuating, which can severely affect the quality of data transmission. On the other hand, emerging energy harvesting technologies enable wireless devices to scavenge energy from the ambient environment [3] and to achieve self-sustainable operation. However, the randomness and intermittence of renewable energy also bring design challenges.

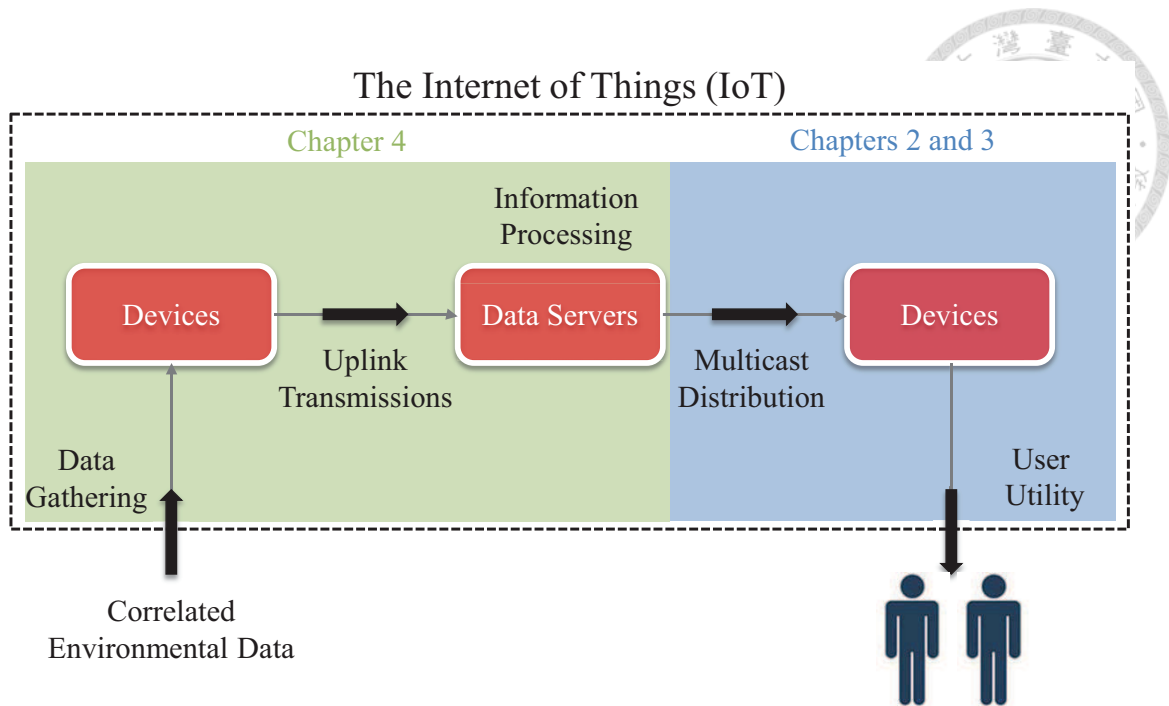


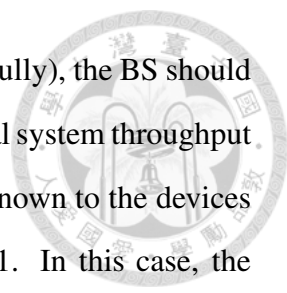
Figure 1.1: Illustration of the IoT from the viewpoint of data flows.

Therefore, channel fluctuations and energy variations should also be important considerations in radio resource allocation design.

1.1 Selfish Devices and Incomplete Information

Unlike most of the existing works, we also consider selfishness of IoT devices and incomplete information of the network environment. Incomplete information means that the network environment, such as channel conditions and energy states, is only known to devices themselves. To optimize the network performance, feedback of the incomplete information from devices is required. Note that overall network optimization usually sacrifices individual performance of some devices. Therefore, devices may be selfish and feedback their own incomplete information dishonestly so as to maximize their own performance. Therefore, the overall network operation may not be optimal.

Consider a very simple toy model where there exist a base station (BS) and 3 wireless devices. Each device requires one data packet. The BS has 2 radio resource blocks where one radio resource block can be used to transmit one packet. Suppose that devices 1 and 2 both have packet success probability (PSP) 0.9 and device 3 has PSP 0.2. To maximize



the system throughput (expected number of packets received successfully), the BS should transmit one packet to device 1 and one packet to device 2. The optimal system throughput is 1.8. However, the throughput of device 3 is 0. If the PSP is only known to the devices and feedback is required, device 3 can untruthfully feedback PSP 1. In this case, the BS may transmit one packet to device 1 and one packet to device 3. By such untruthful feedback, device 3 gets throughput 0.1, higher than that in the optimal resource allocation. However, the real system throughput becomes 1.1, which is less than the optimal system throughput 1.8. From this example, we see that selfishness and incomplete information of devices can cause severe system performance degradation. Traditional solutions that do not consider selfishness and incomplete information may not work effectively. To this end, we adopt a mechanism design approach to designing novel resource allocation mechanisms.

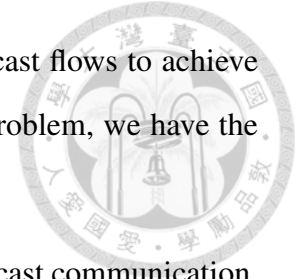
1.2 Problem Overviews and Contributions

In this dissertation, we play the role of the radio resource providers. We aim to design IoT radio resource allocation mechanisms where IoT devices and servers who use radio resources are the participants. Selfishness of IoT devices and incomplete information of the network environment are considered. By using the divide-and-conquer method, we formulate the resource allocation problems in the IoT scenarios of information gathering and distribution, as illustrated in Fig. 1.1. Novel resource allocation mechanisms are proposed to induce truthful information feedback from selfish devices so as to achieve optimal resource allocation. The problem overviews and contributions for each design block are given as follows:

1.2.1 Strategy-Proof Resource Allocation Mechanism for Multi-Flow Wireless Multicast (Chapter 2)

In Chapter 2, we consider downlink multimedia multicast. The BS can send multiple multicast flows to multiple groups of devices. The channel-quality information (CQI) is

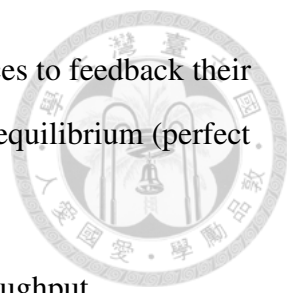
devices' private information. Resource allocation to multiple multicast flows to achieve maximum system throughput is the major objective. To solve the problem, we have the following contributions:



1. We provide the theoretical foundation for the multi-flow multicast communication, constructing an application-layer error correction framework and designing an on-demand resource allocation mechanism for the future Multimedia Broadcast Multicast Services (MBMS).
2. The proposed mechanism performs access control via pricing. The proposed pricing scheme only enables the users with the channel qualities better than the system-defined threshold to join the mechanism and gain positive utility.
3. The proposed mechanism induces truthful feedback of the CQI in a dominant-strategy equilibrium (strategy-proofness).
4. The resource allocation in the equilibrium is Pareto efficient. No other resource allocation can make all the users better off in utility.
5. The resource allocation also achieves flow-level weighted max-min and proportional fairness.
6. There is no net payment from the BS to the devices. In other words, the BS does not need to pay to ensure truthful feedback (budget balance).

1.2.2 Wireless Multicast over Time-Varying Channels for Energy-Harvesting Devices (Chapter 3)

Chapter 3 studies the downlink multicast scenario on an infinite time horizon. Common data multicast, e.g., small data and control signal transmissions, to energy-harvesting devices over time-varying channels is considered. The energy and channel states of the devices are time-varying and only known to themselves. We aim to decide resource allocation to different multicast flows over time to achieve maximum system throughput. Our contributions are given as follows:

- 
1. We propose a resource allocation mechanism induces the devices to feedback their true energy and channel state information in a perfect ex-post equilibrium (perfect ex-post incentive compatibility).
 2. The equilibrium resource allocation maximizes the system throughput.
 3. The payment is always made from the devices to the BS The BS does not need to pay to ensure truthful feedback (budget balance).
 4. Moreover, all devices will obtain higher utility when joining the proposed resource allocation mechanism (individual rationality).

1.2.3 On Maximizing Data Fidelity in Energy-Harvesting IoT: A Mechanism Design Approach (Chapter 4)

Chapter 4 focuses on correlated data gathering of energy-harvesting devices. The data correlations and the energy states are only known to devices. A node activation decision problem over an infinite time horizon is studied, with spatial-temporal data correlations and incomplete information on the data statistics and the energy states. Resource allocation to devices for information gathering and uplink transmissions to achieve maximum system data fidelity is then the major design goal. Our contributions are given as follows:

1. The proposed node activation mechanism ensures truthful feedback of the true data statistics and energy states in a perfect ex-post equilibrium (perfect ex-post incentive compatibility).
2. The proposed node activation mechanism maximizes the system data fidelity.
3. The proposed node activation mechanism also ensures that the payment is always made from the data servers to the BS. In other words, the BS does not need to pay to guarantee truthful feedback (budget balance).
4. All data servers and their sensor nodes will join the proposed node activation mechanism to obtain higher utility than without joining (individual rationality).

1.3 Mechanism Design

A mechanism design approach is adopted in this dissertation to inducing truthful feedback of incomplete information from selfish devices to achieve desirable resource allocation. Before going to the design details of following chapters, we provide some basic knowledge of mechanism design.

1.3.1 Basic Knowledge

Mechanism design is a sub-field of economics and game theory that takes an engineering approach to designing mechanisms or incentives to achieve desirable outcomes in a strategic setting. Such a strategic design is necessary since players are selfish, act rationally, and usually have private preferences. In the following, we use resource allocation mechanism to shortly explain mechanism design. A mechanism designer first designs an outcome rule, i.e., a resource allocation rule plus a pricing rule. The game induced by the mechanism has the following main components:

- **Players:** Devices are players in the game.
- **Types:** Channel conditions, energy states, and data correlations are types of players. Types are usually incomplete information that is known to players themselves, but not known to each other or the mechanism designer.
- **Strategies:** Players have strategies that decide how to report types to the mechanism.
- **Outcomes:** With the reported types received and according to the resource allocation rules and the pricing rules, the mechanism decides resource allocation and prices charged to devices.
- **Utility:** Players have different utility with respect to the outcomes.

1.3.2 Equilibrium Concepts

The main objective in mechanism design is to design the resource allocation rule and the pricing rule such that reporting the true types maximizes players' utility in an equilibrium.

The most well-known equilibrium concept is a Nash equilibrium, which states that in an equilibrium each player will select a utility-maximizing strategy given the strategies of the other players. Although the Nash equilibrium concept is fundamental, it makes very strong assumptions about players' information and beliefs: Each player must have perfect information about the types of the other players.

A stronger solution concept is a dominant-strategy equilibrium. In a dominant-strategy equilibrium each player has the same utility-maximizing strategy regardless of the strategies of other players. A dominant-strategy equilibrium is very robust, as it makes no assumptions about the information available to players about each other. As will be shown in Chapter 2, the proposed mechanism will be implemented in a truthful dominant-strategy equilibrium.

1.3.3 Infinite Time Horizon Mechanisms

Mechanism design for infinite time horizons is required when the types, i.e., channel conditions, energy states, and data correlations, vary with time and are incomplete information. In addition to the basic components in Chapter 1.3.1, we should also consider Markov type transitions and ex-post utility:

- Markov type transitions: Players have different types in different time slots. We assume that types have Markov transitions. That is, the types of the players in the next time slot only depend on the types and the resource allocation in the current time slot.
- Ex-post utility: Players also have different utility with respect to the outcomes. A slight refinement from one-shot utility is that we define utility in the ex-post stage. An ex-post stage is defined as the timing after players report the types in each time slot. Therefore, ex-post utility represents the utility seen in the ex-post stage of each time slot.

With the refinement of ex-post utility, the equilibrium concept we will use in infinite time horizon mechanisms is a perfect ex-post equilibrium. A perfect ex-post equilibrium

means that each player maximizes the ex-post utility in any subgame by playing a strategy given the strategies of the other players. The perfect ex-post equilibrium concept is also strong in infinite time horizon mechanisms as it makes no assumptions about the type information available to players about each other in each time slot. As will be shown in Chapters 3 and 4, the proposed mechanisms will be implemented in a truthful perfect ex-post equilibrium.

To sum up, according to different network scenarios on one-shot or infinite time horizons, different mechanisms will be proposed and different equilibrium concepts will be applied. Desirable properties of the outcomes will also be analyzed. More design details, equilibria, and property analysis will be provided in the following chapters.



Chapter 2

Strategy-Proof Resource Allocation

Mechanism for Multi-Flow Wireless

Multicast

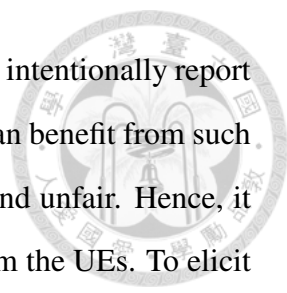
2.1 Introduction

Wireless multicast/broadcast, also known as one-to-many communication, is a promising technology for delivering information from a server to a group of wireless users. As users have become more data hungry and service demanding, multicast/broadcast service is a solution that can cater this need efficiently. One-to-many communication can be performed via unicast. Employing unicast involves multiple transmissions to a group of users which results in severe waste of radio resources especially when the group size gets larger. Therefore, wireless multicast techniques have been extensively studied and widely used because of the efficient usage of radio resources. However, wireless multicast requires the network, including the server and routers, to route packets such that each user receives a copy. Route establishment is then one of the most basic and challenging issues in wireless multicast. Many multicast protocols come up with solutions to set up and maintain routes. In addition, on the basis of multicast routing, the issues on network resource utilization, packet scheduling, adaptive rate control, power control, and throughput maximization,

have been jointly investigated [4].

Multicast/broadcast service is supported in the 4G communication networks such as Long Term Evolution Advanced (LTE-A) and Worldwide Interoperability for Microwave Access (WiMAX) IEEE 802.16m. In 3GPP LTE systems, Multimedia Broadcast Multicast Services (MBMS) is a mechanism for multicasting video streams [5]. To provide transmission reliability, application-layer error correction framework is applied. By applying fountain (rateless erasure) coding techniques [6], application-layer data files are encoded into source data packets and repair data packets, which provide redundancy for data delivery [7]. Recently, 3GPP has started working on providing dynamic and on-demand MBMS [8]. Dynamic radio resource allocation and adaptive error correction configuration could be applied to ensure efficient resource utilization and user satisfaction for multi-flow multicast video services. As different users may face different wireless channel qualities, one key issue for multicast configuration is to determine the appropriate application-layer error correction level so that the users are satisfied with the reception quality. On the other hand, since radio resources are limited, resource allocation among different multicast streams needs to be carefully considered. Our previous works investigated adaptive modulation/coding schemes [9], game-theoretic configuration [10], and optimal pricing [11] for wireless multicast. On the basis of the previous works, a new research problem of resource allocation for wireless multicast in the next-generation networks will be of interest.

In this research work, we provide the theoretical foundation for the multi-flow multicast communication schemes, which will be an indispensable part of the future MBMS wireless multimedia delivery. In the proposed scenario, a base station (BS) is capable of sending multiple data flows to multiple groups of user equipments (UEs). The BS aims to provide efficient and fair multicast services by sending redundancy for data delivery, which requires the feedback of the channel-quality information (CQI) from the UEs. The channel qualities are, in general, time-varying and can only be correctly measured by the UEs themselves, which means the CQI is the UEs' private information. Regarding the CQI feedback, this chapter further considers the rational and selfish user characteristic.



When the UEs have the private CQI, the rational and selfish UEs may intentionally report the false CQI to manipulate the BS's multicast configuration if they can benefit from such untruthful feedback. The multicast service may turn out inefficient and unfair. Hence, it will be a significant issue to ensure reliable and truthful feedback from the UEs. To elicit the true CQI and to achieve efficient and fair network operation, we propose a multicast resource allocation mechanism with the designs of the access-control pricing scheme and the weighted water-filling resource allocation. Our analysis indicates that the proposed mechanism can elicit the true CQI from the UEs, avoiding any manipulation of multicast configuration and thereby guaranteeing efficient and fair network operation. The detailed contributions are stated as follows:

1. We provide the theoretical foundation for the multi-flow multicast communication, constructing the application-layer error correction framework and designing the on-demand resource allocation mechanism for the future MBMS.
2. The proposed mechanism performs access control via pricing. The proposed pricing scheme enables the UEs with the channel qualities better than the system-defined threshold to join the mechanism and gain positive utility. On the other hand, the UEs with the channel qualities worse the threshold will not join the mechanism since they will never gain positive utility.
3. The proposed mechanism is strategy-proof. It induces the selfish UEs to truthfully report their private CQI. Therefore, the system operates at the truth-revealing dominant-strategy equilibrium.
4. The resource allocation at the equilibrium operating point is Pareto efficient. No other resource allocation can make all the UEs better off in utility. The resource allocation also achieves flow-level weighted max-min and proportional fairness. Moreover, there is no net payment from the BS to the UEs. In other words, the BS does not need to pay the UEs to ensure strategy-proofness of the proposed mechanism (weak budget balance).

2.2 Related Work

Many research papers studied the issues on multicast flow accommodation and resource allocation. Some papers conducted theoretical analysis on the maximum concurrent flow problem in wireless networks. Tu studied the efficient utilization of network resources for increasing the number of concurrent multimedia flows when a channel becomes saturated [12]. Jain et al. worked on maximizing throughput in any given wireless network with any given traffic workload, using a conflict graph to model wireless interference [13]. As the throughput maximization problem was shown to be NP-hard, they instead provided methods to compute the upper and lower bounds for this problem. Kodialam et al. analyzed the problem of joint flow routing and transmission scheduling to achieve given throughput [14, 15]. They developed sufficient and necessary conditions and derived upper bounds for the achievable throughput. Wan et al. investigated the maximum concurrent flow problem in multi-hop wireless networks subject to both bandwidth and interference constraints [16, 17]. They also developed polynomial-time algorithms to derive approximation bounds. Kumar et al. conducted the study of the maximum throughput capacity of the network given the collection of source-destination pairs [18]. The algorithmic aspects of the above problem were discussed as well. Ozdaglar and Bertsekas proposed a method for solving the multi-commodity flow problem, relying on the convexity of the cost function [19].

Some papers focused on designing efficient resource allocation methods that improve wireless networks' ability to accommodate more multicast flows. Cruz et al. used a primal-dual approach to compute joint routing, scheduling, and power control policies [20]. Middleton et al. developed a framework allowing scheduling, routing, and power allocation for multiple flows in polynomial-time [21]. Their study was subsequently extended to allocate resources in networks with streaming-packet data flows [22]. Baghaie et al. studied multi-flow transmission in delay constrained wireless multi-hop networks to minimize power consumption for prolonging network life [23]. Tu et al. investigated video multicasting in large-scale areas using wireless mesh networks. They designed a set of heuristic-based algorithms to improve network throughput [24]. Some other pa-

pers also investigated the issue on private information in multicast networks. In [25, 26], Gopinathan et al. studied the multicast problem in an ad-hoc wireless network. They designed inter-node cost sharing schemes for the information dissemination to achieve group strategy-proofness. They also showed that to achieve group strategy-proofness a compromise in routing optimality and budget balance is inevitable.

Jakubczak and Katabi proposed SoftCast, a novel cross-layer design for video multicast [27, 28]. SoftCast provides a joint source-channel coding scheme linearly transforming a video stream into coded packets such that each packet contains approximately the same amount of information and is uncorrelated to each other. In this way, each receiver can decode the received packets into the video whose quality is proportional to its channel quality. As the authors proposed and demonstrated SoftCast in a single-flow scenario, SoftCast configuration in a multi-flow scenario will also be of interest. In a multi-flow scenario, whether the system applies SoftCast or other coding schemes, feedback of the CQIs from the UEs may be needed to decide the redundancy level of each flow and to optimize the system performance. Therefore, resource allocation mechanism design with feedback decisions in a multi-flow scenario will be important and interesting.

In summary, different from the papers of [25, 26] that designed the cost sharing methods for single-flow multicast, this chapter proposes a resource allocation framework with feedback decisions for multi-flow multicast. Besides, unlike the other previous works, this chapter makes the practical assumption that UEs are self-interested, have private CQI, and make feedback decisions in a distributed way. While the system requires the UEs' private CQI, the UEs that are selfish in improving their own performance may manipulate the multicast configuration by falsely reporting the CQI. Without the correct CQI, the resource allocation may turn out inefficient and unfair. With regard to the issue on UEs' manipulating the system operation, this chapter is the first applying incentive mechanism design to propose a resource allocation mechanism in a multi-flow multicast scenario. The proposed mechanism is shown to induce the selfish UEs to reveal the true CQI and to achieve efficient and fair system operation.

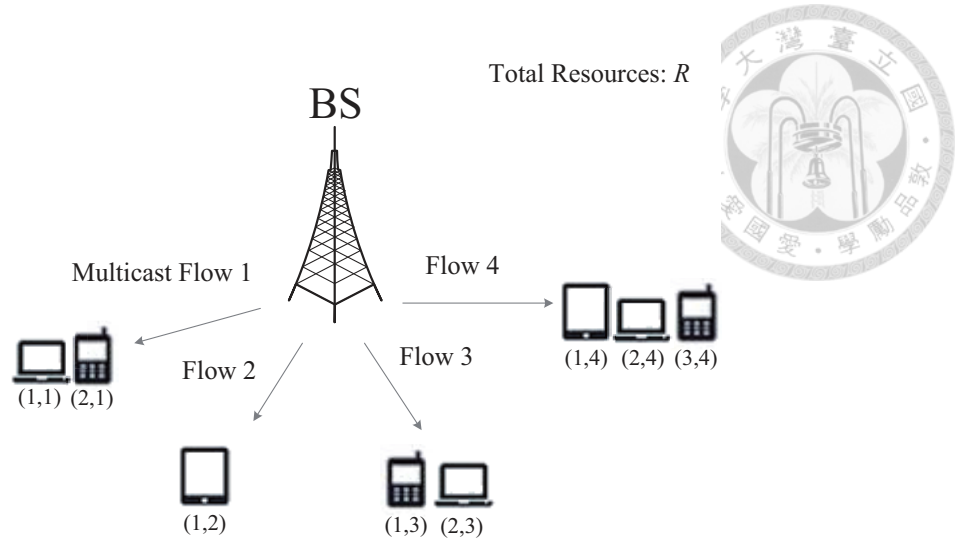


Figure 2.1: System model. The BS provides multiple multicast flows to wireless UEs.

2.3 Multicast System Model

We consider a wireless multicast system consisting of a BS and multiple wireless UEs, as illustrated in Fig. 2.1. Time is divided into periods of equal length and the system has R resource blocks in each time period. The BS provides a set of multicast flows $\mathcal{G} = \{1, 2, \dots, G\}$ where each flow g is accessed by a group of UEs $\mathcal{N}_g = \{1, 2, \dots, N_g\}$. We denote each UE i accessing flow g by UE (i, g) , $i \in \mathcal{N}_g$ and $g \in \mathcal{G}$. Note that each UE only accesses one flow, i.e., each UE belongs to only one group. Throughout the rest of the paper, we will use the terms flow and group interchangeably.

2.3.1 Multicast Flows

The number of packets in flow g is denoted by M_g . For simplicity, we assume that each packet has equal length and transmission of one packet requires one resource block. Each flow can be either loss-tolerant or loss-sensitive. a UE that accesses a loss-tolerant flow obtains a fixed amount of utility from each packet received, and the utility reaches the maximum once it receives all the packets. In contrast, a UE that accesses a loss-sensitive flow must receive all the packets to obtain the maximum utility; otherwise, it gains nothing.

2.3.2 Lossy Channels and Generalized Erasure Coding

Wireless channels are not perfect in general. Transmission through wireless channels may suffer from packet loss. To accommodate dynamic channel fading scenarios, we assume that each UE experiences the constant channel quality in a time period, but the channel quality varies from period to period. In the rest of the paper, we will study a single time period. Nonetheless, the designs and analysis can be applied to multiple time periods as well.

We use the binary-symmetric channel model [29]. Each UE (i, g) suffers from constant bit error probability (BEP) $b_{i,g}$, $0 \leq b_{i,g} \leq 1$. Since each packet in a flow is assumed to have equal length, UE (i, g) suffers from constant packet error probability (PEP) $e_{i,g} = 1 - (1 - b_{i,g})^L$ where L is the packet length. Note that each UE's CQI, i.e., BEP and PEP, are assumed to be private information. This assumption is reasonable as only the receiver can correctly measure its channel quality.

Since the channels are lossy and unreliable, we apply the generalized erasure coding [30, 31] to control error.¹ The generalized erasure coding transforms a flow of M_g packets into a longer flow of coded packets such that the data contents can be fully recovered from any M_g out of the coded packets. Thus, if a UE obtains a sufficient number of the coded packets $j \geq M_g$, it obtains the full valuation. However, if a UE obtains an insufficient number of the coded packets $j < M_g$, it can recover only the portion j/M_g of the original packets. We define the UE's valuation with respect to the number of the received coded packets j as follows.

Definition 2.1. [UE's valuation] *If flow g is loss-tolerant, UE (i, g) 's valuation function with respect to the number of the received coded packets j is*

$$v_g(j) = \min \left\{ 1, \frac{j}{M_g} \right\} \quad (2.1)$$

¹As 3GPP MBMS has attracted a lot of attention in recent year, we follow the specification of 3GPP MBMS and propose a resource allocation framework that uses the fountain codes for application-layer error correction. The basic ideas of the proposed resource allocation framework may be applied with specific designs for different coding schemes.

If flow g is loss-sensitive, UE (i, g) 's valuation function is

$$v_g(j) = \begin{cases} 1, & j \geq M_g \\ 0, & \text{otherwise} \end{cases} \quad (2.2)$$



2.3.3 UEs' Utility

UEs receive any packet the BS transmits in perfect channels. However, this is not the case when the channels are lossy. In the lossy binary-symmetric channels, when the BS transmits A_g (coded) packets in flow g , UE (i, g) with the PEP $e_{i,g}$ will receive j packets, $0 \leq j \leq A_g$, with probability $\binom{A_g}{j} (1 - e_{i,g})^j e_{i,g}^{A_g-j}$. Thus, each UE (i, g) 's valuation on the flow transmitted, denoted by $v_g(e_{i,g}, A_g)$, is derived in Proposition 2.1. In the system meaning, UE (i, g) 's valuation $v_g(e_{i,g}, A_g)$ can be viewed as the expected normalized throughput.

Proposition 2.1. *The BS transmits A_g packets in flow g . If flow g is loss-tolerant, UE (i, g) 's valuation function is*

$$v_g(e_{i,g}, A_g) = \sum_{j=0}^{A_g} \min \left\{ 1, \frac{j}{M_g} \right\} \binom{A_g}{j} (1 - e_{i,g})^j e_{i,g}^{A_g-j} \quad (2.3)$$

If flow g is loss-sensitive, UE (i, g) 's valuation function is

$$v_g(e_{i,g}, A_g) = \begin{cases} \sum_{j=M_g}^{A_g} \binom{A_g}{j} (1 - e_{i,g})^j e_{i,g}^{A_g-j}, & A_g \geq M_g \\ 0, & \text{otherwise} \end{cases} \quad (2.4)$$

Lemma 2.1 shows that UE (i, g) 's valuation function $v_g(e_{i,g}, A_g)$ is strictly decreasing with respect to the PEP $e_{i,g}$ and strictly increasing with respect to the number of the transmitted packets A_g . We put the proof for Lemma 2.1 in Appendix A.1.

Lemma 2.1. *Whether flow g is loss-tolerant or loss-sensitive, each UE (i, g) 's valuation function $v_g(e_{i,g}, A_g)$ has the following two properties:*

1. $v_g(e_{i,g}, A_g)$ is strictly decreasing with respect to $e_{i,g}$.



Table 2.1: Notation of the multicast system model

R	Total resource blocks in the system.
\mathcal{G}	The set of multicast flows. $\mathcal{G} = \{1, 2, \dots, G\}$.
M_g	The number of original packets of flow g .
A_g	The number of coded packets of flow g .
\mathcal{N}_g	The group of UEs accessing flow g . $\mathcal{N}_g = \{1, 2, \dots, N_g\}$.
UE (i, g)	UE i accessing flow g .
$b_{i,g}$	The true BEP of UE (i, g) . $0 \leq b_i \leq 1$.
$e_{i,g}$	The true PEP of UE (i, g) . $e_{i,g} = 1 - (1 - b_{i,g})^L$ where L is the packet length.
$v_g(e_{i,g}, A_g)$	The valuation function of UE (i, g) defined in Proposition 2.1.
$c_g(A_g)$	The price function for flow g .
$u_{i,g}(e_{i,g}, A_g)$	The utility function of UE (i, g) defined in Definition 2.2.

2. $v_g(e_{i,g}, A_g)$ is strictly increasing with respect to A_g .

In the next section, we will propose a resource allocation mechanism along with a pricing scheme. The pricing scheme means that the BS charges a price for each UE's accessing a flow. The price function for flow g , denoted by $c_g(A_g)$, is a function of the number of transmitted packets A_g . It will be designed in Chapter 2.4.1. With the price function, we define UE (i, g) 's utility function, denoted by $u_{i,g}(e_{i,g}, A_g)$, as the valuation function minus the price function in Definition 2.2. The notation is summarized in Table 2.1.

Definition 2.2. [UE's utility] UE (i, g) 's utility function $u_{i,g}(e_{i,g}, A_g)$ is defined as the valuation function $v_g(e_{i,g}, A_g)$ minus the price function $c_g(A_g)$.

$$u_{i,g}(e_{i,g}, A_g) = v_g(e_{i,g}, A_g) - c_g(A_g) \quad (2.5)$$

2.4 Resource Allocation Problem and Mechanism Design

In the proposed multicast system, the BS has no information on the UEs' PEPs. The most direct way is to request the private PEP information from the UEs. However, as the UEs are self-interested in nature, they may falsely report the PEPs if doing so increases their own utility. Without the correct PEP feedback, the resource allocation may be suboptimal. In the following, we design a truth-revealing resource allocation mechanism that can elicit

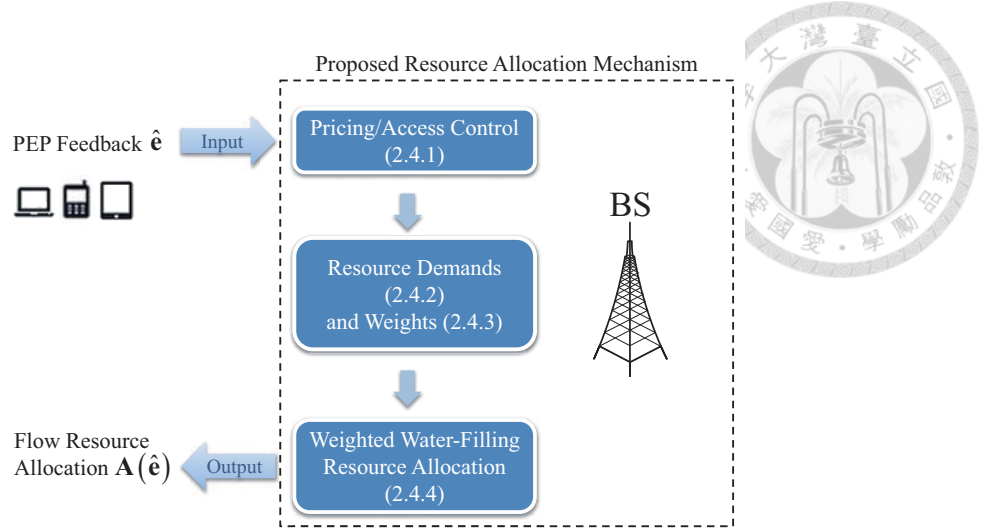


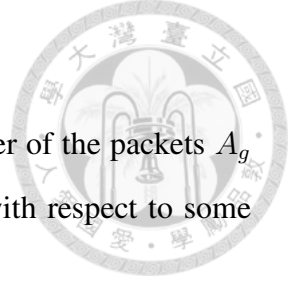
Figure 2.2: The flow diagram of the proposed resource allocation mechanism.

the true PEP information from the UEs. Recall that time is divided into periods. Though the mechanism is proposed for a single time period, it can be run in every time period. Mathematically, the proposed mechanism (the BS) requires each UE to report the private PEP information $\hat{e}_{i,g}$. With the reported PEP profile $\hat{\mathbf{e}} = (\hat{e}_{i,g})_{i \in \mathcal{N}_g, g \in \mathcal{G}}$, the BS decides the resource allocation profile

$$\mathbf{A}(\hat{\mathbf{e}}) = (A_1(\hat{\mathbf{e}}), A_2(\hat{\mathbf{e}}), \dots, A_G(\hat{\mathbf{e}})), \text{ s.t. } \sum_{g=1}^G A_g(\hat{\mathbf{e}}) \leq R \quad (2.6)$$

where $A_g(\hat{\mathbf{e}})$ is the number of the packets transmitted to each group $g \in \mathcal{G}$. Note that the reported PEP profile $\hat{\mathbf{e}}$ may not be the true PEP profile $\mathbf{e} = (e_{i,g})_{i \in \mathcal{N}_g, g \in \mathcal{G}}$. Therefore, our design goals are (1) to elicit the true PEP information from the UEs $\hat{\mathbf{e}} = \mathbf{e}$ (truth-revelation in Chapter 2.6) and (2) to achieve efficient and fair resource allocation (efficiency and fairness properties in Chapter 2.7).

In design of the mechanism, we consider UEs' group resource demands and priority (weights). A weighted water-filling method is proposed to allocate resources [32]. The flow diagram of the proposed mechanism is given in Fig. 2.2, and the detailed designs are specified as follows.



2.4.1 Pricing and Access Control

The BS decides the price function $c_g(A_g)$ for transmitting the number of the packets A_g in flow g . We design the price function as the valuation function with respect to some system-defined PEP value $e_{c,g}$, $0 \leq e_{c,g} \leq 1$.

Design 2.1. [Price function] The price function $c_g(A_g)$ is the valuation function with respect to some system-defined PEP value $e_{c,g}$, $0 \leq e_{c,g} \leq 1$.

$$c_g(A_g) = v_g(e_{c,g}, A_g) \quad (2.7)$$

The design of the price functions has one major advantage of access control. When joining the mechanism, the UEs with the PEPs less than $e_{c,g}$ gain positive utility, and the UEs with the PEPs greater than $e_{c,g}$ gain negative utility. In other words, $e_{c,g}$ is like a threshold that enables only the UEs with the PEPs less than $e_{c,g}$ to join the mechanism. In the rest of the paper, we will focus on the UEs joining the mechanism, assuming that all UEs have the PEPs $e_{i,g} < e_{c,g}$.

Lemma 2.2. For UE (i, g) , the utility function $u_{i,g}(e_{i,g}, A_g)$ is positive if $e_{i,g} < e_{c,g}$; the utility function is non-positive if $e_{i,g} \geq e_{c,g}$.

$$\begin{cases} u_{i,g}(e_{i,g}, A_g) > 0, & e_{i,g} < e_{c,g} \\ u_{i,g}(e_{i,g}, A_g) \leq 0, & e_{i,g} \geq e_{c,g} \end{cases} \quad (2.8)$$

Proof. Note $c_g(A_g) = v_g(e_{c,g}, A_g)$. From Lemma 2.1, we know that $v_g(e_{i,g}, A_g)$ is strictly decreasing with respect to $e_{i,g}$. Thus, if $e_{i,g} < e_{c,g}$, $v_g(e_{i,g}, A_g) > v_g(e_{c,g}, A_g)$; otherwise, $v_g(e_{i,g}, A_g) \leq v_g(e_{c,g}, A_g)$. This implies (2.8). \square

Theorem 2.1. [Access control] UE (i, g) will join the mechanism and obtain positive utility if the PEP $e_{i,g} < e_{c,g}$; otherwise, the UE will not join the mechanism. In the system meaning, the proposed mechanism grants access to each UE with the PEP $e_{i,g} < e_{c,g}$.

Proof. This is the direct result of Lemma 2.2. \square

2.4.2 UE Resource Demands and Group Resource Demands

Another advantage of the proposed price functions is that each UE (i, g) 's utility function $u_{i,g}(e_{i,g}, A_g)$ will be single-peaked over the number of the packets A_g . This is shown in Lemmas 2.3 and 2.4. For UE (i, g) (with the PEP $e_{i,g} < e_{c,g}$), we define

$$\Delta v_g(e_{i,g}, A_g) = v_g(e_{i,g}, A_g + 1) - v_g(e_{i,g}, A_g) \quad (2.9)$$

as the gradient of the UE's valuation function with respect to A_g (valuation gradient function for short). We also define

$$\begin{aligned} \Delta u_{i,g}(e_{i,g}, A_g) &= u_{i,g}(e_{i,g}, A_g + 1) - u_{i,g}(e_{i,g}, A_g) \\ &= \Delta v_g(e_{i,g}, A_g) - \Delta v_g(e_{c,g}, A_g) \end{aligned} \quad (2.10)$$

as the gradient of the UE's utility function (utility gradient function for short). These gradient functions will be used in Lemmas 2.3, 2.4, and 2.5. The proofs for Lemmas 2.3 and 2.4 can be found in Appendices A.2 and A.3.

Lemma 2.3. *The valuation gradient function $\Delta v_g(e_{i,g}, A_g)$ is single-peaked with respect to $e_{i,g}$. Denote the point on the $e_{i,g}$ -axis that maximizes $\Delta v_g(e_{i,g}, A_g)$ by $e_g^*(A_g)$. The function $e_g^*(A_g)$ is strictly increasing with respect to A_g .*

Lemma 2.4. *For UE (i, g) (with the PEP $e_{i,g} < e_{c,g}$), the utility function $u_{i,g}(e_{i,g}, A_g)$ is single-peaked. Mathematically, there exists unique $d_{i,g}$ such that $u_{i,g}(e_{i,g}, A_g)$ is maximized at $A_g = d_{i,g}$, and*

$$\begin{cases} \Delta u_{i,g}(e_{i,g}, A_g) > 0, & A_g < d_{i,g} \\ \Delta u_{i,g}(e_{i,g}, A_g) \geq 0, & A_g = d_{i,g} \\ \Delta u_{i,g}(e_{i,g}, A_g) < 0, & A_g > d_{i,g} \end{cases} \quad (2.11)$$

From Lemma 2.4, each UE (i, g) 's utility is maximized when the number of the transmitted packets is $d_{i,g}$. We call this $d_{i,g}$ UE (i, g) 's resource demand. Note that each UE

(i, g) with different PEP values $e_{i,g}$ may have different amounts of the resource demand $d_{i,g}$. Therefore, we can define a function $d_g(e_{i,g}) = d_{i,g}$ as the UE resource demand function in flow g . The UE resource demand function is an increasing function of $e_{i,g}$, as proven in Lemma 2.5. This means the proposed price functions ensure the UEs with the lower PEPs to demand less, and vice versa.

Lemma 2.5. *The UE resource demand function $d_g(e_{i,g})$ is an increasing function of $e_{i,g}$.*

Proof. For UE (i, g) , $u_{i,g}(e_{i,g}, A_g)$ is maximized at $A_g = d_g(e_{i,g})$. With (2.10) and the first and second inequalities of (2.11), we have

$$\Delta v_g(e_{i,g}, A_g) - \Delta v_g(e_{c,g}, A_g) \geq 0, \quad A_g \leq d_g(e_{i,g}) \quad (2.12)$$

Consider another UE (j, g) with the PEP $e_{j,g}$ satisfying $e_{i,g} < e_{j,g} < e_{c,g}$. Due to the single-peaked property of the valuation gradient function in Lemma 2.3, (2.12) along with $e_{i,g} < e_{j,g} < e_{c,g}$ implies

$$\Delta v_g(e_{j,g}, A_g) > \Delta v_g(e_{c,g}, A_g), \quad A_g \leq d_g(e_{i,g}) \quad (2.13)$$

Moreover, from (2.10) and the first inequality of (2.11), for UE (j, g) we have

$$\Delta v_g(e_{j,g}, A_g) - \Delta v_g(e_{c,g}, A_g) > 0, \quad A_g < d_g(e_{j,g}) \quad (2.14)$$

Checking the conditions of (2.13) and (2.14), we must have $d_g(e_{j,g}) \geq d_g(e_{i,g})$ for $e_{j,g} > e_{i,g}$. □

In fact, the UE resource demand function is an increasing step (staircase) function. This is because the resource allocation, as well as the resource demand, only takes integer values, and different PEP values on a consecutive interval may correspond to the same integer value of the resource demand. Such a step-like property of the UE resource demand function will result in similar step-like behavior of the UE's utility function, as will be seen in Fig. 2.4 in Chapter 2.8.1.

We can directly use every UE's resource demand for resource allocation. However, as each group may have numerous UEs, a resource allocation method that considers every UE's resource demand will be complex. A simpler way is to propose a flow-level method that jointly uses a single UE's resource demand to represent the group resource demand, and a group weight to take the number of the UEs in the group into consideration. We design the group resource demand $D_g(\mathbf{e}_g)$ as the k_g -th minimum resource demand of the UEs in flow g where $k_g \in \mathcal{N}_g$. According to Lemma 2.5, the group resource demand is also the resource demand of the UE with the k_g -th minimum PEP.

Design 2.2. [Group resource demand] In flow g , the group resource demand $D_g(\mathbf{e}_g)$ is defined as the k_g -th minimum resource demand of the UEs in the flow. It is also the resource demand of the UE with the k_g -th minimum PEP.

$$\begin{aligned} D_g(\mathbf{e}_g) &= \min \{k_g; d_g(e_{1,g}), d_g(e_{2,g}), \dots, d_g(e_{N_g,g})\} \\ &= d_g(\min \{k_g; \mathbf{e}_g\}) \end{aligned} \quad (2.15)$$

where $k_g \in \mathcal{N}_g$, $\mathbf{e}_g = (e_{1,g}, e_{2,g}, \dots, e_{N_g,g})$ is the PEP profile of the UEs in flow g , and $\min \{k_g; \cdot\}$ selects the k_g -th minimum input element.

Besides reducing the complexity, the design of the group resource demand has another good property: In consideration of limited resources, the selection of k_g means that we fulfill the resource demands of the UEs with the first k_g minimum PEPs. For the other UEs with the PEPs greater than the k_g -th minimum PEP and less than $e_{c,g}$, we grant them access (Theorem 2.1) but do not guarantee to fulfill their resource demands.

2.4.3 Group Weights

As mentioned above, group weights that consider the number of the UEs in each group are also used for resource allocation. To be specific, the weight w_g for each group g is designed as an increasing and concave function of the number of the UEs \hat{N}_g that report $\hat{e}_{i,g} < e_{c,g}$. (We have assumed that each UE has the PEP $e_{i,g} < e_{c,g}$ for simplicity. Though the UEs may falsely report the PEPs, they may not report the PEPs higher than

$e_{c,g}$. Otherwise, they gain nothing. Thus, $\hat{N}_g = N_g$.) This design is desirable in that a group with more UEs will have a higher weight and thus higher priority to gain resources. However, the increment of the weight becomes less when the number of UEs increases, which also balances the resource allocation to each group. One possible design of the weight is as follows.

Design 2.3. [Group weight] The group weight w_g is increasing and concave with respect to the number of the UEs N_g . One simple candidate is a log function

$$w_g = \log(1 + N_g) \quad (2.16)$$

2.4.4 Weighted Water-Filling Resource Allocation

The core of the proposed mechanism is the weighted water-filling resource allocation. It has low complexity. With the proposed price functions, group resource demands, and group weights, the overall procedures for resource allocation are specified as follows.

1. [Pricing] The BS sets the price function $c_g(A_g)$ for each group g as in Design 2.1.
2. [Requesting the PEP feedback] The BS requires each UE (i, g) to report the PEP $\hat{e}_{i,g}$. Note that the reported PEP may not be the true PEP.
3. [Computing the group resource demands] Receiving the PEP feedback, the BS computes each UE (i, g) 's "reported" resource demand $d_g(\hat{e}_{i,g})$ that maximizes the "reported" utility function $\hat{u}_{i,g}(A_g) = v_g(\hat{e}_{i,g}, A_g) - c_g(A_g)$. The BS further decides the group resource demand $D_g(\hat{\mathbf{e}}_g)$ as the k_g -th minimum reported resource demand as in Design 2.2 where $\hat{\mathbf{e}}_g = (\hat{e}_{1,g}, \hat{e}_{2,g}, \dots, \hat{e}_{N_g,g})$ denotes the reported PEP profile of the UEs in group g .
4. [Computing the weights] The BS sets the weight w_g for each group g as an increasing and concave function of the number of UEs N_g . For example, the BS sets $w_g = \log(1 + N_g)$.

5. [*Sorting the groups*] The BS sorts all groups in increasing order of the weighted resource demands $\{D_g(\hat{\mathbf{e}}_g)/w_g\}_{g \in \mathcal{G}}$. Without loss of generality, we assume that all groups satisfy this increasing order of the weighted resource demands

$$\frac{D_1(\hat{\mathbf{e}}_1)}{w_1} \leq \frac{D_2(\hat{\mathbf{e}}_2)}{w_2} \leq \dots \leq \frac{D_G(\hat{\mathbf{e}}_G)}{w_G} \quad (2.17)$$

6. [*Weighted water-filling resource allocation*] The BS allocates the total resources R to the sorted groups round-by-round: In the r -th round, $r = 1, 2, \dots, G$, we define a resource allocation base $a_r(\hat{\mathbf{e}})$ in (2.18). The BS allocates to every sorted group g , $g = r, r + 1, \dots, G$, the resources $w_g a_r(\hat{\mathbf{e}})$ (on the base $a_r(\hat{\mathbf{e}})$ and proportional to the weight w_g), until either group r 's unsatisfied resource demand, $D_r(\hat{\mathbf{e}}_r) - w_r \sum_{l=1}^{r-1} a_l(\hat{\mathbf{e}})$, is satisfied or the total unallocated resources, $R - \sum_{l=1}^{r-1} a_l(\hat{\mathbf{e}}) \sum_{h=l}^G w_h$, are allocated. According to this procedure, the resource allocation base $a_r(\hat{\mathbf{e}})$, $r = 1, 2, \dots, G$, can be expressed iteratively

$$a_r(\hat{\mathbf{e}}) = \min \left\{ \frac{D_r(\hat{\mathbf{e}}_r) - w_r \sum_{l=1}^{r-1} a_l(\hat{\mathbf{e}})}{w_r}, \frac{R - \sum_{l=1}^{r-1} a_l(\hat{\mathbf{e}}) \sum_{h=l}^G w_h}{\sum_{h=r}^G w_h} \right\} \quad (2.18)$$

The resource allocation to each sorted group g is

$$A_g(\hat{\mathbf{e}}) = w_g \sum_{r=1}^g a_r(\hat{\mathbf{e}}) \quad (2.19)$$

7. [*Charging*] The BS charges each UE in each group g the price $c_g(A_g(\hat{\mathbf{e}}))$.

Instead of the iterative expressions in (2.18) and (2.19), the resource allocation can also be directly expressed in terms of the group resource demands $\{D_g(\hat{\mathbf{e}}_g)\}_{g \in \mathcal{G}}$. We first define $(G + 1)$ traffic cases for the group resource demands where the traffic case C_j , $j = 0, 1, \dots, G$, is

$$\begin{cases} \frac{D_g(\hat{\mathbf{e}}_g)}{w_g} \leq \frac{R - \sum_{k=1}^{g-1} D_k(\hat{\mathbf{e}}_k)}{\sum_{k=g}^G w_k}, & g \leq j \\ \frac{D_g(\hat{\mathbf{e}}_g)}{w_g} > \frac{R - \sum_{k=1}^j D_k(\hat{\mathbf{e}}_k)}{\sum_{k=j+1}^G w_k}, & \text{otherwise} \end{cases} \quad (2.20)$$

Note that the group resource demands must fall in one of $(G + 1)$ traffic cases. In traffic case C_j , $j = 0, 1, \dots, G$, groups 1 to j 's resource demands are satisfied and groups $(j + 1)$ to G 's resource demands are not satisfied. Thus, the resource allocation $A_g(\hat{\mathbf{e}})$ in each traffic case can be derived in Design 2.4.

Design 2.4. [Weighted resource allocation] Without loss of generality, the group resource demands $\{D_g(\hat{\mathbf{e}}_g)\}_{g \in \mathcal{G}}$ satisfy the weighted increasing order. When the group resource demands fall in traffic case C_j , $j = 0, 1, \dots, G$, the resource allocation is

$$A_g(\hat{\mathbf{e}}) = \begin{cases} D_g(\hat{\mathbf{e}}_g), & g \leq j \\ \frac{w_g(R - \sum_{k=1}^j D_k(\hat{\mathbf{e}}_k))}{\sum_{k=j+1}^G w_k}, & \text{otherwise} \end{cases} \quad (2.21)$$

Proof. Adding $\sum_{l=1}^{r-1} a_l(\hat{\mathbf{e}})$ to both sides of (2.18), we have

$$\sum_{l=1}^r a_l(\hat{\mathbf{e}}) = \min \left\{ \frac{D_r(\hat{\mathbf{e}}_r)}{w_r}, \frac{R - \sum_{l=1}^{r-1} a_l(\hat{\mathbf{e}}) \sum_{h=l}^{r-1} w_h}{\sum_{h=r}^G w_h} \right\} \quad (2.22)$$

Further using (2.19) and the fact that $\sum_{l=1}^{r-1} a_l(\hat{\mathbf{e}}) \sum_{h=l}^{r-1} w_h = \sum_{h=1}^{r-1} w_h \sum_{l=1}^h a_l(\hat{\mathbf{e}}) = \sum_{h=1}^{r-1} A_h(\hat{\mathbf{e}})$, we can derive the resource allocation to each group g

$$A_g(\hat{\mathbf{e}}) = \min \left\{ D_g(\hat{\mathbf{e}}_g), \frac{w_g(R - \sum_{h=1}^{g-1} A_h(\hat{\mathbf{e}}))}{\sum_{h=g}^G w_h} \right\} \quad (2.23)$$

Given traffic case C_j as in (2.20), we can derive A_1, A_2, \dots, A_G iteratively and obtain (2.21) (The derivation process is skipped to save space). In other words, groups 1 to j 's resource demands are satisfied, and groups $(j + 1)$ to G 's resource demands are not satisfied. \square

Lastly, for the use of notation in the rest of the paper, we denote the reported PEP profile by $\hat{\mathbf{e}} = (\hat{\mathbf{e}}_{i,g}, \hat{\mathbf{e}}_{-(i,g)})$ where $\hat{\mathbf{e}}_{-(i,g)}$ is the reported PEP profile of the UEs other than UE (i, g) . We also denote the reported PEP profile of the UEs in flow g by $\hat{\mathbf{e}}_g = (\hat{\mathbf{e}}_{i,g}, \hat{\mathbf{e}}_{-i,g})$ where $\hat{\mathbf{e}}_{-i,g}$ is the reported PEP profile of the UEs in flow g other than UE (i, g) . The notation of the proposed mechanism is summarized in Table 2.2.

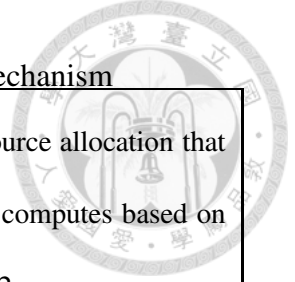


Table 2.2: Notation of the multicast resource allocation mechanism

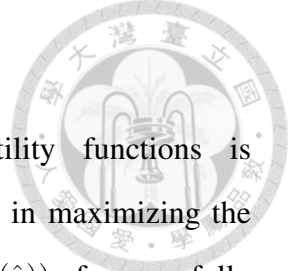
$c_g(A_g)$	The price function for flow g defined in Design 2.1.
$d_g(e_{i,g})$	The resource demand of UE (i, g) . It is defined as the resource allocation that maximizes UE (i, g) 's utility.
$d_g(\hat{e}_{i,g})$	The "reported" resource demand of UE (i, g) that the BS computes based on the reported PEP $\hat{e}_{i,g}$.
$D_g(\mathbf{e}_g)$	The group resource demand of flow g defined in Design 2.2.
$D_g(\hat{\mathbf{e}}_g)$	The "reported" group resource demand of flow g that the BS computes based on the reported PEPs $\hat{\mathbf{e}}_g$.
w_g	The weight for flow g defined in Design 2.3.
$A_g(\hat{\mathbf{e}})$	The resource allocation to flow g defined in Design 2.4.
$\hat{e}_{i,g}$	The reported PEP of UE (i, g) .
$\hat{\mathbf{e}}$	The overall reported PEP profile. $\hat{\mathbf{e}} = (\hat{e}_{i,g})_{i \in \mathcal{N}_g, g \in \mathcal{G}} = (\hat{e}_{i,g}, \hat{\mathbf{e}}_{-(i,g)})$.
$\hat{\mathbf{e}}_{-(i,g)}$	The reported PEP profile of the UEs other than UE (i, g) .
$\hat{\mathbf{e}}_g$	The reported PEP profile of the UEs in flow g . $\hat{\mathbf{e}}_g = (\hat{e}_{1,g}, \hat{e}_{2,g}, \dots, \hat{e}_{N_g,g}) = (\hat{e}_{i,g}, \hat{\mathbf{e}}_{-i,g})$.
$\hat{\mathbf{e}}_{-i,g}$	The reported PEP profile of the UEs in flow g other than UE (i, g) .

2.5 Resource Allocation Game

In the proposed resource allocation mechanism, the selfish UEs report the PEPs to maximize their own utility. We formulate the feedback decisions of the UEs as a strategic game and apply game theory to analyze it. The aim of the game-theoretic analysis is to derive a desirable operating steady state, specifically, truth-revealing dominant-strategy equilibrium at which the resource allocation is efficient and fair. Even though each UE may act selfishly and try to manipulate the multicast configuration, the proposed mechanism ensures the robustness and optimality of the system. In the following, we construct a resource allocation game model for the proposed mechanism and introduce the dominant-strategy solution concept.

The resource allocation game is $G = (N, S, U, E)$ where each component is specified as below.

- Player set N : Each UE (i, g) , $i \in \mathcal{N}_g$ and $g \in \mathcal{G}$, is a player in the game. Therefore, the player set is $N = \{\mathcal{N}_g \times \mathcal{G}\}$. We may use the terms UE and player interchangeably.
- Strategy space S : Each player (i, g) 's strategy is to report the PEP $\hat{e}_{i,g}$. All possible strategies of player (i, g) form the strategy set $\hat{E}_{i,g} = \{\hat{e}_{i,g} : 0 \leq \hat{e}_{i,g} \leq 1\}$. Thus,



the game has the strategy space $S = \prod_{i \in \mathcal{N}_G, g \in \mathcal{G}} \hat{E}_{i,g}$.

- Set of the utility functions U : The set of the utility functions is $U = \{u_{i,g}(e_{i,g}, A_g(\hat{\mathbf{e}}))\}_{i \in \mathcal{N}_G, g \in \mathcal{G}}$. Each player (i, g) is selfish in maximizing the valuation, i.e., the expected normalized throughput, $v_g(e_{i,g}, A_g(\hat{\mathbf{e}}))$ of successfully receiving and decoding the data flow. However, the BS also charges the price $c_g(A_g(\hat{\mathbf{e}}))$ for transmitting the data flow. Hence, as defined in Definition 2.2, each player (i, g) 's utility function is the valuation $v_g(e_{i,g}, A_g(\hat{\mathbf{e}}))$ minus the price $c_g(A_g(\hat{\mathbf{e}}))$,

$$u_{i,g}(e_{i,g}, A_g(\hat{\mathbf{e}})) = v_g(e_{i,g}, A_g(\hat{\mathbf{e}})) - c_g(A_g(\hat{\mathbf{e}})) \quad (2.24)$$

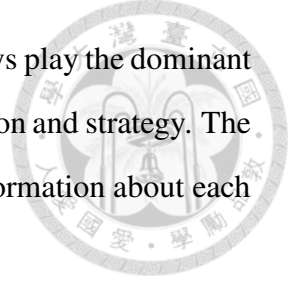
To alleviate the complex notation, we use $u_{i,g}(\hat{\mathbf{e}})$ to denote player (i, g) 's utility function for short in the rest of the paper.

- Set of the true PEPs E : The set of the true PEPs is $E = \{e_{i,g}\}_{i \in \mathcal{N}_G, g \in \mathcal{G}}$. Note that each player (i, g) 's true PEP $e_{i,g}$ is private information.

The solution concept that will be used is dominant-strategy equilibrium. The dominant-strategy solution concept is stronger and harder to achieve than the well-known Nash solution concept [33]. Note that every player has the private PEP information. The Nash solution concept that requires perfect information of all players' preferences cannot be applied. Instead, the dominant-strategy solution concept that requires no private information is used (This is why the dominant-strategy solution concept is stronger and harder to achieve). The formal definition of the dominant-strategy solution concept is as follows.

Definition 2.3. [*Dominant strategy*] Player (i, g) 's strategy $\hat{e}_{i,g}^*$ is a dominant strategy if it maximizes player (i, g) 's utility for all possible strategies of the other players, $u_{i,g}(\hat{e}_{i,g}^*, \hat{\mathbf{e}}_{-(i,g)}) \geq u_{i,g}(\hat{e}_{i,g}, \hat{\mathbf{e}}_{-(i,g)}) \forall \hat{e}_{i,g} \neq \hat{e}_{i,g}^*$ and $\forall \hat{\mathbf{e}}_{-(i,g)}$.

Definition 2.4. [*Dominant-strategy equilibrium*] The strategy profile $\hat{\mathbf{e}}^*$ is a dominant-strategy equilibrium if $\hat{e}_{i,g}^*$ is a dominant strategy for every player (i, g) .



When every player has a dominant strategy, every player can always play the dominant strategy to maximize its utility without knowing any other's information and strategy. The game then reaches a dominant-strategy equilibrium, requiring no information about each other.

2.6 Strategy-Proofness – Truth-Revealing Equilibrium

In the proposed resource allocation game, we prove that each UE (i, g) has the dominant strategy to report the true PEP, $\hat{e}_{i,g}^* = e_{i,g}$. The game reaches the truth-revealing dominant-strategy equilibrium $\hat{e}^* = \mathbf{e}$. Hence, the proposed mechanism is strategy-proof [34].

Definition 2.5. [Strategy-proofness] *A mechanism is strategy-proof if the game induced by the mechanism reaches the truth-revealing dominant-strategy equilibrium.*

The flow of the proofs are as follows. We first show how each UE influences the group resource demand by changing its strategy in Lemma 2.6. We also show that how the change of the group resource demand influences the resource allocation in Lemma 2.7. Based on these two lemmas, each UE is shown to have the truth-revealing dominant strategy in Theorem 2.2.

Lemma 2.6. *Each UE (i, g) can influence the group resource demand $D_g(\hat{\mathbf{e}}_g)$ by changing its strategy $\hat{e}_{i,g}$ in the following three cases:*

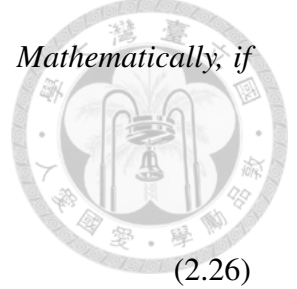
1. *If UE (i, g) 's true resource demand is greater than the group resource demand, it cannot influence the group resource demand by increasing its strategy. It can only decrease the group resource demand by decreasing its strategy. Mathematically, if $d_g(e_{i,g}) > D_g(e_{i,g}, \hat{e}_{-i,g})$,*

$$\begin{cases} D_g(\hat{\mathbf{e}}_g) = D_g(e_{i,g}, \hat{e}_{-i,g}), & \hat{e}_{i,g} > e_{i,g} \\ D_g(\hat{\mathbf{e}}_g) \leq D_g(e_{i,g}, \hat{e}_{-i,g}), & \hat{e}_{i,g} < e_{i,g} \end{cases} \quad (2.25)$$

2. *If UE (i, g) 's true resource demand is less than the group resource demand, it cannot influence the group resource demand by decreasing its strategy. It can only*

increase the group resource demand by increasing its strategy. Mathematically, if $d_g(e_{i,g}) < D_g(e_{i,g}, \hat{e}_{-i,g})$,

$$\begin{cases} D_g(\hat{e}_g) \geq D_g(e_{i,g}, \hat{e}_{-i,g}), & \hat{e}_{i,g} > e_{i,g} \\ D_g(\hat{e}_g) = D_g(e_{i,g}, \hat{e}_{-i,g}), & \hat{e}_{i,g} < e_{i,g} \end{cases} \quad (2.26)$$



3. If UE (i, g) 's true resource demand is the group resource demand, $d_g(e_{i,g}) = D_g(e_{i,g}, \hat{e}_{-i,g})$, it can increase/decrease the group resource demand by increasing/
decreasing its strategy.

Proof. The proofs for cases 1 and 2 are similar, so we only prove case 1. Case 3 is straightforward, so we do not show it here. In case 1, according to Lemma 2.5 and Design 2.2, the condition $d_g(e_{i,g}) > D_g(e_{i,g}, \hat{e}_{-i,g})$ implies

$$\begin{aligned} d_g(e_{i,g}) > D_g(e_{i,g}, \hat{e}_{-i,g}) &= d_g(\min \{k_g; e_{i,g}, \hat{e}_{-i,g}\}) \\ \Leftrightarrow e_{i,g} > \min \{k_g; e_{i,g}, \hat{e}_{-i,g}\} \end{aligned} \quad (2.27)$$

Inequality (2.27) then implies (2.25). □

Lemma 2.7. *Without loss of generality, we assume that the group resource demands $\{D_g(\hat{e}_g)\}_{g \in \mathcal{G}}$ satisfy the weighted increasing order. We also assume that the group resource demands $\{D_g(\hat{e}_g)\}_{g \in \mathcal{G}}$ are in traffic case C_j , $j = 0, 1, \dots, G$. The following two statements are true:*

1. *For $g = 1, 2, \dots, j$, group g can acquire more/fewer resources by increasing/decreasing the group resource demand.*
2. *For $g = j + 1, j + 2, \dots, G$, group g cannot acquire more resources by increasing the group resource demand. It can only acquire fewer resources by decreasing the group resource demand.*

Proof. We drop the notation \hat{e} and \hat{e}_g for short. When the group resource demands are in traffic case C_j , groups 1 to j fulfill their group resource demands but groups $(j+1)$ to G do not fulfill their group resource demands. According to (2.18), we know the resource allocation base

$$a_g = \begin{cases} \frac{D_g - w_g \sum_{l=1}^{g-1} a_l}{w_g}, & g \leq j \\ \frac{R - \sum_{l=1}^{g-1} a_l \sum_{h=l}^G w_h}{\sum_{h=g}^G w_h}, & \text{otherwise} \end{cases} \quad (2.28)$$

[Case 1: $g = 1, 2, \dots, j$. Group g fulfills its group resource demand.] If group g increases its group resource demand from D_g to D'_g (i.e., $D'_g > D_g$), group g will increase its order from g to some $k \geq g$. Since groups 1 to $(g-1)$'s orders are not affected, the resource allocation bases a_1 to a_{g-1} are not affected as well. Then according to (2.19), the resource allocation to group g becomes

$$A'_g = w_g \left(\sum_{r=1}^{g-1} a_r + \sum_{r=g}^k a'_r \right) \quad (2.29)$$

where a'_r is the new resource allocation base in the r -th round for $r = g, g+1, \dots, k$. Obviously, the new resource allocation base a'_g in the g -th round should be greater than or equal to a_g , i.e., $a'_g \geq a_g$, since the group with the new order g (group g if $D'_g/w_g < D_{g+1}/w_{g+1}$, or group $(g+1)$ otherwise) must have greater group resource demand. Therefore, we have

$$A'_g = w_g \left(\sum_{r=1}^{g-1} a_r + \sum_{r=g}^k a'_r \right) \geq w_g \sum_{r=1}^g a_r = A_g \quad (2.30)$$

which means group g acquires more resources by increasing its group resource demand.

On the other hand, if group g decreases its group resource demand from D_g to D'_g (i.e., $D'_g < D_g$), group g will decrease its order from g to some $k \leq g$. Note that groups 1 to $(k-1)$'s orders are not affected, and neither are the resource allocation bases a_1 to



a_{k-1} . Then the resource allocation to group g becomes

$$A'_g = w_g \left(\sum_{r=1}^{k-1} a_r + a'_k \right) \quad (2.31)$$

where a'_k is the new resource allocation base in the k -th round. Note that group k fulfills its group resource demand as in (2.28). Also note that group g decreases its order from g to some smaller k , which implies $D'_g/w_g \leq D_k/w_k$. We must have $a'_k \leq a_k$. Therefore,

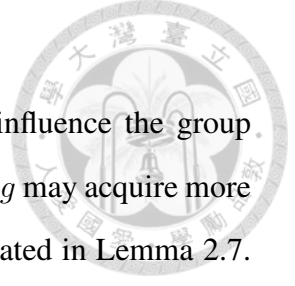
$$A'_g = w_g \left(\sum_{r=1}^{k-1} a_r + a'_k \right) \leq w_g \sum_{r=1}^g a_r = A_g \quad (2.32)$$

which means group g acquires fewer resources by decreasing its group resource demand.

[Case 2: $g = j + 1, j + 2, \dots, G$. Group g does not fulfill its group resource demand.] The proof for case 2 is quite similar so we do not repeat the details. The only difference is that group g cannot acquire more resources by increasing its group resource demand. Since group g does not fulfill its group resource demand, even if group g increases its group resource demand, the resource allocation base in the g -th round will not be affected. Therefore, group g can only acquire fewer resources by decreasing its group resource demand. \square

Theorem 2.2. [Strategy-proofness] *Each UE (i, g) has the truth-revealing dominant strategy $\hat{e}_{i,g}^* = e_{i,g}$ that maximizes its utility. Therefore, the resource allocation game G reaches the truth-revealing dominant-strategy equilibrium $\hat{\mathbf{e}}^* = \mathbf{e}$.*

Proof. When UE (i, g) plays the truth-revealing strategy $\hat{e}_{i,g} = e_{i,g}$, there are three possibilities for the relationship between UE (i, g) 's true resource demand $d_g(e_{i,g})$ and the group resource demand $D_g(e_{i,g}, \hat{e}_{-i,g})$: (a1) $d_g(e_{i,g}) > D_g(e_{i,g}, \hat{e}_{-i,g})$, (a2) $d_g(e_{i,g}) < D_g(e_{i,g}, \hat{e}_{-i,g})$, and (a3) $d_g(e_{i,g}) = D_g(e_{i,g}, \hat{e}_{-i,g})$. Given the group resource demand $D_g(e_{i,g}, \hat{e}_{-i,g})$, there are also two possibilities: (b1) Group g fulfills its group resource demand, and (b2) group g does not fulfill its group resource demand. Therefore, there are totally six possibilities that UE (i, g) 's true resource demand $d_g(e_{i,g})$ is greater than/less than/equal to the group resource demand $D_g(e_{i,g}, \hat{e}_{-i,g})$, and group g fulfills its group



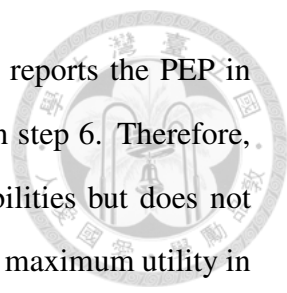
resource demand or not.

Now if UE (i, g) plays a different strategy $\hat{e}_{i,g} \neq e_{i,g}$, it can influence the group resource demand $D_g(\hat{e})$ as stated in Lemma 2.6. Also note that group g may acquire more or fewer resources when changing the group resource demands as stated in Lemma 2.7. We take the first possibility, (a1) and (b1), for example. If UE (i, g) increases its strategy $\hat{e}_{i,g} > e_{i,g}$, the group resource demand remains unchanged (Lemma 2.6). This implies unchanged resource allocation and unchanged UE (i, g) 's utility. If UE (i, g) decreases its strategy $\hat{e}_{i,g} < e_{i,g}$, the group resource demand decreases as well (Lemma 2.6). This implies less resource allocation (Lemma 2.7) and lower UE (i, g) 's utility (Lemma 2.4). The other five possibilities can be analyzed in a similar way (we do not repeat here). Therefore, we can make the following six statements that are always true:

1. If (a1) and (b1), $A_g(\hat{e}) \leq A_g(e_{i,g}, \hat{e}_{-(i,g)}) < d_g(e_{i,g})$.
2. If (a2) and (b1), $A_g(\hat{e}) \geq A_g(e_{i,g}, \hat{e}_{-(i,g)}) > d_g(e_{i,g})$.
3. If (a3) and (b1), $A_g(\hat{e}) \geq A_g(e_{i,g}, \hat{e}_{-(i,g)}) = d_g(e_{i,g})$ for $\hat{e}_{i,g} > e_{i,g}$ and $A_g(\hat{e}) \leq A_g(e_{i,g}, \hat{e}_{-(i,g)}) = d_g(e_{i,g})$ for $\hat{e}_{i,g} < e_{i,g}$.
4. If (a1) and (b2), $A_g(\hat{e}) \leq A_g(e_{i,g}, \hat{e}_{-(i,g)}) < d_g(e_{i,g})$.
5. If (a2) and (b2), $A_g(\hat{e}) = A_g(e_{i,g}, \hat{e}_{-(i,g)}) > d_g(e_{i,g})$.
6. If (a3) and (b2), $A_g(\hat{e}) \leq A_g(e_{i,g}, \hat{e}_{-(i,g)}) = d_g(e_{i,g})$.

Finally, as Lemma 2.4 states that UE (i, g) 's utility function is single-peaked and maximized at $d_g(e_{i,g})$, we always have $u_{i,g}(e_{i,g}, \hat{e}_{-(i,g)}) \geq u_{i,g}(\hat{e}) \forall \hat{e}_{i,g} \neq e_{i,g}$ in all of the six possibilities. In other words, UE (i, g) has the truth-revealing dominant strategy $\hat{e}_{i,g}^* = e_{i,g}$ that maximizes the utility. Therefore, game G reaches the truth-revealing dominant-strategy equilibrium $\hat{e}^* = e$. □

Remarks: There are six possibilities that the UE's true resource demand is greater than/less than/equal to the group resource demand, and the group resource demand is satisfied or not. The UE's utility with respect to the reported PEP in all six possibilities will be drawn



in Fig. 2.4 in Chapter 2.8.1. Recall in Chapter 2.4.4 that each UE reports the PEP in step 2, and the mechanism computes the resource allocation result in step 6. Therefore, when reporting the PEP, each UE only knows the above six possibilities but does not know in which possibility it is. Note that each UE always obtains the maximum utility in each possibility by reporting the true PEP, but may obtain less utility in some possibilities by reporting the false PEP. Therefore, it has no incentive to report the false PEP. The proposed mechanism is "ex-ante" strategy-proof. Taking this one step further, after the mechanism gives the resource allocation result, each UE knows exactly in which case it is. Again, since each UE always obtains the maximum utility by reporting the true PEP, it still has no incentive to change the strategy (report false PEP). Hence, the proposed mechanism is also "ex-post" strategy-proof. Another thing worth mentioning is that after the mechanism gives the resource allocation result, the UE knowing in which case it is may obtain the same maximum utility by reporting the false PEP. One may wonder if the UE has the incentive or any benefit to report such a false PEP? The answer is no. Since reporting such a false PEP does not affect the resource allocation result and the UE's utility at all, it brings no benefit and will be meaningless to play such a strategy.

Lastly, in the system meaning, the proposed mechanism enables the system to reach the equilibrium operating point where the BS collects the true PEP information from the UEs and allocates resources accordingly. The resource allocation at the truth-revealing dominant-strategy equilibrium, or shortly, the equilibrium resource allocation is given in Theorem 2.3.

Theorem 2.3. [Equilibrium resource allocation] *Without loss of generality, the true group resource demands $\{D_g(\mathbf{e}_g)\}_{g \in \mathcal{G}}$ satisfy the weighted increasing order. If the group resource demands fall in traffic case C_j , $j = 0, 1, \dots, G$, the equilibrium resource allocation is*

$$A_g^*(\mathbf{e}) = \begin{cases} D_g(\mathbf{e}_g), & g \leq j \\ \frac{w_g(R - \sum_{k=1}^j D_k(\mathbf{e}_k))}{\sum_{k=j+1}^G w_k}, & \text{otherwise} \end{cases} \quad (2.33)$$

Proof. Please refer to the proof for Design 2.4. □



2.7 Desirable Properties of the Equilibrium Resource Allocation

Besides the truth-revealing property, we further show that the equilibrium resource allocation has several desirable properties, including flow-level weighted max-min fairness, flow-level weighted proportional fairness, Pareto efficiency, and (weak) budget balance. We briefly introduce these properties as follows.

Max-min fairness and proportional fairness are two of the most important system design issues. A resource allocation satisfies weighted max-min fairness if it is not possible to increase a group's weighted resource acquisition without simultaneously decreasing another group's weighted resource acquisition that is already fewer [35]. A resource allocation exhibits weighted proportional fairness if it maximizes the product of all groups' resource acquisition with the weight in the exponent [35, 36]. Pareto efficiency is another key system design issue defined as a resource allocation upon which no UE can be made better off in utility without making at least one other UE worse off in utility [34]. Lastly, (weak) budget balance means that there is a net payment from the UEs to the mechanism, not from the mechanism to the UEs. In other words, the BS does not need to pay the UEs to ensure strategy-proofness [34].

In the following analysis, we drop the notation \mathbf{e} and $\hat{\mathbf{e}}$ for short. We focus on the effective resource allocation $\min\{A_g, D_g\}$ since each UE (i, g) 's resource acquisition exceeding the resource demand contributes negative value to its utility (the single-peaked property of the utility function in Lemma 2.4). Also note that any resource allocation \mathbf{A} must satisfy the resource constraint $\sum_{g=1}^G A_g \leq R$.

Theorem 2.4. [Weighted max-min fairness] *The equilibrium resource allocation \mathbf{A}^* is*

flow-level weighted max-min fair. Mathematically, \mathbf{A}^* satisfies

$$\begin{aligned} & \exists \mathbf{A} \neq \mathbf{A}^* \text{ and } h \in \mathcal{G}, \min \{A_h, D_h\} > \min \{A_h^*, D_h\} \\ \Rightarrow & \exists k \in \mathcal{G}, \frac{\min \{A_k, D_k\}}{w_k} < \frac{\min \{A_k^*, D_k\}}{w_k} \leq \frac{\min \{A_h^*, D_h\}}{w_h} \end{aligned} \quad (2.34)$$

Proof. Suppose that the group resource demands fall in traffic case C_j , $j = 0, 1, \dots, G$.

From (2.33), we know

$$\begin{aligned} \frac{\min \{A_1^*, D_1\}}{w_1} & \leq \dots \leq \frac{\min \{A_j^*, D_j\}}{w_j} \leq \frac{\min \{A_{j+1}^*, D_{j+1}\}}{w_{j+1}} \\ & = \dots = \frac{\min \{A_G^*, D_G\}}{w_G} \end{aligned} \quad (2.35)$$

Suppose that there exists another resource allocation \mathbf{A} such that

$$\min \{A_h, D_h\} > \min \{A_h^*, D_h\} \text{ for some } h \in \mathcal{G} \quad (2.36)$$

This h must satisfy $h > j$ according to (2.33) and (2.35). Thus, we have

$$\frac{\min \{A_g^*, D_g\}}{w_g} < \frac{\min \{A_h^*, D_h\}}{w_h} \quad \forall g \neq h \quad (2.37)$$

Because $\sum_{g=1}^G \min \{A_g^*, D_g\} = \min \left\{ R, \sum_{g=1}^G D_g \right\} \geq \sum_{g=1}^G \min \{A_g, D_g\}$, there must exist some $k \in \mathcal{G}$ such that $\min \{A_k, D_k\} < \min \{A_k^*, D_k\}$. Therefore, we have

$$\frac{\min \{A_k, D_k\}}{w_k} < \frac{\min \{A_k^*, D_k\}}{w_k} \leq \frac{\min \{A_h^*, D_h\}}{w_h} \quad (2.38)$$

□

Theorem 2.5. [Weighted proportional fairness] *The equilibrium resource allocation \mathbf{A}^* is flow-level weighted proportionally fair. Mathematically, \mathbf{A}^* solves the objective function*

$$\max_{\mathbf{A}} \prod_{g=1}^G \min \{A_g, D_g\}^{w_g} \quad (2.39)$$

Proof. Suppose that the group resource demands fall in traffic case C_j , $j = 0, 1, \dots, G$. In the following, B_g is used to denote $\min\{A_g, D_g\}$ for short. Dividing the objective function of (2.39) by $\prod_{g=1}^G w_g^{w_g}$, we get a new objective function $\prod_{g=1}^G (B_g/w_g)^{w_g}$ with the same solution. Applying the arithmetic mean-geometric mean inequality to $\prod_{g=j+1}^G (B_g/w_g)^{w_g}$, we have

$$\begin{aligned} \prod_{g=1}^G \left(\frac{B_g}{w_g}\right)^{w_g} &\leq \left(\frac{\sum_{g=j+1}^G B_g}{\sum_{g=j+1}^G w_g}\right)^{\sum_{g=j+1}^G w_g} \prod_{g=1}^j \left(\frac{B_g}{w_g}\right)^{w_g} \\ &\leq \left(\frac{R - \sum_{g=1}^j B_g}{\sum_{g=j+1}^G w_g}\right)^{\sum_{g=j+1}^G w_g} \prod_{g=1}^j \left(\frac{B_g}{w_g}\right)^{w_g} \end{aligned} \quad (2.40)$$

The equality of (2.40) holds if and only if

$$B_g = \frac{w_g \left(R - \sum_{k=1}^j B_k\right)}{\sum_{k=j+1}^G w_k}, \quad \forall g > j \quad (2.41)$$

We let

$$H = \left(\frac{R - \sum_{g=1}^j B_g}{\sum_{g=j+1}^G w_g}\right)^{\sum_{g=j+1}^G w_g} \prod_{g=1}^j \left(\frac{B_g}{w_g}\right)^{w_g} \quad (2.42)$$

for short. Differentiating H by B_j and rearranging it, we have

$$\begin{aligned} \frac{\partial H}{\partial B_j} &= \frac{\sum_{g=j}^G w_g}{\sum_{g=j+1}^G w_g} \left(\frac{R - \sum_{g=1}^{j-1} B_g}{\sum_{g=j}^G w_g} - \frac{B_j}{w_j}\right) \\ &\quad \times \left(\frac{R - \sum_{g=1}^j B_g}{\sum_{g=j+1}^G w_g}\right)^{(\sum_{g=j+1}^G w_g - 1)} \left(\frac{B_j}{w_j}\right)^{(w_j-1)} \prod_{g=1}^{j-1} \left(\frac{B_g}{w_g}\right)^{w_g} \end{aligned} \quad (2.43)$$

Equation (2.43) tells that H is an increasing function of B_j , i.e., $\partial H/\partial B_j \geq 0$, if and only if

$$B_j \leq \frac{w_j \left(R - \sum_{k=1}^{j-1} B_k\right)}{\sum_{k=j}^G w_k} \quad (2.44)$$

Given the condition of (2.44), if continuing to differentiate H by B_{j-1} , we can derive

that H is an increasing function of B_{j-1} and B_j if and only if

$$B_g \leq \frac{w_g (R - \sum_{k=1}^{g-1} B_k)}{\sum_{k=g}^G w_k}, \quad g = j-1, j \quad (2.45)$$



Applying the same procedure iteratively to $B_{j-2}, \dots,$ and B_1 , we can derive that H is an increasing function of $B_g \forall g \leq j$ if and only if

$$B_g \leq \frac{w_g (R - \sum_{k=1}^{g-1} B_k)}{\sum_{k=g}^G w_k}, \quad \forall g \leq j \quad (2.46)$$

Then (2.40) along with the above analysis on H becomes

$$\begin{aligned} \prod_{g=1}^G \left(\frac{B_g}{w_g} \right)^{w_g} &\leq \left(\frac{R - \sum_{g=1}^j B_j}{\sum_{g=j+1}^G w_g} \right)^{\sum_{g=j+1}^G w_g} \prod_{g=1}^j \left(\frac{B_g}{w_g} \right)^{w_g} \\ &\leq \left(\frac{R - \sum_{g=1}^j A_g^*}{\sum_{g=j+1}^G w_g} \right)^{\sum_{g=j+1}^G w_g} \prod_{g=1}^j \left(\frac{A_g^*}{w_g} \right)^{w_g} \end{aligned} \quad (2.47)$$

The equality of (2.47) holds if and only if (2.41) and (2.46) hold. This is uniquely satisfied by \mathbf{A}^* . \square

Theorem 2.6. [Pareto efficiency] *The equilibrium resource allocation \mathbf{A}^* is Pareto efficient. Mathematically, \mathbf{A}^* satisfies*

$$\begin{aligned} \exists \mathbf{A} \neq \mathbf{A}^*, i \in \mathcal{N}_G, \text{ and } g \in \mathcal{G}, u_{i,g}(e_{i,g}, A_g) &> u_{i,g}(e_{i,g}, A_g^*) \\ \Rightarrow \exists l \in \mathcal{N}_K \text{ and } k \in \mathcal{G}, u_{l,k}(e_{l,k}, A_k) &< u_{l,k}(e_{l,k}, A_k^*) \end{aligned} \quad (2.48)$$

Proof. Assume that the group resource demands fall in traffic case $C_j, j = 0, 1, \dots, G$. Recall in Lemma 2.4 that each UE's utility function is single-peaked. First, if $A_g \neq A_g^*$ for $g \leq j$, at least the UE in group g whose resource demand is the group resource demand D_g obtains less utility. Second, if $A_g < A_g^*$ for $g > j$, at least the UE in group g whose resource demand is the group resource demand D_g obtains less utility. Lastly, if $A_g > A_g^*$ for $g > j$, since $\sum_{g=1}^G \min \{A_g^*, D_g\} = \min \left\{ R, \sum_{g=1}^G D_g \right\} \geq \sum_{g=1}^G \min \{A_g, D_g\}$, there must exist some k such that $\min \{A_k, D_k\} < \min \{A_k^*, D_k\}$. Then at least the UE

Table 2.3: Parameter setting

	Meaning	Default value
R	The number of resource blocks.	10000 – 12000
\mathcal{G}	The set of flows. Flows 1, 3, ..., 19 are loss-tolerant. Flows 2, 4, ..., 20 are loss-sensitive.	{1, 2, ..., 20}
M_g	The number of original packets of flow g .	500
$\mathcal{N}_{\mathcal{G}}$	The group of UEs in flow g .	Random in [10, 100]
$e_{c,g}$	The PEP threshold for flow g .	0.2
$e_{i,g}$	The PEP of UE (i, g) .	Uniform in $(0, e_{c,g})$
k_g	The indicator for the group resource demand of flow g .	$\min \{20, N_g\}$
w_g	The weight of flow g .	$\log(1 + N_g)$

in group k whose resource demand is the group resource demand D_k obtains less utility. Therefore, even if there exists $\mathbf{A} \neq \mathbf{A}^*$ such that $u_{i,g}(e_{i,g}, A_g) > u_{i,g}(e_{i,g}, A_g^*)$, there must exist some l and k such that $u_{l,k}(e_{l,k}, A_k) < u_{l,k}(e_{l,k}, A_k^*)$. \square

Theorem 2.7. [Budget balance] *The equilibrium resource allocation \mathbf{A}^* is (weak) budget-balanced. Mathematically, the UEs' total payment at the equilibrium resource allocation \mathbf{A}^* satisfies*

$$\sum_{g=1}^G N_g c_g(A_g^*) \geq 0 \quad (2.49)$$

Proof. Note $c_g(A_g) = v_g(e_{c,g}, A_g) \geq 0 \forall g \in \mathcal{G}$. This then implies (2.49). \square

2.8 Numerical Simulation Results

In this section, we numerically evaluate the proposed resource allocation mechanism. We also show the performance of the proposed mechanism in the 3GPP MBMS simulation.

2.8.1 Numerical Analysis

The default parameter setting for the numerical analysis is given in Table 2.3. The results are plotted for a single network instance if not specially mentioned. First, we verify the property of access control of the proposed pricing method (Theorem 2.1). Fig. 2.3 shows the UE's utility functions (the expected normalized throughput minus the cost)

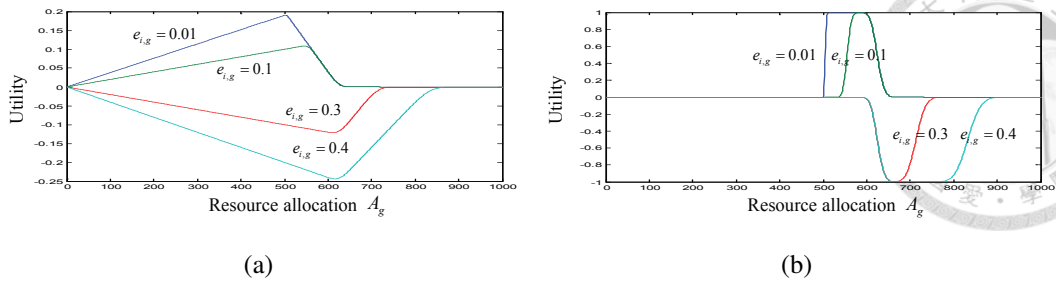


Figure 2.3: The UE's utility under different PEP values. (a) Loss-tolerant flow. (b) Loss-sensitive flow.

corresponding to different PEP values $e_{i,g} = 0.01, 0.1, 0.3,$ and 0.4 , in both of the loss-tolerant and the loss-sensitive flows. The UE's utility functions are positive with the PEP 0.01 and 0.1 less than the PEP threshold $e_{c,g} = 0.2$, and negative with the PEP 0.3 and 0.4 greater than the PEP threshold. Hence, the proposed pricing method performs access control that allows only the UEs with the PEPs less than the PEP threshold to join the mechanism and gain positive utility.

We also verify the property of truth-revelation of the proposed mechanism (Theorem 2.2). Note that there are totally six possibilities that the UE's true resource demand is greater than/less than/equal to the group resource demand, and the group fulfills its group resource demand or not. Fig. 2.4 shows the UE's utility function (the expected normalized throughput minus the cost) with respect to the reported PEP $\hat{e}_{i,g}$ in all six possibilities. The step-like behavior of the utility function is due to the step-like property of the UE resource demand function, as explained in Chapter 2.4.2. In each possibility, the UE always obtains the maximum utility by reporting the true PEP $\hat{e}_{i,g} = e_{i,g}$. Even though the UE may obtain the the same maximum utility by reporting the false PEP, the UE has no incentive to do so, as discussed in the remarks in Chapter 2.6. Hence, the proposed mechanism ensures truth-revelation.

Lastly, we evaluate the performance of the proposed mechanism in weighted proportional fairness (Theorem 2.5) and weighted max-min fairness (Theorem 2.4) in Fig. 2.5(a) and Fig. 2.5(b), respectively. We compare the proposed mechanism with a weighted scheme and a random scheme. The weighted scheme allocates resources with the same weight setting except for gathering the private PEP information. The random scheme allo-

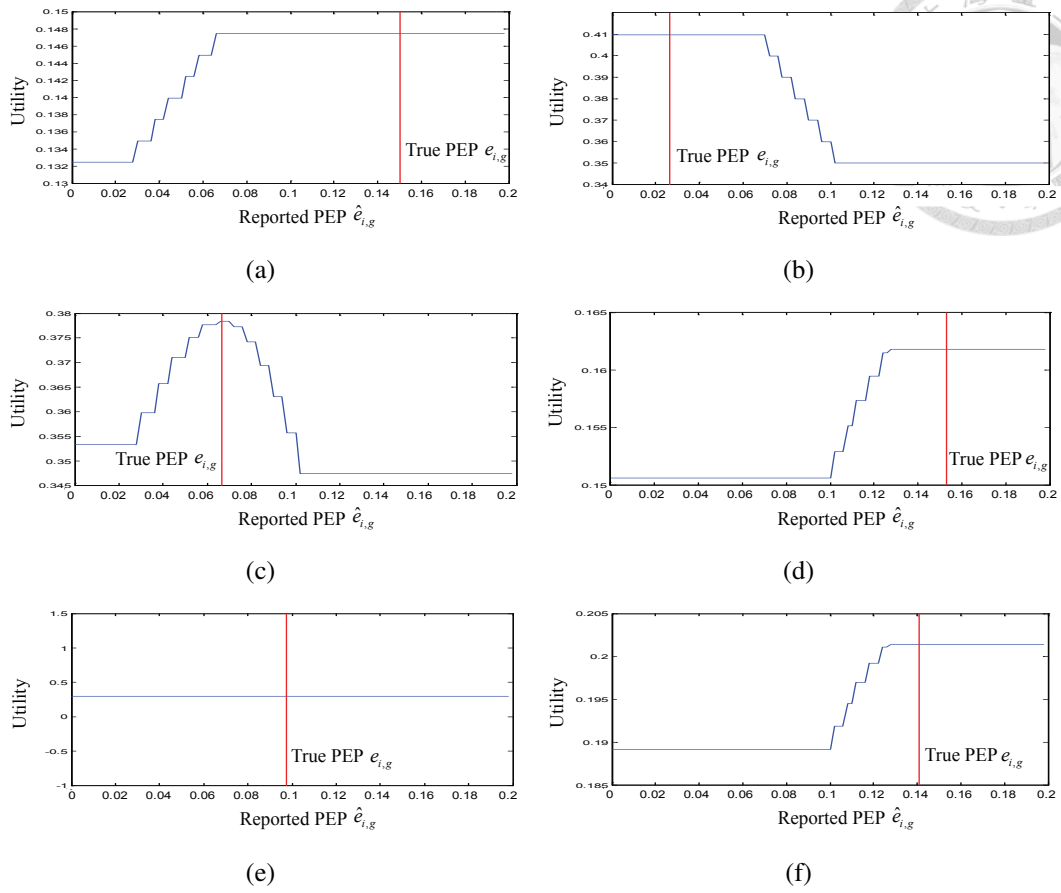


Figure 2.4: The UE’s utility with respect to the reported PEP. (a) The UE’s true resource demand is ”greater” than the group resource demand, and the group ”fulfills” its group resource demand. (b) ”less” and ”fulfill”. (c) ”equal” and ”fulfill”. (d) ”greater” and ”not fulfill”. (e) ”less” and ”not fulfill”. (f) ”equal” and ”not fulfill”.

cates resource randomly without considering the private PEP information and the weights (The results of the random scheme are averaged over 100 runs). Fig. 2.5(a) shows the weighted proportional-fairness metric, i.e., the objective function of (2.39), under different numbers of the resource blocks R from 10000 to 12000. The proposed mechanism always outperforms the other two schemes. This is because the proposed mechanism can collect the true PEP information and accordingly compute the true resource demand of each group. In this way, the resource allocation is always effective and there will be no resource waste. Fig. 2.5(b) shows the weighted effective resource allocation $\min \{A_g, D_g\} / w_g$ to each group, given the number of resource blocks $R = 11000$. The proposed mechanism achieves weighted max-min fairness in the sense that it is impossible to increase the (weighted effective) resources allocated to one group without simultaneously decreasing the resources allocated to another group that are already fewer. This

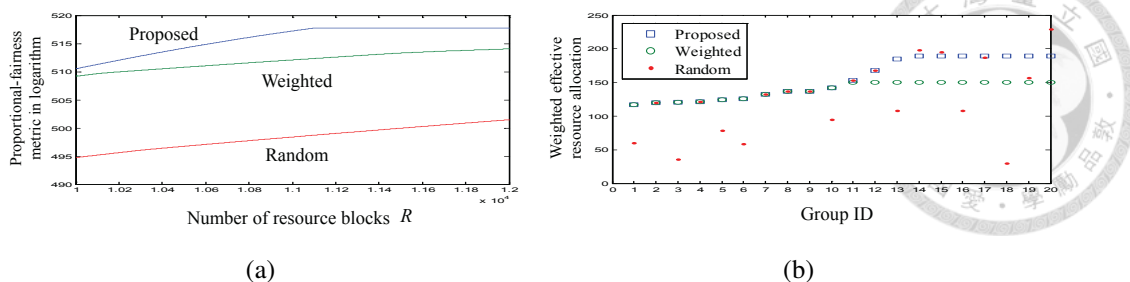


Figure 2.5: Performance comparison among the proposed mechanism, the weighted scheme, and the random scheme: (a) Weighted proportional fairness. (b) Weighted max-min fairness.

can be seen in Fig. 2.5(b) as the proposed mechanism always allocates more resources to each group than the weighted scheme. Although the random scheme allocates more resources to groups 14, 15, and 20 than the proposed mechanism, this brings the tradeoff in decreasing the resources allocated to groups 1, 3, 5, 6, 10, and 13 that are already fewer.

2.8.2 3GPP MBMS Simulation

We also conduct the 3GPP MBMS simulation to evaluate the proposed resource allocation mechanism. The simulation platform includes the video and LTE simulation modules. The video module is implemented from SVEF [37], which is a JSVM [38] based video streaming framework. Raw FOREMAN [39] video with CIF format is encoded into 10-second, 2-layer H.264 video with the average bitrate 3.84 Mbps. The encoded video is further fragmented and resynthesized into 300 packets with the fixed packet size 128 Kb. The LTE simulation module is based on LTE specification [40]. There are five multicast groups with different number of UEs in one cell. The channel bandwidth is 20 MHz. 64 QAM modulation is adopted to achieve the maximum channel capacity 37.52 Mbps. Assuming that the channel capacity is divided into 128-Kb resource blocks (one resource block can be used to transmit one video packet), the system has the maximum number of resource blocks $R_{max} = 3000$ in 10 seconds. The packet error rate (PER) of each UE is obtained from the LTE simulator [41]. The proposed access-control scheme is used to select the UEs with $PER < 0.5$. The proposed mechanism is then used to append redundancy packets to each video. The encoded video packets with redundancy are trans-

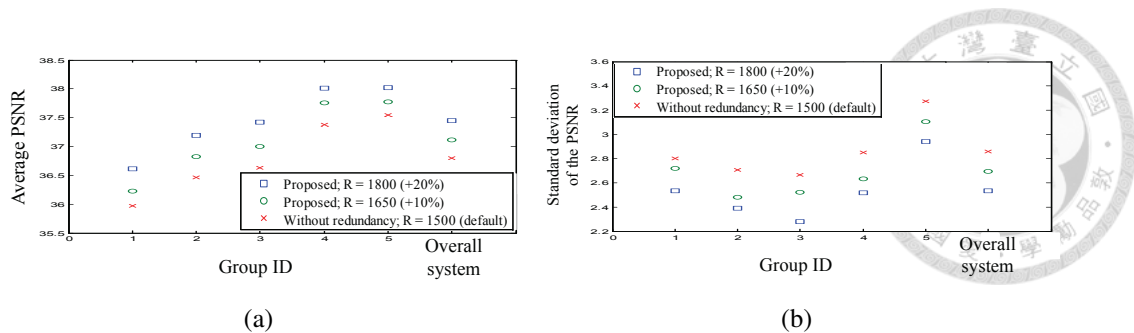


Figure 2.6: PSNR evaluation of the proposed mechanism in LTE MBMS: (a) Average PSNR. (b) Standard deviation of the PSNR.

mitted according to 3GPP MBMS protocol [5]. After each UE receives the video packets, error correction is performed and the peak signal-to-noise ratio (PSNR) is computed from the original video and the recovered one. By using PSNR as the performance metric, we run the simulation under three resource constraint levels: $R = 1500$ (default), 1650 (10% more), and 1800 (20% more). The simulation results are averaged over 10 runs.

Fig. 2.6 shows the average PSNR of each multicast group and the overall system. When $R = 1500$, by transmitting all the video flows without redundancy, the system has the average PSNR 36.79 dB and the standard deviation 2.86 dB. When the number of resource blocks increases by 10% ($R = 1650$) and 20% ($R = 1800$), the proposed mechanism brings higher average PSNR to each group and the system. The average PSNR of the system increases by 0.33 dB and 0.66 dB, respectively. Moreover, the standard deviation of the PSNR of each group and the system decreases. This means the proposed mechanism reduces the PSNR difference among the UEs in each group as well as the PSNR difference among all groups. With the above simulation results, the proposed mechanism is shown to improve 3GPP MBMS, providing more efficient (higher average PSNR) and fairer (lower standard deviation) multicast operation.

2.9 Summary

In this chapter, we address the resource allocation problem in the multi-flow multicast scenario from the perspective of incentive mechanism design. Unlike the other previous works, this chapter considers the UEs' selfish characteristic and private CQI. The pro-

posed resource allocation mechanism is desirable in many aspects. It achieves access control. Only the UEs with the PEPs less than the system-defined PEP threshold have the incentive to join the mechanism. The proposed mechanism also ensures truth-revelation. The system operation reaches the equilibrium where all of the UEs reveal their true PEPs to the BS. With truthful PEP feedback, the resource allocation at the truth-revealing equilibrium is further proven to be efficient, fair, and (weak) budget-balanced.



Chapter 3

Wireless Multicast over Time-Varying Channels for Energy-Harvesting Devices

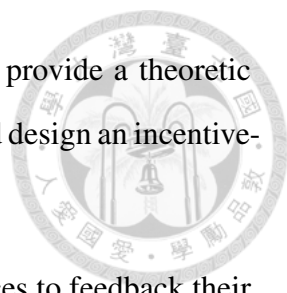
3.1 Introduction

In recent years, energy consumption has emerged as a key design issue for next-generation wireless networks. The renewable energy supply becomes a desirable alternative to decrease the use of fossil fuels and the emission of greenhouse gases. To achieve this, energy harvesting is a novel technology that enables wireless devices to scavenge energy from the ambient environment [3]. Energy harvesting not only means obtaining energy from rich sources including solar power, electromagnetic waves, thermal energy, wind energy, and kinetic energy. It also contains the process of storing energy for a period of time, and using the energy for wireless communications. Energy harvesting also provides many promising advantages that cannot be provided by conventional energy supply, such as prolonged lifetime of mobile devices and self-sustaining operation of wireless networks. Despite the advantages, the random and intermittent characteristics of renewable energy also impose new design challenges to wireless communications. Unlike the conventional networks with fixed energy supply, the available energy in energy-harvesting networks

is time-varying and bounded by the harvested and stored energy. With the advantages and challenges, energy harvesting becomes an important design consideration of future protocols.

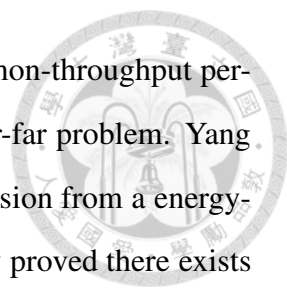
On the other hand, radio resource efficiency is another key design objective in wireless networks. When devices request the same data, e.g., firmware updates, software updates, or group messages [42], wireless multicast is a promising mode for data delivery with the efficient use of radio resources. As wireless channels are not perfect and devices may face different wireless channel conditions, the designs of efficient application error correction frameworks and on-demand resource allocation mechanisms are important for future multicast transmission [10, 43]. Inspired by the efficient use of energy and radio resources, we are interested in exploiting the potential of renewable energy in wireless multicast, which should be one of the future developments in the next-generation wireless communications.

In this chapter, we provide a theoretic model for energy-harvesting enabled wireless multicast over time-varying channels. In the proposed scenario, a base station (BS) is capable of sending multiple data flows to devices in multiple time slots. To receive data, the devices are capable of harvesting energy from the environment but also suffer from channel variations. To provide the efficient and fair multicast, the BS requires the devices to feedback the energy states and channel states (states for short). The states are in general time-varying and only known to the devices themselves. Regarding this, this chapter further considers the rational and selfish user characteristics. Devices controlled by rational and selfish users may intentionally feedback the false state information to manipulate the BS's multicast if they can benefit from such false feedback. The multicast may turn out inefficient and unfair. Therefore, to ensure reliable and truthful feedback from the devices becomes an important issue. To this end, we propose an incentive-based multicast resource allocation mechanism that can elicit the true state information from the devices (incentive compatibility), avoiding any manipulation of multicast and thereby guaranteeing efficient and fair network operation. The detailed contributions are stated as follows:

- 
1. Taking into account energy and radio resource efficiency, we provide a theoretic foundation for energy-harvesting enabled wireless multicast and design an incentive-based multicast resource allocation mechanism.
 2. The proposed resource allocation mechanism induces the devices to feedback their true state information in each time slot (incentive compatibility). The system then operates at the truth-revealing equilibrium.
 3. The resource allocation at the equilibrium point maximizes the system throughput.
 4. The payment is always made from the devices to the BS (budget balance). In other words, the BS does not need to pay the devices to ensure truthful feedback. Moreover, all devices will obtain higher utility when joining the proposed resource allocation mechanism (individual rationality).

3.2 Related Works

Transmission scheduling with renewable energy is a mature research area. In the following, we review some state of the art. Ozel et al. considered data transmission of an energy harvesting node in a wireless fading channel [44]. They studied optimal off-line transmission policies that maximize the throughput and minimize the transmission completion time. They also considered optimal on-line policies solved via stochastic dynamic programming. Near-optimal policies were also proposed with reduced complexity. Ho and Zhang considered energy allocation of point-point wireless communications over a finite horizon with time-varying channel conditions and energy sources [45]. With available side information on the channel conditions and harvested energy, optimal water-filling energy allocation policies were proposed to maximize the throughput. Ju and Zhang studied a wireless powered network where the users first harvest the wireless energy broadcast by the access point in the downlink and then send their independent information to the access point in the uplink [46]. The maximum sum-throughput was shown to be unfair in that substantially more time is allocated to the near users than the far users, of which



the problem was called doubly near-far. They then proposed a common-throughput performance metric with an efficient algorithm to solve the doubly near-far problem. Yang et al. investigated the completion time minimization of data transmission from a energy-harvesting transmitter to two users in a broadcast channel [47]. They proved there exists a cut-off power level: if the optimal total transmit power is lower than this cut-off level, all transmit power is allocated to the stronger user and vice versa. Accordingly, they proposed an algorithm converging to the optimal off-line scheduling policy. Xu and Zhang considered point-to-point data transmission of a transmitter with the time-varying energy constraint and the non-ideal circuit power consumption [48]. To maximize the average throughput over a finite horizon, they first studied the off-line optimal transmit power allocation. They also proposed an on-line algorithm with only the past and present energy state information known at the transmitter.

Energy-aware multicast over fading channels is also a topic that has been thoroughly studied [49]. Ko et al. studied a multi-flow multicast scenario where a BS is capable of sending multiple data flows to multiple multicast groups [43]. Under the assumption of the unknown channel quality information, they proposed a resource allocation mechanism that elicits the true channel quality information from the users and achieves efficient and fair network operation. Chuan et al. investigated resource allocation and scheduling for scalable video multicast [50]. They formulated the problem by maximizing the video quality subject to transmission energy and channel access constraints. Their proposed scheme maximizes the video quality while satisfying the energy budget and channel access constraints. Al-Kanj and Dawy studied multicast resource allocation with bit rate adaptation [51]. By dividing mobile users into groups based on their channel conditions, they formulated the problem as a linear mixed integer programming problem that minimizes the total energy consumption. They proposed a near-optimal polynomial time heuristic algorithm to solve the problem. Kuan et al. proposed an erasure-based broadcast scheme to guarantee reliable broadcast transmission in energy-harvesting networks [52]. They proposed three policies to determine the broadcast period for different performance requirements, balancing the tradeoff between reliability and throughput.

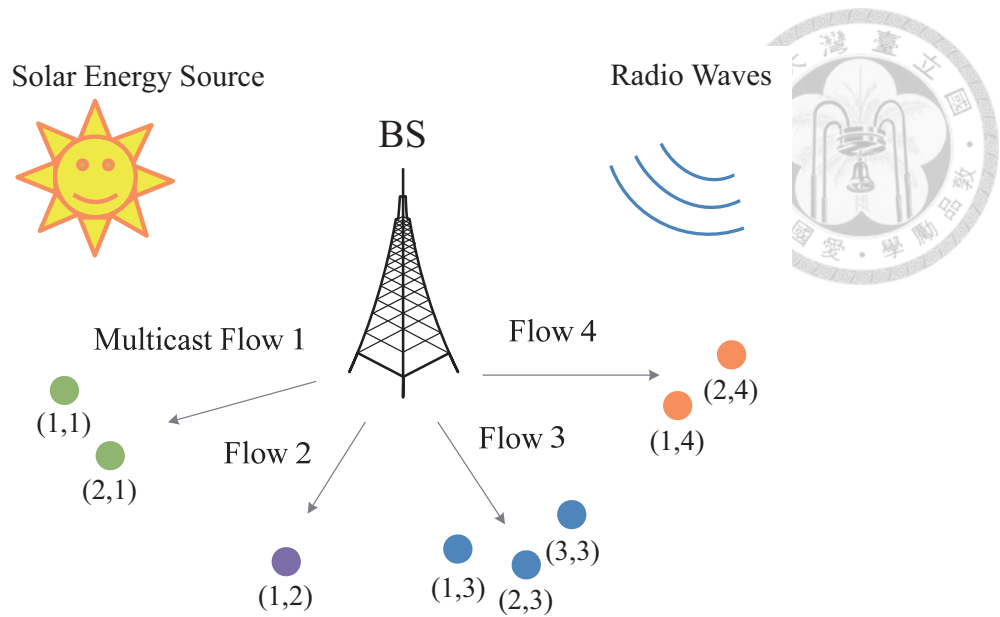
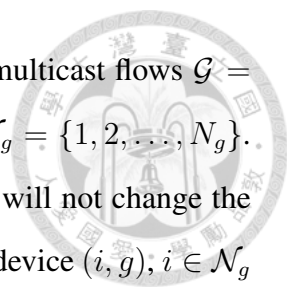


Figure 3.1: System model. The BS provides multiple multicast flows to energy harvesting devices. The energy source can be solar power, radio-frequency (RF) energy, etc. Each device accesses only one flow. Device i accessing flow g is denoted by device (i, g) .

To sum up, the works [44, 45, 48, 52] considered a single transmission flow. Our work differs in that we solve the optimal resource allocation to multiple data transmission flows. Different from [43, 50, 51] that did not consider energy harvesting, this chapter considers renewable energy where the design objective is the best use of renewable energy over time to achieve system efficiency. Moreover, unlike all of these previous works, we further make the practical assumption that devices controlled by rational and selfish users may feedback the false state information to improve their own performance. Such an assumption was considered in our previous work [43] for multi-flow multicast in a one-shot scenario. So in this chapter, by further modelling energy variations and channel fluctuations over time, we design a mechanism that gathers the true state information and accordingly allocates resources to multicast flows to achieve desirable properties.

3.3 System Model

We consider a time-slotted wireless network consisting of a BS and multiple wireless devices, as illustrated in Fig. 3.1. We assume that the BS has fixed power supply and the devices can harvest energy from the environment. The system starts in time slot 0 and



has R resource blocks in each time slot. The BS provides a set of multicast flows $\mathcal{G} = \{1, 2, \dots, G\}$ where each flow g is accessed by a group of devices $\mathcal{N}_g = \{1, 2, \dots, N_g\}$. It is assumed that each device only accesses one multicast flow and will not change the access over time. Thus, each device i accessing flow g is denoted by device (i, g) , $i \in \mathcal{N}_g$ and $g \in \mathcal{G}$. In each time slot $t = 0, 1, 2, \dots$, each multicast flow g is assumed to have constant m_g data packets. This assumption will be relaxed to Markov data sources in Chapter 3.8.2. The BS allocates a_g^t resource blocks to each flow g where one resource block can be used to transmit one packet. The notation $\mathbf{a}^t = (a_g^t)_{g \in \mathcal{G}}$ is used to denote the profile of resource allocation to all flows. The notations $a_g^{\langle t \rangle}$ and $a_g^{\langle q \geq t \rangle}$ are used to denote the resource allocation to flow g in all time t and all time $q \geq t$, respectively. (Without special mention, the use of notation $\langle \cdot \rangle$ in the superscript has the same meaning in the rest of paper.) On the other hand, the devices can harvest energy from the environment. The devices consume energy to receive and decode multicast data¹. We assume that receiving and decoding one packet requires one resource block and consumes one unit of energy.

3.3.1 Types of Multicast Flows

We consider two types of multicast flows: loss-tolerant and loss-sensitive. A loss-tolerant flow means that a device obtains a fixed amount of throughput from each packet received, and the throughput reaches the maximum once the device receives all of the packets. In contrast, A loss-sensitive flow means that a device must receive all of the packets to obtain the maximum throughput; otherwise, it gains nothing. Since the channels are lossy as will be discussed in Chapter 3.3.3, the generalized erasure coding [30, 31] is then applied to control error. Specifically, in each time slot t , the BS applies generalized erasure coding to transform m_g packets of each flow g into a_g^t coded packets (i.e., transmit a_g^t packets in flow g). The data contents can be fully recovered from any m_g out of the coded packets. So if a device receives a sufficient number of the coded packets $j \geq m_g$, it obtains the maximum throughput in both types of data. If a device receives insufficient number of the coded packets $j < m_g$, it obtains j/m_g and zero throughput in the loss-tolerant and

¹The devices also consume energy for other tasks such as feedbacking the state and computing the utility. We will explain later why the energy consumption of these tasks can be negligible.

loss-sensitive types of data, respectively.



3.3.2 Energy Arrivals and Markov Energy States

Each device can harvest energy from the environment to receive and decode multicast data. Each device (i, g) 's energy arrival in each time slot t is modeled by an independent and identically distributed (i.i.d.) discrete random variable $e_{i,g}$ [53, 45].² The harvested energy in time slot t will be ready for use in the next time $(t + 1)$. The energy arrivals of different devices can be correlated and different, which may be related to each device's energy-harvesting environment such as the physical location. The system energy arrivals, i.e., the collection of the energy arrival of each device, in each time slot is denoted by $\mathbf{e} = (e_{i,g})_{i \in \mathcal{N}_g, g \in \mathcal{G}}$. The system energy arrivals other than device (i, g) is denoted by $\mathbf{e}_{-(i,g)} = (e_{j,k})_{j \in \mathcal{N}_k, k \in \mathcal{G}, (j,k) \neq (i,g)}$.

At the beginning of each time t , the energy stored in each device (i, g) is called the energy state and denoted by $es_{i,g}^t \in \mathcal{ES}_{i,g} = \{0, 1, \dots, EC_{i,g}\}$ where $EC_{i,g}$ is the energy capacity. Recall that receiving and decoding one packet requires one resource block and one unit of energy. The relationship of the energy states between any two consecutive time slots is given as follows:

$$es_{i,g}^{t+1} = \min (es_{i,g}^t - \min(es_{i,g}^t, a_g^t) + e_{i,g}, EC_{i,g}), \quad (3.1)$$

where a_g^t is the number of resource blocks allocated to flow g in time slot t . From (3.1), one can note that the energy state has the Markov transition. The energy state transition probability of each device (i, g) is denoted by

$$E_{i,g}(es_{i,g}^{t+1} | es_{i,g}^t, a_g^t). \quad (3.2)$$

The system energy state is denoted by $\mathbf{es}^t = (es_{i,g}^t)_{i \in \mathcal{N}_g, g \in \mathcal{G}}$, with the energy state transi-

²The i.i.d. assumption of the energy arrivals should be reasonable since the duration of a resource block is usually on the order of millisecond, while the energy harvesting process, e.g., solar and wind power, typically remains constant for seconds.

tion probability

$$E(\mathbf{es}^{t+1}|\mathbf{es}^t, \mathbf{a}^t). \quad (3.3)$$

The system energy state other than device (i, g) is denoted by $\mathbf{es}_{-(i,g)}^t = (eS_{j,k}^t)_{j \in \mathcal{N}_k, k \in \mathcal{G}, (j,k) \neq (i,g)}$, with the energy state transition probability

$$E_{-(i,g)}(\mathbf{es}_{-(i,g)}^{t+1}|\mathbf{es}_{-(i,g)}^t, \mathbf{a}^t). \quad (3.4)$$

3.3.3 Fading Channels and Markov Channel States

Transmission through wireless channels suffers from packet loss. To accommodate dynamic channel fading scenarios, we assume that each device experiences the constant channel quality in a time slot, but the channel quality has the Markov transition from one time slot to the next time slot [54, 55]. Specifically, each device (i, g) has the packet success probability, i.e., channel state, $cs_{i,g}^t \in \mathcal{CS}_{i,g}$ in each time slot t where $\mathcal{CS}_{i,g}$ is the set of all possible channel states. The channel state transition probability is given as

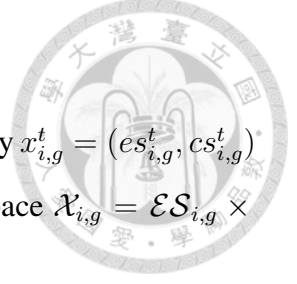
$$C_{i,g}(cs_{i,g}^{t+1}|cs_{i,g}^t). \quad (3.5)$$

The system channel state is denoted by $\mathbf{cs}^t = (cs_{i,g}^t)_{i \in \mathcal{N}_g, g \in \mathcal{G}}$, with the channel state transition probability

$$C(\mathbf{cs}^{t+1}|\mathbf{cs}^t). \quad (3.6)$$

The system channel state other than device (i, g) is denoted by $\mathbf{cs}_{-(i,g)}^t = (cs_{j,k}^t)_{j \in \mathcal{N}_k, k \in \mathcal{G}, (j,k) \neq (i,g)}$, with the channel state transition probability

$$C_{-(i,g)}(\mathbf{cs}_{-(i,g)}^{t+1}|\mathbf{cs}_{-(i,g)}^t). \quad (3.7)$$



3.3.4 Joint States and Information Assumptions

For the ease of notation, the joint energy and channel state is denoted by $x_{i,g}^t = (es_{i,g}^t, cs_{i,g}^t)$ and called the state for short. Note that the state $x_{i,g}^t$ has the state space $\mathcal{X}_{i,g} = \mathcal{E}\mathcal{S}_{i,g} \times \mathcal{C}\mathcal{S}_{i,g}$. From (3.2) and (3.5), the state transition probability is

$$X_{i,g}(x_{i,g}^{t+1}|x_{i,g}^t, a_g^t) = E_{i,g}(es_{i,g}^{t+1}|es_{i,g}^t, a_g^t)C_{i,g}(cs_{i,g}^{t+1}|cs_{i,g}^t). \quad (3.8)$$

The system state in time slot t is denoted by $\mathbf{x}^t = (x_{i,g}^t)_{i \in \mathcal{N}_g, g \in \mathcal{G}}$, with the system state space $\mathcal{X} = \times_{i \in \mathcal{N}_g, g \in \mathcal{G}} \mathcal{X}_{i,g}$ and the system state transition probability

$$X(\mathbf{x}^{t+1}|\mathbf{x}^t, \mathbf{a}^t) = E(\mathbf{es}^{t+1}|\mathbf{es}^t, \mathbf{a}^t)C(\mathbf{cs}^{t+1}|\mathbf{cs}^t). \quad (3.9)$$

The system state other than device (i, g) is denoted by $\mathbf{x}_{-(i,g)}^t = (x_{j,k}^t)_{j \in \mathcal{N}_k, k \in \mathcal{G}, (j,k) \neq (i,g)}$, with the system state space $\mathcal{X}_{-(i,g)} = \times_{j \in \mathcal{N}_k, k \in \mathcal{G}, (j,k) \neq (i,g)} \mathcal{X}_{j,k}$ and the system state transition probability

$$X_{-(i,g)}(\mathbf{x}_{-(i,g)}^{t+1}|\mathbf{x}_{-(i,g)}^t, \mathbf{a}^t) = E_{-(i,g)}(\mathbf{es}_{-(i,g)}^{t+1}|\mathbf{es}_{-(i,g)}^t, \mathbf{a}^t)C_{-(i,g)}(\mathbf{cs}_{-(i,g)}^{t+1}|\mathbf{cs}_{-(i,g)}^t). \quad (3.10)$$

We assume that the BS can measure the energy-harvesting and channel environment to know the system state dynamics $X(\mathbf{x}^{t+1}|\mathbf{x}^t, \mathbf{a}^t)$.³ The BS will also broadcast this information to each device. However, the exact state $x_{i,g}^t$ of each device (i, g) is only known to the device itself. Such an assumption of incomplete state information should be more reasonable than complete state information. The Bayesian update of the state information will be derived in Chapter 3.4.3.

3.3.5 One-Shot and Long-Term Throughput

We assume that each device cares about its own throughput performance. Recall that receiving and decoding one packet requires one resource block and one unit of energy.

³The BS can deploy sensor nodes in the area to measure the energy-harvesting and channel environment to get the system state dynamics.

When the BS transmits a_g^t packets in flow g , device (i, g) will successfully receive j packets, $0 \leq j \leq \min(es_{i,g}^t, a_g^t)$, with probability

$$p(x_{i,g}^t, a_g^t, j) = \binom{\min(es_{i,g}^t, a_g^t)}{j} (cs_{i,g}^t)^j (1 - cs_{i,g}^t)^{\min(es_{i,g}^t, a_g^t) - j}. \quad (3.11)$$

Thus, each device (i, g) 's one-shot throughput in time slot t is given as follows:

Definition 3.1. [One-shot throughput] If flow g is loss-tolerant, the one-shot throughput of device (i, g) in time slot t is

$$v_g(x_{i,g}^t, a_g^t) = \sum_{j=0}^{\min(es_{i,g}^t, a_g^t)} \min(1, \frac{j}{m_g}) p(x_{i,g}^t, a_g^t, j). \quad (3.12)$$

If flow g is loss-sensitive, the one-shot throughput of device (i, g) in time slot t is

$$v_g(x_{i,g}^t, a_g^t) = \begin{cases} \sum_{j=m_g}^{\min(es_{i,g}^t, a_g^t)} p(x_{i,g}^t, a_g^t, j), & a_g^t \geq m_g \\ 0, & \text{otherwise} \end{cases}. \quad (3.13)$$

With the one-shot throughput, we can further define the long-term throughput (or throughput for short). The throughput of each device seen in time slot t is the time-discounted sum of the one-shot throughput in each time slot $q \geq t$.

Definition 3.2. [Throughput] The throughput of device (i, g) seen in time slot t is

$$\sum_{q=t}^{\infty} \beta^{q-t} \mathbb{E} [v_g(x_{i,g}^q, a_g^q)], \quad (3.14)$$

where β , $0 \leq \beta \leq 1$, is the discount factor.

In the following we define the weighted system throughput:

Definition 3.3. [Weighted system throughput] The weighted system throughput seen in time slot t is

$$\sum_{i \in \mathcal{N}_g, g \in \mathcal{G}} \sum_{q=t}^{\infty} \beta^{q-t} w_g \mathbb{E} [v_g(x_{i,g}^q, a_g^q)], \quad (3.15)$$

where w_g is the weight for flow g .

The weight w_g for flow g can be designed as a decreasing function of the number of the devices $|\mathcal{N}_g|$ in flow g . As throughput maximization always brings unfair resource allocation, maximizing the weighted system throughput can balance the throughput performance of devices especially when there are huge differences in the number of devices in different flows. One possible design of the weight is as follows.

Design 3.1. [Flow weight] The flow weight w_g is decreasing with respect to the number of the devices N_g . One simple candidate is

$$w_g = \frac{\log(1 + N_g)}{N_g}. \quad (3.16)$$

3.4 Resource Allocation Problem and Mechanism Design

In the proposed framework, the BS allocates resources to each multicast flow in each time slot. The goal is to maximize the weighted system throughput defined in Definition 3.3. Note that the throughput is a function of the devices' states as shown in (3.15) of Definition 3.3. As the BS has no exact knowledge of the states, the BS may require the devices feedback the states. The devices are controlled by selfish and rational users. They may falsely feedback to manipulate the resource allocation result if doing so increases their own performance. The system throughput performance may become undesirable. Therefore, in this section we design a resource allocation mechanism that can induce truthful feedback from the devices.

The block diagram of the proposed resource allocation mechanism is shown in Fig. 3.2. The proposed resource allocation mechanism first requires the feedback of the states from the devices. Each device will make a feedback strategy that decides how to feedback the state in each time slot. Then we design a resource allocation policy and a pricing policy. The resource allocation policy decides how the BS allocates resources to each multicast flow in each time slot. It is designed to maximize the weighted system throughput. The pricing policy decides how the BS charges each device in each time slot. it is de-

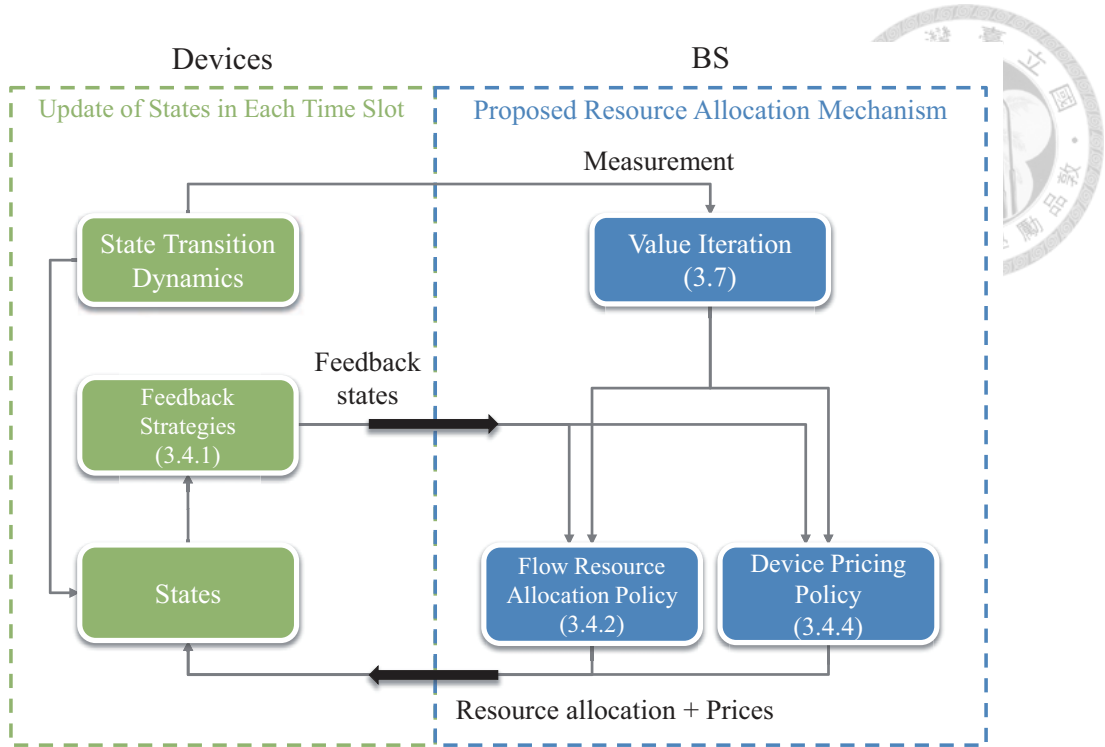


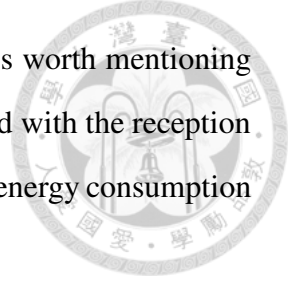
Figure 3.2: The block diagram of the proposed resource allocation mechanism. The detailed designs are specified in each subsection.

signed to ensure truthful feedback from the devices and to achieve several other desirable properties. Also, a value iteration algorithm is proposed to derive the resource allocation policy and the pricing policy. The detailed designs are specified in each subsection.

3.4.1 Feedback Strategies of the Devices

Before the proposed resource allocation mechanism starts, each device (i, g) makes a feedback strategy $s_{i,g} = \hat{x}_{i,g}^{(t)}$ upon which device (i, g) feeds back the state $\hat{x}_{i,g}^t$ in each time slot t . Note that truthful feedback means $\hat{x}_{i,g}^t = x_{i,g}^t$. The collection of all devices' feedback states up to time $(t - 1)$ is called the history in time slot t and denoted by $h^t = \hat{\mathbf{x}}^{(q \leq t-1)}$. The feedback state $\hat{x}_{i,g}^t$ in each time slot t should depend on the history h^t and device (i, g) 's true state $x_{i,g}^t$. In other words, the feedback state should be $\hat{x}_{i,g}^t(h^t, x_{i,g}^t)$. However, we just use $\hat{x}_{i,g}^t$ for the ease of notation in the rest of the paper. The strategy profile of all devices is denoted by $\mathbf{s} = \hat{\mathbf{x}}^{(t)}$ where $\hat{\mathbf{x}}^{(t)} = (\hat{x}_{i,g}^t)_{i \in \mathcal{N}_g, g \in \mathcal{G}}$ is the feedback states of all devices in time slot t . The strategy profile of all devices other than device (i, g) is denoted by $\mathbf{s}_{-(i,g)} = \hat{\mathbf{x}}_{-(i,g)}^{(t)}$ where $\hat{\mathbf{x}}_{-(i,g)}^{(t)} = (\hat{x}_{j,k}^t)_{j \in \mathcal{N}_k, k \in \mathcal{G}, (j,k) \neq (i,g)}$ is the feedback

states of all devices other than device (i, g) in time slot t . Lastly, it is worth mentioning that the feedback of the state information can be a few bits. Compared with the reception and decoding of multicast packets that are on the order of 10^5 bits, the energy consumption for the feedback should be negligible.



3.4.2 Flow Resource Allocation Policy

Since the system has the Markov state transition in (3.9), Markov decision processes [56], which provide a mathematical framework for decision making under uncertainty, will be a powerful tool. We propose a Markov resource allocation policy under which the BS allocates resources according to the feedback of the current state only. To be specific, the proposed resource allocation policy is denoted by $\pi^* = (\pi_g^*)_{g \in \mathcal{G}}$ under which the resource allocation to each flow g is $a_g^t = \pi_g^*(\hat{\mathbf{x}}^t)$, given the current feedback state $\hat{\mathbf{x}}^t$ in each time slot t . The resource allocation policy π^* is designed to maximize the weighted system throughput as follows.

Design 3.2. [Resource allocation policy] The resource allocation policy π^* is designed to maximize the weighted system throughput given any initial system state $\tilde{\mathbf{x}}^0$:

$$\begin{aligned} \pi^* &= \arg \max_{\mathbf{a}^{(t)}} \sum_{i \in \mathcal{N}_g, g \in \mathcal{G}} \sum_{t=0}^{\infty} \beta^t w_g \mathbb{E} [v_g(\tilde{x}_{i,g}^t, a_g^t) | \tilde{\mathbf{x}}^0] \\ s.t. \quad &\sum_{g \in \mathcal{G}} \pi_g^* \leq R, \end{aligned} \quad (3.17)$$

where the system state $\tilde{\mathbf{x}}^t$ satisfies the system state transition probability in (3.9) with $\mathbf{a}^t = \pi^*(\tilde{\mathbf{x}}^t)$.⁴

Given the feedback state $\hat{\mathbf{x}}^t$ in each time slot t , the resource allocation to each multicast flow g is $a_g^t = \pi_g^*(\hat{\mathbf{x}}^t)$.

It is useful to denote the weighted system throughput in (3.17) by the value function

⁴Because of the stationary Markov state transition and stationary throughput function of each device, the optimal policy for this particular maximization problem is indeed stationary and a function of the current state only.

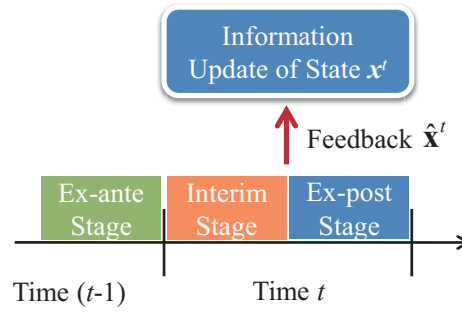


Figure 3.3: Illustration of three different information stages in a time slot. Each time slot can be broken into ex-ante, interim, and ex-post stages according to what information is known at different time instants.

V^* :

$$V^*(\tilde{\mathbf{x}}^0) = \sum_{i \in \mathcal{N}_g, g \in \mathcal{G}} \sum_{t=0}^{\infty} \beta^t w_g \mathbb{E} [v_g(\tilde{x}_{i,g}^t \pi_g^*(\tilde{\mathbf{x}}^t)) | \tilde{\mathbf{x}}^0]. \quad (3.18)$$

For the use in the pricing policy in 3.4.4, it is also useful to denote the weighted system throughput other than device (i, g) by the value function $V_{-(i,g)}^*$. On the other hand, we can also design a resource allocation policy $\pi^{-(i,g)}$ that maximizes the weighted system throughput with device (i, g) excluded from the system in a similar way in Design 3.2. Under $\pi^{-(i,g)}$, we can also denote the weighted system throughput with device (i, g) excluded by $V^{-(i,g)}$. The algorithm for deriving the resource allocation policies and the value functions will be given in Chapter 3.7.

3.4.3 Bayesian Update of the State Information

In the following, we discuss how the BS and each device update the probability mass function (pmf) of the system state $\Delta(\mathbf{x}^t)$ with the feedback state $\hat{\mathbf{x}}^t$ and history h^t . As depicted in Fig. 3.3, each time t can be broken into the ex-ante, interim, and ex-post stages [57] with respect to what information is known to the BS and the devices:

- Ex-ante stage: The system enters the ex-ante stage right before entering time t . The BS knows the pmf $\Delta(\mathbf{x}^t | h^t)$ derived via the state transition probability in (3.9) as



follows:

$$\Delta(\mathbf{x}^t|h^t) = \sum_{\mathbf{x}^{t-1} \in \mathcal{X}} \Delta(\mathbf{x}^{t-1}|h^t) X(\mathbf{x}^t|\mathbf{x}^{t-1}, \pi^*(\hat{\mathbf{x}}^{t-1})). \quad (3.19)$$

where $\Delta(\mathbf{x}^{t-1}|h^t)$ is the pmf of the system state in the ex-post stage of time $(t - 1)$ that will shown in point 3.

Similarly, each device (i, g) knows the pmf $\Delta(\mathbf{x}^t|x_{i,g}^{t-1}, h^t)$ derived as follows:

$$\Delta(\mathbf{x}^t|x_{i,g}^{t-1}, h^t) = \sum_{\mathbf{x}_{-(i,g)}^{t-1} \in \mathcal{X}_{-(i,g)}} \Delta(\mathbf{x}^{t-1}|x_{i,g}^{t-1}, h^t) X(\mathbf{x}^t|\mathbf{x}^{t-1}, \pi^*(\hat{\mathbf{x}}^{t-1})), \quad (3.20)$$

- Interim stage: The system enters the interim stage at the beginning of time t and before each device feedbacks the state. The BS still knows the pmf $\Delta(\mathbf{x}^t|h^t)$ as in the ex-ante stage. Each device (i, g) knows its current state $x_{i,g}^t$ and updates the pmf $\Delta(\mathbf{x}^t|x_{i,g}^t, h^t)$ as follows:

$$\Delta(\mathbf{x}^t|x_{i,g}^t, h^t) = \sum_{\mathbf{x}_{-(i,g)}^{t-1} \in \mathcal{X}_{-(i,g)}} \Delta(\mathbf{x}^{t-1}|x_{i,g}^{t-1}, h^t) X_{-(i,g)}(\mathbf{x}_{-(i,g)}^t|\mathbf{x}_{-(i,g)}^{t-1}, \pi^*(\hat{\mathbf{x}}^{t-1})). \quad (3.21)$$

- Ex-post stage: The system enters the ex-post stage right after each device feedbacks the state. The BS updates the pmf $\Delta(\mathbf{x}^t|h^{t+1})$ by the Bayes' rule as follows:

$$\Delta(\mathbf{x}^t|h^{t+1}) = \frac{\Delta(\mathbf{x}^t|h^t)\Delta(\hat{\mathbf{x}}^t|\mathbf{x}^t, h^t)}{\sum_{\mathbf{x}^t \in \mathcal{X}} \Delta(\mathbf{x}^t|h^t)\Delta(\hat{\mathbf{x}}^t|\mathbf{x}^t, h^t)}. \quad (3.22)$$

Similarly, each device (i, g) updates the pmf $\Delta(\mathbf{x}^t|x_{i,g}^t, h^{t+1})$ as follows:

$$\Delta(\mathbf{x}^t|x_{i,g}^t, h^{t+1}) = \frac{\Delta(\mathbf{x}^t|x_{i,g}^t, h^t)\Delta(\hat{\mathbf{x}}^t|\mathbf{x}^t, h^t)}{\sum_{\mathbf{x}_{-(i,g)}^t \in \mathcal{X}_{-(i,g)}} \Delta(\mathbf{x}_{-(i,g)}^t|h^t)\Delta(\hat{\mathbf{x}}^t|\mathbf{x}_{-(i,g)}^t, h^t)}. \quad (3.23)$$

We will only focus on the ex-post stage, since any properties that are ex-post must be interim and ex-ante as well. So without special mention, the weighted system throughput

defined in Definition 3.3 and everything else that will be defined or designed later are all in the ex-post manner.



3.4.4 Device Pricing Policy

We also propose a pricing policy by which the BS charges each device to ensure truthful feedback and to achieve desirable properties. The basic idea of the proposed pricing policy comes from the Vickrey-Clarke-Groves (VCG) mechanism [58, 59, 60] but we extend it from one shot to multiple time slots.

In each time slot t with the feedbacks state $\hat{\mathbf{x}}^t$, to ensure truthful feedback, the BS pays each device (i, g) the one-shot price $\sum_{j \in \mathcal{N}_k, k \in \mathcal{G}, (j,k) \neq (i,g)} \frac{w_k}{w_g} v_k(\hat{x}_{j,k}^t, \pi_k^*(\hat{\mathbf{x}}^t))$, i.e., the one-shot system throughput other than device (i, g) . To balance the payment, the BS also charges each device the one-shot price

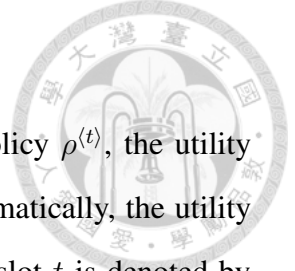
$$\kappa_{i,g}^t(h^t, \hat{\mathbf{x}}^t) = \frac{1}{w_g} \left\{ V^{-(i,g)}(\hat{\mathbf{x}}_{-(i,g)}^t) - \beta \mathbb{E} \left[V^{-(i,g)}(\mathbf{x}_{-(i,g)}^{t+1}) | h^{t+1} \right] \right\}, \quad (3.24)$$

where $h^{t+1} = (h^t, \hat{\mathbf{x}}^t)$. Just as in the VCG mechanism, we want the time discounted sum of $\kappa_{i,g}^t$ to be $V^{-(i,g)}$, i.e., the weighted system throughput with device (i, g) excluded from the system. However, directly using the VCG mechanism to charge the one-shot system throughput with device (i, g) excluded from the system, $\sum_{j \in \mathcal{N}_k, k \in \mathcal{G}, (j,k) \neq (i,g)} \frac{w_k}{w_g} v_k(\hat{x}_{j,k}^t, \pi_k^{-(i,g)}(\hat{\mathbf{x}}_{-(i,g)}^t))$, cannot make the time discounted sum equal to $V^{-(i,g)}$. Therefore, we find another way to decompose $V^{-(i,g)}$ in time into $\kappa_{i,g}^t$ in (3.24). As will be shown in Lemma 3.1, the time discounted sum of $\kappa_{i,g}^t$ is indeed $V^{-(i,g)}$. Therefore, the overall pricing policy denoted by $\rho^{(t)} = (\rho_{i,g}^{(t)})_{i \in \mathcal{N}_g, g \in \mathcal{G}}$ is designed as follows:

Design 3.3. [Pricing policy] The one-shot price the BS charges each device (i, g) in time slot t is

$$\rho_{i,g}^t(h^t, \hat{\mathbf{x}}^t) = - \sum_{j \in \mathcal{N}_k, k \in \mathcal{G}, (j,k) \neq (i,g)} \frac{w_k}{w_g} v_k(\hat{x}_{j,k}^t, \pi_k^*(\hat{\mathbf{x}}^t)) + \kappa_{i,g}^t(h^t, \hat{\mathbf{x}}^t), \quad (3.25)$$

where $\kappa_{i,g}^t$ is given in (3.24).



3.4.5 Ex-Post Utility of the Devices

With the proposed resource allocation policy π^* and the pricing policy $\rho^{(t)}$, the utility of each device is defined as the throughput minus the price. Mathematically, the utility function of each device (i, g) after the feedback history h^t in time slot t is denoted by $u_{i,g}(\mathbf{s}|x_{i,g}^t, h^{t+1})$:

Definition 3.4. [Ex-post utility] In each time slot t , the utility of device (i, g) is

$$u_{i,g}(\mathbf{s}|x_{i,g}^t, h^{t+1}) = \sum_{q=t}^{\infty} \beta^{q-t} \mathbb{E} [v_g(x_{i,g}^q, \pi_g^*(\hat{\mathbf{x}}^q)) - \rho_{i,g}^q(h^q, \hat{\mathbf{x}}^q)|x_{i,g}^t, h^{t+1}], \quad (3.26)$$

where $h^{t+1} = (h^t, \hat{\mathbf{x}}^t)$.

3.5 Resource Allocation Game

In the proposed resource allocation mechanism, each device feedbacks the state information to maximize its own utility. Since the state transition is Markov and the exact states are only known to the devices themselves, the devices' decision making can be formulated as a stochastic game with incomplete information [61]. The induced resource allocation game is denoted by $G = (\mathcal{N}, \mathbf{x}^{(t)}, \mathbf{s}, X, \mathcal{S}, \mathbf{u})$ where each component is specified as below:

- Player set \mathcal{N} : Each device $(i, g) \in \mathcal{N} = \mathcal{N}_g \times \mathcal{G}$ is a player in the game.
- State profile $\mathbf{x}^{(t)}$: Each device (i, g) 's state $x_{i,g}^t$ in time slot t is only known to itself. The state information is updated after feedback in each time slot as shown in Chapter 3.4.3.
- Strategy profile \mathbf{s} : Each device (i, g) has a strategy $s_{i,g} = \hat{x}_{i,g}^{(t)}$ that feedbacks the state $\hat{x}_{i,g}^t$ in each time slot t . The strategy profile is $\mathbf{s} = \hat{\mathbf{x}}^{(t)}$.
- State transition probability X : Derived from (3.9), the state transition probability under the proposed resource allocation policy π^* is $\mathbf{X}(\mathbf{x}^{t+1}|\mathbf{x}^t, \pi^*(\hat{\mathbf{x}}^t))$. We have assumed that the state transition probability is known to the BS and each device.

- Utility profile \mathbf{u} : Each device (i, g) has the utility function $u_{i,g}$ as shown in Definition 3.4. The utility profile is $\mathbf{u} = (u_{i,g})_{i \in \mathcal{N}_g, g \in \mathcal{G}}$.

We will use the solution concept "perfect ex-post equilibrium" to analyze the proposed resource allocation game. A perfect ex-post equilibrium is a refinement of a subgame perfect equilibrium [62] where the strategies form an ex-post equilibrium in any subgame. It is a stronger solution concept than Bayesian equilibrium and Nash equilibrium that require Bayesian and complete information, respectively. The formal definition of a perfect ex-post equilibrium is given as follows:

Definition 3.5. [*Perfect ex-post equilibrium*] The strategy profile \mathbf{s}^* is a perfect ex-post equilibrium if

$$u_{i,g}(\mathbf{s}^* | x_{i,g}^t, h^{t+1}) \geq u_{i,g}(s_{i,g}, \mathbf{s}_{-(i,g)}^* | x_{i,g}^t, h^{t+1}) \quad \forall (i, g), t, \mathbf{x}^t, h^t, m, s_{i,g} \neq s_{i,g}^*. \quad (3.27)$$

It is well-known that a strategy profile is a subgame perfect equilibrium if and only if there are no profitable one-shot deviations. The definitions of one-shot deviation strategy and the one-shot deviation principle [63, 64] for the proposed resource allocation game are given as follows:

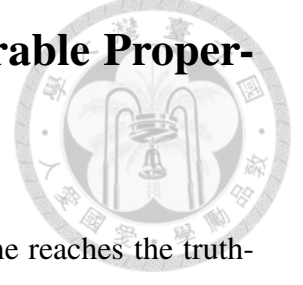
Definition 3.6. [*One-shot deviation strategy*] A strategy $s'_{i,g} = \hat{x}_{i,g}^{t,(q)}$ is a one-shot deviation from another strategy $s_{i,g} = \hat{x}_{i,g}^{(q)}$ after some history h^t in time slot t if $\hat{x}_{i,g}^{t,(q)} \neq \hat{x}_{i,g}^t$ and $\hat{x}_{i,g}^{t,(q)} = \hat{x}_{i,g}^q \quad \forall q > t$.

Definition 3.7. [*One-shot deviation principle*] The strategy profile \mathbf{s}^* is a perfect ex-post equilibrium if and only if

$$u_{i,g}(\mathbf{s}^* | x_{i,g}^t, h^{t+1}) \geq u_{i,g}(s_{i,g}, \mathbf{s}_{-(i,g)}^* | x_{i,g}^t, h^{t+1}) \quad \forall (i, g), t, \mathbf{x}^t, h^t, s_{i,g} \quad (3.28)$$

where $s_{i,g}$ is any one-shot deviation strategy from $s_{i,g}^*$ after history h^t .

3.6 Truth-Revealing Equilibrium and Desirable Properties



We prove in Theorem 3.1 that the proposed resource allocation game reaches the truth-revealing perfect ex-post equilibrium $\mathbf{s}^* = \mathbf{x}^{(t)}$. The proposed resource allocation mechanism is then called ex-post incentive compatible. Before that we first show the following lemma about $\kappa_{i,g}^t$ that will be used in the proof for Theorem 3.1.

Lemma 3.1. *Given any strategy $s_{i,g} = \hat{x}_{i,g}^{(q \geq t)}$ of device (i, g) and the truthful feedback strategies $\mathbf{s}_{-(i,g)}^* = \mathbf{x}_{-(i,g)}^{(q \geq t)}$ of the other devices after any history h^t , the time discounted sum of $\kappa_{i,g}^t$ is*

$$\sum_{q=t}^{\infty} \beta^{q-t} \mathbb{E} \left[\kappa_{i,g}^q(h^q, \hat{x}_{i,g}^q, \mathbf{x}_{-(i,g)}^q) | h^{t+1} \right] = \frac{1}{w_g} V^{-(i,g)}(\mathbf{x}_{-(i,g)}^t), \quad (3.29)$$

where $h^{q+1} = (h^q, \hat{x}_{i,g}^q, \mathbf{x}_{-(i,g)}^q) \forall q \geq t$.

Proof. From (3.24), we know $\forall q \geq t$

$$\begin{aligned} \beta^{q-t} \mathbb{E} \left[\kappa_{i,g}^q(h^q, \hat{x}_{i,g}^q, \mathbf{x}_{-(i,g)}^q) | h^{t+1} \right] &= \frac{1}{w_g} \beta^{q-t} \mathbb{E} \left[V^{-(i,g)}(\mathbf{x}_{-(i,g)}^q) | h^{t+1} \right] \\ &\quad - \frac{1}{w_g} \beta^{q+1-t} \mathbb{E} \left[V^{-(i,g)}(\mathbf{x}_{-(i,g)}^{q+1}) | h^{t+1} \right], \end{aligned} \quad (3.30)$$

where $\mathbb{E} \left[V^{-(i,g)}(\mathbf{x}_{-(i,g)}^t) | h^{t+1} \right] = V^{-(i,g)}(\mathbf{x}_{-(i,g)}^t)$. Therefore, (3.29) can be easily derived by summing (3.30) $\forall q \geq t$. \square

Theorem 3.1. *[Ex-post incentive compatibility] The proposed resource allocation mechanism is ex-post incentive compatible. That is, the proposed game reaches the truth-revealing perfect ex-post equilibrium $\mathbf{s}^* = \mathbf{x}^{(t)}$.*

Proof. The proof follows the one-shot deviation principle. Given $\mathbf{s}_{-(i,g)}^* = \mathbf{x}_{-(i,g)}^{(q \geq t)}$ after any history h^t , we show that $s_{i,g}^* = x_{i,g}^{(q \geq t)}$ always brings higher utility than any one-shot deviation strategy.

From (3.26) and (3.25), each device (i, g) 's utility after history h^t under the truth-revealing strategy profile $\mathbf{s}^* = \mathbf{x}^{(q \geq t)}$ is

$$\begin{aligned} u_{i,g}(\mathbf{s}^* | x_{i,g}^t, h^{t+1}) &= \sum_{q=t}^{\infty} \beta^{q-t} \mathbb{E} \left[\sum_{j \in \mathcal{N}_k, k \in \mathcal{G}} \frac{w_k}{w_g} v_k(x_{j,k}^q, \pi_k^*(\mathbf{x}^q)) - \kappa_{i,g}^q(h^q, \mathbf{x}^q) | h^t, \mathbf{x}^t \right] \\ &= \frac{1}{w_g} [V^*(\mathbf{x}^t) - V^{-(i,g)}(\mathbf{x}_{-(i,g)}^t)], \end{aligned} \quad (3.31)$$

where the last equality comes from (3.18) and Lemma 3.1. If device (i, g) plays any one-shot deviation strategy $s_{i,g} = (\hat{x}_{i,g}^t, x_{i,g}^{(q > t)})$ that only deviates after history h^t in time slot t , its utility becomes

$$u_{i,g}(s_{i,g}, \mathbf{s}_{-(i,g)}^* | x_{i,g}^t, h^{t+1}) = \frac{1}{w_g} [V'(\mathbf{x}^t) - V^{-(i,g)}(\mathbf{x}_{-(i,g)}^t)], \quad (3.32)$$

where

$$V'(\mathbf{x}^t) = \sum_{j \in \mathcal{N}_k, k \in \mathcal{G}} \left\{ w_k v_k(x_{j,k}^t, \pi_k^*(\hat{x}_{i,g}^t, \mathbf{x}_{-(i,g)}^t)) + \sum_{q=t+1}^{\infty} \beta^{q-t} w_k \mathbb{E} [v_k(x_{j,k}^q, \pi_k^*(\mathbf{x}^q)) | \mathbf{x}^t] \right\}. \quad (3.33)$$

According to (3.17) and (3.18), since $\mathbf{a}^q = \pi^*(\mathbf{x}^q) \forall q \geq t$ maximizes the weighted system throughput, we know $V^*(\mathbf{x}^t) \geq V'(\mathbf{x}^t)$. Therefore, $u_{i,g}(\mathbf{s}^* | x_{i,g}^t, h^{t+1}) \geq u_{i,g}(s_{i,g}, \mathbf{s}_{-(i,g)}^* | x_{i,g}^t, h^{t+1}) \forall (i, g), t, \mathbf{x}^t, h^t$. In other words, the proposed resource allocation game has the truth-revealing perfect ex-post equilibrium $\mathbf{s}^* = \mathbf{x}^{(t)}$. The proposed resource allocation mechanism is ex-post incentive compatible. \square

Theorem 3.1 means that the proposed resource allocation mechanism allows the system to reach the equilibrium point where the BS always collects the true state information from the devices in each time slot. The equilibrium is perfect in that if each device is allowed to change a feedback strategy in each time slot, each device still always feeds back the true state information. The equilibrium is also ex-post in that after the true state information is revealed in the ex-post stage of each time slot, each device will not regret the strategy it has made before the proposed resource allocation mechanism starts.



In the following propositions, we show the resource allocation, the history, and the state information at the truth-revealing equilibrium.

Proposition 3.1. [Equilibrium resource allocation] *The equilibrium resource allocation to flow g in time slot t is $a_g^{*,t} = \pi_g^*(\mathbf{x}^t)$.*

Proposition 3.2. [Equilibrium history and state information] *The equilibrium history in time slot t is $h^{*,t} = \mathbf{x}^{(q \leq t-1)}$. In the ex-post stage of time t , the BS and each device knows the exact state \mathbf{x}^t .*

Since the states have the Markov transition, Proposition 3.2 implies that once the true state \mathbf{x}^t is revealed in each time slot t , the BS and each device only need to memorize \mathbf{x}^t . No need to memorize the history $h^{*,t}$ at all. At the truth-revealing equilibrium, the BS and each device can also easily compute the prices and the utility given in Propositions 3.3 and 3.4, respectively. Since each device's computation of the utility is quite simple at the truth-revealing equilibrium, the energy consumption for the computation should be negligible compared with the reception and decoding of multicast packets.

Proposition 3.3. [Equilibrium price] *The (long-term) equilibrium price seen in time slot t is*

$$\sum_{q=t}^{\infty} \beta^{q-t} \mathbb{E} [\rho_{i,g}^{*,q} | \mathbf{x}^t] = \frac{1}{w_g} [-V_{-(i,g)}^*(\mathbf{x}^t) + V^{-(i,g)}(\mathbf{x}_{-(i,g)}^t)] \quad (3.34)$$

where $\rho_{i,g}^{*,q} = \rho_{i,g}^q(h^{*,q}, \mathbf{x}^q)$.

Proof. From (3.25), we have

$$\begin{aligned} \sum_{q=t}^{\infty} \beta^{q-t} \mathbb{E} [\rho_{i,g}^{*,q} | \mathbf{x}^t] &= - \sum_{q=t}^{\infty} \beta^{q-t} \sum_{\substack{(j,k) \neq (i,g) \\ j \in \mathcal{N}_k, k \in \mathcal{G}}} \frac{w_k}{w_g} \mathbb{E} [v_k(\hat{x}_{j,k}^q, \pi_k^*(\mathbf{x}^q)) | \mathbf{x}^t] \\ &\quad + \sum_{q=t}^{\infty} \beta^{q-t} \mathbb{E} [\kappa_{i,g}^q(h^{*,q}, \mathbf{x}^q) | \mathbf{x}^t] \\ &= \frac{1}{w_g} [-V_{-(i,g)}^*(\mathbf{x}^t) + V^{-(i,g)}(\mathbf{x}_{-(i,g)}^t)], \end{aligned} \quad (3.35)$$

where in the last equality the first term comes from the definition of $V_{-(i,g)}^*$ and the second term comes from Lemma 3.1. □

Proposition 3.4. [Ex-post equilibrium utility] *The equilibrium utility of each device (i, g) seen in time slot t is*

$$u_{i,g}(\mathbf{s}^* | x_{i,g}^t, h^{*,t+1}) = \frac{1}{w_g} [V^*(\mathbf{x}^t) - V_{-(i,g)}^-(\mathbf{x}_{-(i,g)}^t)]. \quad (3.36)$$

In addition to the property of truth-revelation, the proposed resource allocation mechanism also achieves several desirable properties, including maximum weighted system throughput, budget balance, and individual rationality, all in the ex-post manner [34]. Maximum weighted system throughput means that the equilibrium resource allocation is the most efficient since no other allocation can achieve greater weighted system throughput.

Theorem 3.2. [Maximum weighted ex-post system throughput] *The proposed resource allocation mechanism achieves maximum weighted system throughput.*

$$\pi^* = \arg \max_{\mathbf{a}^{(q \geq t)}} \sum_{i \in \mathcal{N}_g, g \in \mathcal{G}} \sum_{q=t}^{\infty} \beta^{q-t} w_g \mathbb{E} [v_g(x_{i,g}^q, a_g^t) | \mathbf{x}^t]. \quad (3.37)$$

Proof. Recall in Design 3.2 that the proposed resource allocation policy π^* is designed to maximize the weighted system throughput. Therefore, the proof follows Design 3.2 and Theorem 3.1. □

Budget balance means that the net payment is always from the devices to the BS, but not from the BS to the devices. This property is desirable in that the BS does not need to pay the devices to ensure truthful feedback [34]. We show that the proposed resource allocation mechanism achieves ex-post budget balance.

Theorem 3.3. [Ex-Post Budget balance] *The proposed resource allocation mechanism is ex-post budget-balanced.*

$$\sum_{i \in \mathcal{N}_g, g \in \mathcal{G}} \sum_{q=t}^{\infty} \beta^{q-t} \mathbb{E} [\rho_{i,g}^{*,q} | \mathbf{x}^t] \geq 0 \quad (3.38)$$

Proof. Since $\pi^{-(i,g)}$ maximizes the weighted system throughput with device (i, g) excluded from the system, we know

$$V^{-(i,g)}(\mathbf{x}_{-(i,g)}^t) \geq V_{-(i,g)}^*(\mathbf{x}^t). \quad (3.39)$$

Therefore, (3.38) is a direct result from (3.34) and (3.39). \square

Lastly, individual rationality is also important in mechanism design. While devices can decide to join a mechanism or not, individual rationality means that all devices are willing to join to obtain as much utility as without joining. We show that the proposed resource allocation mechanism achieves ex-post individual rationality.

Theorem 3.4. [*Ex-Post Individual rationality*] *The proposed resource allocation mechanism is ex-post individual rational.*

$$u_{i,g}(\mathbf{s}^* | x_{i,g}^t, h^{*,t+1}) \geq 0 \quad \forall i \in \mathcal{N}_g, g \in \mathcal{G}. \quad (3.40)$$

Proof. Since π^* maximizes the weighted system throughput, we know

$$V^*(\mathbf{x}^t) \geq V^{-(i,g)}(\mathbf{x}_{-(i,g)}^t). \quad (3.41)$$

Therefore, from (3.36) and (3.41), we know (3.40) must hold. \square

To sum up, the proposed resource allocation mechanism is ex-post incentive compatible that reaches the truth-revealing perfect ex-post equilibrium. At the truth-revealing equilibrium, the proposed resource allocation mechanism also achieves maximum weighted ex-post system throughput, ex-post budget balance, and ex-post individual rationality.

3.7 Value Iteration for the Resource Allocation Policy

Recall in Design 3.2 and Theorem 3.2 that the proposed resource allocation policy π^* maximizes the weighted system throughput at the truth-revealing equilibrium. Since the proposed resource allocation policy and the state transition are both Markov, the resource



Algorithm 3.1: Value iteration algorithm for multicast resource allocation

- 1: Initialize $V^*(\mathbf{x}) \forall \mathbf{x}$.
 - 2: Repeat
 - 3: $\delta \leftarrow 0$
 - 4: For each \mathbf{x}
 - 5: $v \leftarrow V^*(\mathbf{x})$
 - 6: $V^*(\mathbf{x}) \leftarrow \max_{\mathbf{a}} \left\{ \sum_{i \in \mathcal{N}_g, g \in \mathcal{N}_g} w_g v_g(x_{i,g}, a_g) + \beta \sum_{\mathbf{x}' \in \mathcal{X}} X(\mathbf{x}' | \mathbf{x}, \mathbf{a}) V^*(\mathbf{x}') \right\}$
 - 7: $\delta \leftarrow \max(\delta, |v - V^*(\mathbf{x})|)$
 - 8: Until $\delta < \epsilon$ (a small positive number)
 - 9: Output the value function V^* and the policy π^*
 - 10: $\pi^*(\mathbf{x}) = \arg \max_{\mathbf{a}} \left\{ \sum_{i \in \mathcal{N}_g, g \in \mathcal{N}_g} w_g v_g(x_{i,g}, a_g) + \beta \sum_{\mathbf{x}' \in \mathcal{X}} X(\mathbf{x}' | \mathbf{x}, \mathbf{a}) V^*(\mathbf{x}') \right\}$
-

allocation problem is essentially a Markov decision process. Recall in (3.18) that the value function V^* represents the weighted system throughput under the resource allocation policy π^* . We may also express V^* in a recursive form as follows:

$$V^*(\mathbf{x}) = \max_{\mathbf{a}} \left\{ \sum_{i \in \mathcal{N}_g, g \in \mathcal{G}} w_g v_g(x_{i,g}, a_g) + \beta \sum_{\mathbf{x}' \in \mathcal{X}} X(\mathbf{x}' | \mathbf{x}, \mathbf{a}) V^*(\mathbf{x}') \right\}. \quad (3.42)$$

Equation (3.42) is usually referred to as the Bellman equation. There are several algorithms for solving the Bellman equation. One of the most widely used is value iteration due to its many advantages, such as quick convergence and easy implementation, especially when the state space is very large [65]. The value iteration algorithm for deriving the resource allocation policy π^* and the value function V^* is given in Algorithm 3.1. It involves the arbitrary initialization of the value function V^* (line 1) and the iterative update of the value function according to the Bellman equation in (3.42) (lines 2 to 7). We may also update the value function $V_{-(i,g)}^*$ at the same time in lines 1 to 7. The update process repeats until the convergence criterion is met, i.e., the update error δ is less than the specified error tolerance ϵ (line 8). Lastly, the value iteration algorithm outputs the desirable value function V^* and the resource allocation policy π^* (lines 9 and 10). The same value iteration algorithm can also be used to derive the resource allocation policy $\pi^{-(i,g)}$ and $V^{-(i,g)}$, respectively.

To derive the optimal solutions via the value iteration algorithm, the number of iterations is $Poly(|\mathcal{X}|^{\sum_{g \in \mathcal{G}} |\mathcal{N}_g|}, |\mathcal{A}|, \frac{1}{1-\beta})$ and the worst-case computational complexity per

iteration is $O(|\mathcal{X}|^{2\sum_{g \in \mathcal{G}} |\mathcal{N}_g|} |\mathcal{A}|)$ where $|\mathcal{A}|$ is the number of possible resource allocation [66].



3.8 Further Discussions

3.8.1 Feedback per n Time Slots

As the proposed resource allocation mechanism requires each device to feedback the state information, signaling overhead may be a concern. To reduce the signaling overhead, we may allow each device to feedback the state information per n time slots where $n = 2, 3, 4, \dots$. In this case, the resource allocation policy becomes $\pi^{*,(0 \leq q \leq n-1)}$ that decides the resource allocation $a_g^{nt+q} = \pi_{i,g}^{*,q}(\hat{\mathbf{x}}^{nt})$ to each flow g in time slot $(nt + q)$ given the feedback state $\hat{\mathbf{x}}^{nt}$ in time slot nt . In other words, the resource allocation in time slot $(nt + q)$ depends on the feedback state information in time slot nt . The resource allocation policy is now designed to maximize the weighted system throughput

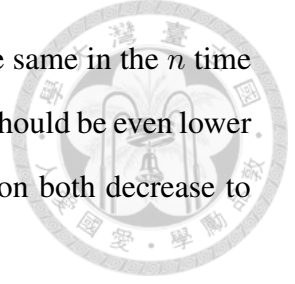
$$V^{*,n}(\mathbf{x}^0) = \max_{\mathbf{a}^{(0 \leq q \leq n-1)}} \left\{ \sum_{i \in \mathcal{N}_g, g \in \mathcal{G}} \sum_{q=0}^{n-1} \beta^q w_g \mathbb{E} [v_g(x_{i,g}^q, a_g^q) | \mathbf{x}^0] + \beta^n \sum_{\mathbf{x}^n \in \mathcal{X}} X^n(\mathbf{x}^n | \mathbf{x}^0, \mathbf{a}^{(0 \leq q \leq n-1)}) V^{*,n}(\mathbf{x}^n) \right\}, \quad (3.43)$$

where $X^n(\mathbf{x}^n | \mathbf{x}^0, \mathbf{a}^{(0 \leq q \leq n-1)})$ is the n -step transition probability satisfying

$$X^n(\mathbf{x}^n | \mathbf{x}^0, \mathbf{a}^{(0 \leq q \leq n-1)}) = \sum_{\mathbf{x}^1, \dots, \mathbf{x}^{n-1} \in \mathcal{X}} \prod_{q=1}^n X(\mathbf{x}^q | \mathbf{x}^{q-1}, \mathbf{a}^{q-1}). \quad (3.44)$$

Comparing (3.42) and (3.43), we know $V^*(\mathbf{x}) \geq V^{*,n}(\mathbf{x})$, i.e., the system throughput is lower under feedback per n time slots. Moreover, to solve the Bellman equation via the value iteration algorithm, the number of iterations becomes $\text{Poly}(|\mathcal{X}|^{\sum_{g \in \mathcal{G}} |\mathcal{N}_g|}, |\mathcal{A}|^n, \frac{1}{1-\beta^n})$ but each iteration becomes more costly with the time complexity $O(|\mathcal{X}|^{2\sum_{g \in \mathcal{G}} |\mathcal{N}_g|} |\mathcal{A}|^n)$. In other words, reducing the signaling overhead may bring the trade-off of lower system throughput and higher time complexity of the value iteration algorithm. To further reduce

the time complexity, we can restrict that the resource allocation is the same in the n time slots, i.e., $\mathbf{a}^0 = \mathbf{a}^1 = \dots = \mathbf{a}^{n-1}$. In this way, the system throughput should be even lower but the number of iterations and the time complexity of each iteration both decrease to $Poly(|\mathcal{X}|^{\sum_{g \in \mathcal{G}} |\mathcal{N}_g|}, |\mathcal{A}|, \frac{1}{1-\beta^n})$ and $O(|\mathcal{X}|^{2\sum_{g \in \mathcal{G}} |\mathcal{N}_g|} |\mathcal{A}|)$, respectively.



3.8.2 Markov Data Sources

So far in this chapter, we have assumed that each flow g has the constant m_g data packets in each time slot t . We may use the Markov data model, assuming that each flow g has m_g^t data packets in time slot t and the data packets satisfy the transition probability $M_g(m_g^{t+1}|m_g^t)$ [67]. We also assume that the data information is known to the BS and also made public to each device. In this Markov data model, the one-shot throughput of each device (i, g) becomes $v_g(x_{i,g}^t, m_g^t, a_g^t)$ that is the same as $v_g(x_{i,g}^t, a_g^t)$ in Definition 3.1, but with m_g replaced by m_g^t . Then the proposed resource allocation mechanism in Chapter 3.4 can be applied. The optimal resource allocation policy becomes $\pi^*(\mathbf{x}^t, \mathbf{m}^t)$ that is a function of the state \mathbf{x}^t and data \mathbf{m}^t in each time slot t . With the extensions above, the proposed resource allocation mechanism can be shown to achieve the truth-revealing equilibrium along with all other desirable properties as in Chapter 3.6. Since the proofs are quite similar, we will not repeat them here.

3.9 Numerical Results

In this section, numerical results are presented to evaluate the proposed resource allocation mechanism. The parameter setting is given as follows: We randomly generate 10 devices and 2 loss-tolerant flows where flow 1 contains 3 devices and flow 2 contains 7 devices. The BS is scheduled to provide one resource block in each time slot, $R = 1$. Each device has the i.i.d. Bernoulli energy arrivals $e_{i,g}$ in each time slot with mean uniformly generated from $[0, 1]$. The energy capacity of each device is 1 unit of energy, $EC_{i,g} = 1$. The wireless channel has two states, $cs_{i,g} = 1, 2$, where 1 means "bad" with packet success probability 0.4 and 2 means "good" with packet success probability 0.8.

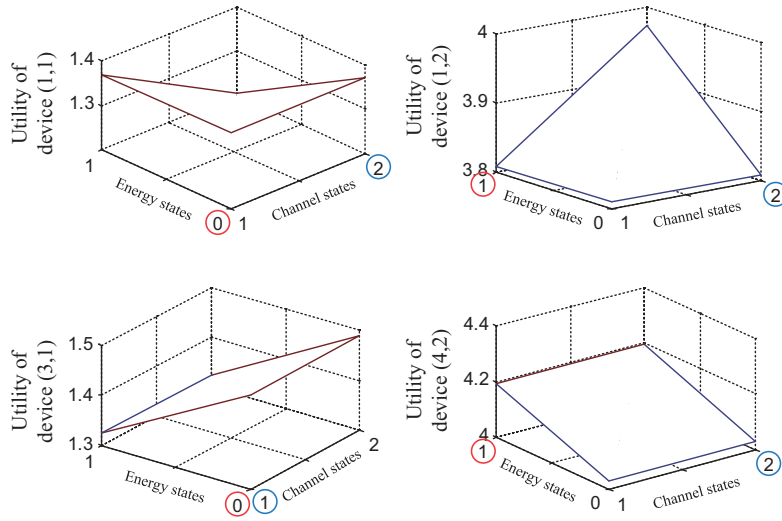
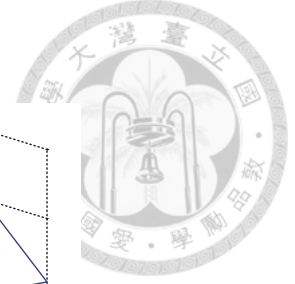


Figure 3.4: The utility of each device in all possible feedback states.

The channel state transition probabilities of each device from state 1 to state 1 and state 2 to state 2 are uniformly generated from $[0, 1]$, respectively. We randomly assign initial energy state $es_{i,g}^0$ and channel state $cs_{i,g}^0$ to each device. The discount factor is $\beta = 0.9$ and the threshold for the value iteration algorithm is $\epsilon = 10^{-6}$. The results are plotted for a single network instance if not specially mentioned.

We first verify the property of truth-revelation. Fig. 3.4 shows the utility of 4 randomly selected devices (2 devices in flow 1 and 2 devices in flow 2) in all possible feedback states in time slot 0. It can be seen that each device always achieves the maximum utility in the true energy and channel states (the circled ones). This is true in each time slot. In other words, the devices will always feedback the true state in each time slot. The proposed resource allocation mechanism then ensures perfect ex-post incentive compatibility. We also verify the properties of budget balance and individual rationality. In Fig. 3.5(a), the net payment from the devices to the BS is greater than zero. Similarly, in Fig. 3.5(b), the utility of each device is always greater than zero. Hence, the proposed resource allocation is both ex-post budget balanced and ex-post individual rational.

In Fig. 3.6, to evaluate the weighted system throughput, we compare the proposed resource allocation mechanism with the other schemes, including the greedy scheme, the

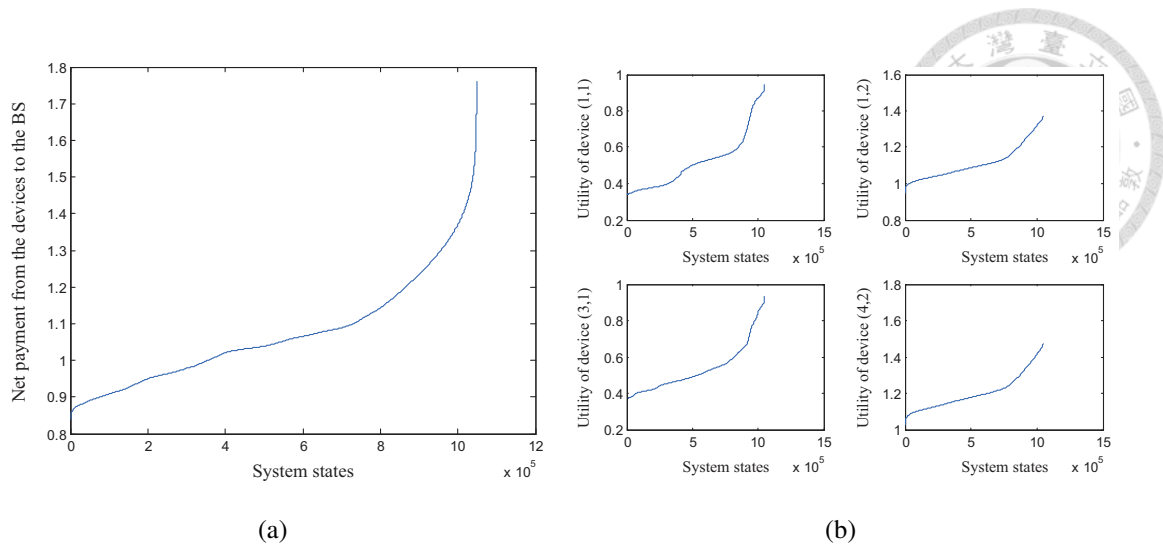


Figure 3.5: Budget balance and individual rationality: (a) The net payment from the devices to the BS in all system states. (b) The utility of each device in all system states.

random scheme, and the partial feedback schemes that collect the feedback of energy states or channel states, but not both. The greedy scheme allocates resources assuming that each device greedily feedbacks the highest energy state and "good" channel state in each time slot. The random scheme allocates resource randomly in each time slot (The results of the random scheme are averaged over 10 runs). Both greedy and random schemes do not collect the feedback information from the devices. It can be seen in Fig. 3.6(a) that the proposed resource allocation mechanism always outperforms the other schemes. This is because the proposed resource allocation mechanism collects the true feedback states and allocates resources in the most efficient way. The two partial feedback schemes outperform the greedy and random schemes that do not collect the feedback information. The partial feedback scheme that collects the feedback of the energy states has better performance since the energy states are affected by the resource allocation and it would be better to know the energy states, instead of the channel states. The random scheme outperforms the greedy scheme. This is because in the random scheme each flow has equal opportunities to gain resources, but in the greedy scheme only one specific flow can gain resources. Thus, the random scheme has better performance.

The discount factor is also varied $\beta = 0, 0.4, 0.8, 0.9, 0.95$ to investigate its impact on the weighted system throughput. Fig. 3.6(b) shows that the weighted system throughput gets higher when the discount factor β increases. We can foresee this result as higher β

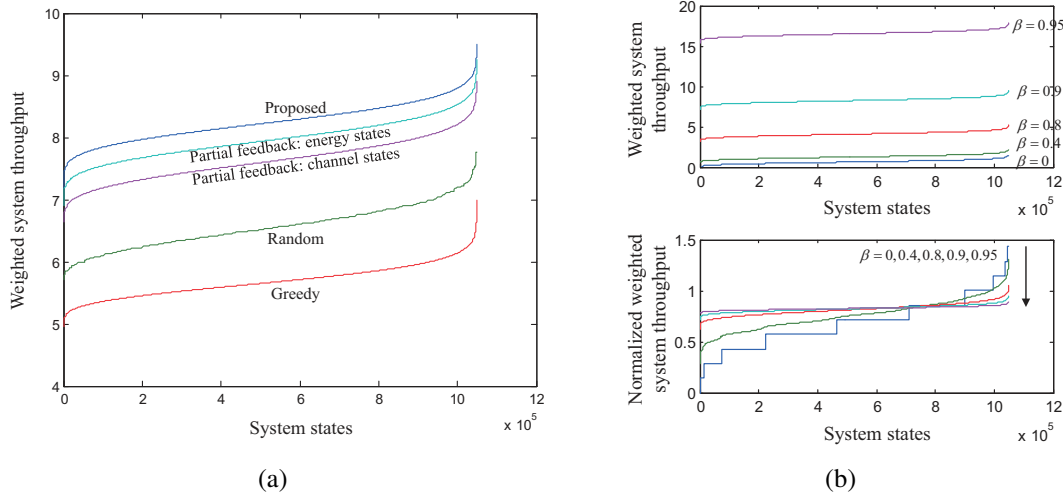
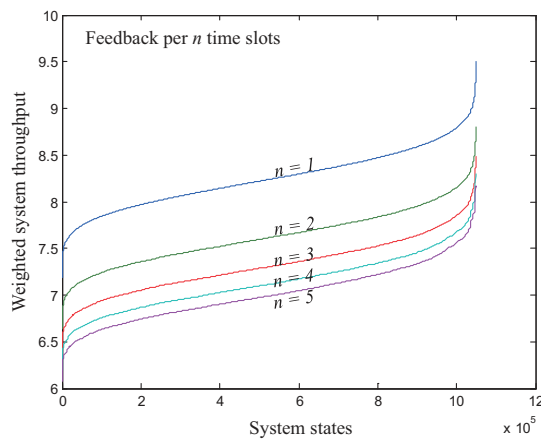


Figure 3.6: Performance comparison in the system throughput: (a) The weighted system throughput of the proposed resource allocation mechanism, and other schemes. (b) The weighted system throughput of the proposed resource allocation mechanism with different values of the discount factor β .

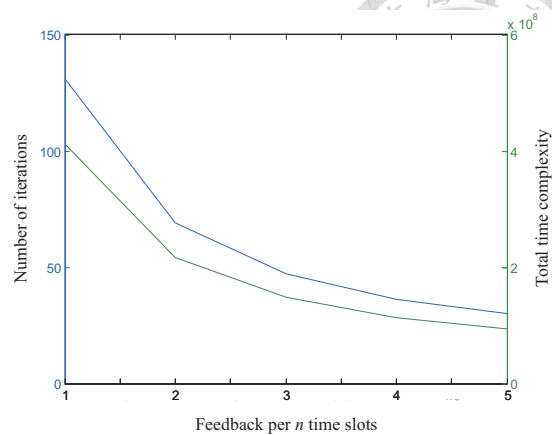
means the proposed resource allocation mechanism takes more future one-shot throughput into account and thus achieves higher weighted system throughput. Another way is to see the weighted system throughput normalized by $(1 - \beta)$. We can find that the normalized weighted system throughput may be high or low in different system states when β is small. On the other hand, when β is large, the normalized weighted system throughput becomes stable around 0.8 in all system states by taking more future one-shot system throughput into account.

We also evaluate the weighted system throughput under different feedback frequencies from per time slot to per 5 time slots. Fig. 3.7(a) shows that the weighted system throughput is lower when n gets larger (the feedback is less frequent). Also, the decrease becomes smaller when n gets larger. The reason is that the difference between the discount factors in the n -th and $(n + 1)$ -th time slots, $\beta^n(1 - \beta)$, is decreasing with respect to n . Thus, there will be less difference to update the feedback states in the n -th and $(n + 1)$ -th time slots when n gets larger. Fig. 3.7(b) shows that the number of iterations and the total time complexity both decrease when n gets larger. In other words, reducing the signalling overhead brings the trade off of lower system throughput and less total time complexity as we have discussed in Chapter 3.8.1.

Lastly, the throughput of each device with/without the weight design is compared in



(a)



(b)

Figure 3.7: Trade-off among the signaling overhead, the system throughput and the time complexity: (a) The weighted system throughput under feedback frequencies from per time slot to per 5 time slots. (b) The number of iterations and the total time complexity under feedback frequencies from per time slot to per 5 time slots.

Fig. 3.8. It can be seen that with the weight design, the throughput of each device in flow 1 (with 3 devices) is higher. The throughput of each device in flow 2 (with 7 devices) and the system throughput are less. This means that the proposed weight design indeed trades the system throughput off for fairer throughput performance among the devices.

3.10 Summary

In this chapter, we investigate multi-flow multicast over time-varying channels for energy-harvesting devices. From the perspective of incentive mechanism design, this chapter solves the resource allocation problem, considering the selfish characteristic and incomplete state information of the devices. The proposed resource allocation mechanism ensures the system to operate at the truth-revealing equilibrium where each device feedbacks the true state information to the BS in each time slot. With truthful feedback, the resource allocation achieves the desirable properties of maximum weighted system throughput, budget balance, and individual rationality. The simple weight design also brings the system fairness to some extent. From the algorithmic viewpoint, the proposed resource allocation policy can be solved via the value iteration algorithm. The system throughput can be traded off for less feedback signaling overhead and time complexity.

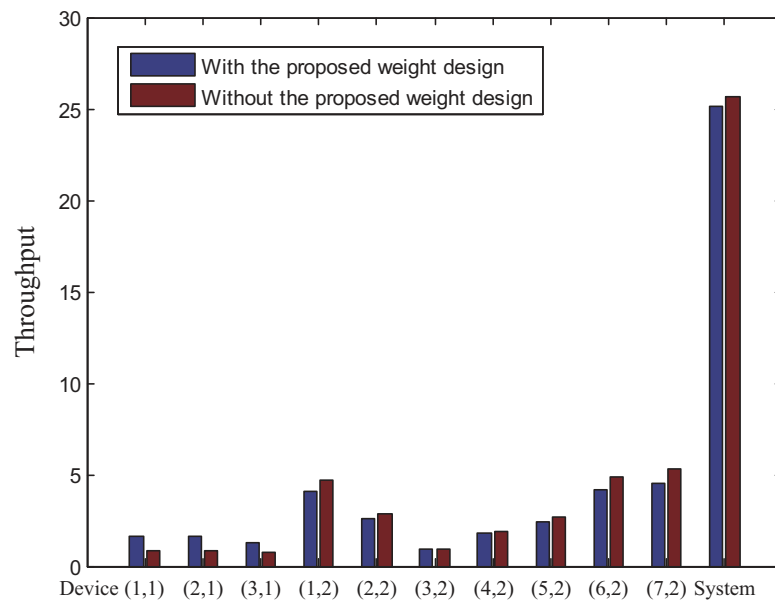


Figure 3.8: Throughput performance of each device and the system with/without the proposed weight design.

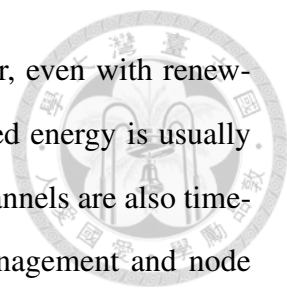


Chapter 4

On Maximizing Data Fidelity in Energy-Harvesting IoT: A Mechanism Design Approach

4.1 Introduction

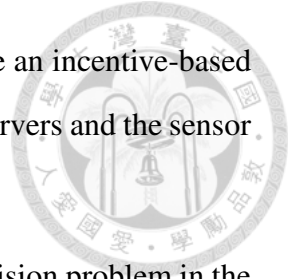
The Internet of things (IoT) is the inter-networking of smart devices, vehicles, and machines, and other items. The key factor for enabling this sophisticated paradigm is the integration of novel communication protocols and technologies [1, 2]. The basic premise of the IoT is to have wireless sensors collaborate directly without human involvement [68]. The wireless sensors can collect data from the environment, which allows other IoT items to further process data and make decisions. Conventional wireless sensors are installed with batteries of limited capacity. Therefore, limited energy is a major bottleneck and minimizing energy consumption to ensure longer network operation is a main design aspect. With the rapid development of energy harvesting technologies [69], wireless sensors now have chances to harvest renewable energy from ambient sources, such as solar power, electromagnetic waves, thermal energy, wind energy, kinetic energy, etc. Essentially, wireless sensors can benefit from the energy harvesting technologies to prolong life time and to achieve better performance [70]. Energy harvesting thus becomes



an important design consideration of future IoT protocols. However, even with renewable energy, wireless sensors cannot always be activated as harvested energy is usually scarce and time-varying, radio resources are limited, and wireless channels are also time-fluctuating. Many research papers endeavor to propose energy management and node activation schemes to achieve throughput maximization, transmission completion time minimization, etc. Moreover, as the environmental data are usually correlated in space and time, achieving high data fidelity, instead of solely maximizing throughput, also becomes a design objective. Even if many existing works optimize different network performance metrics with complete information on energy, channels, and data correlations, optimization is still difficult when such information is incomplete/unknown.

In this chapter, we investigate a node activation decision problem in the energy-harvesting IoT over an infinite time horizon. In the proposed scenario, there are three different groups of entities: a base station (BS), servers, and sensor nodes. The BS has a limited number of radio resources. It manages the network and gives activation to sensor nodes. The servers deploy sensor nodes to sense different environmental data, such as temperature, humidity, pressure, etc. The sensor nodes can harvest energy to sense data and transmit the sensed data through the BS to their servers. The data to be sensed are assumed to have spatial-temporal correlations. Consider the case where two sensor nodes gather data at the same time. When the data have high spatial correlations, the data fidelity, i.e, the meaning and quality of the data, is lower than when the data have low spatial correlations, even if the throughput, i.e., the amount of data gathered, is the same. This is also true for high temporal data correlations. Therefore, the design metric should be data fidelity in the server layer, not merely throughput in the sensor node layer. Furthermore, we make a practical assumption that the data statistics (correlations) and the energy states are only known to the servers and the sensor nodes, respectively. To achieve efficient node activation, the BS requires the servers and the sensor nodes to feedback the data statistics and the energy states. Considering the rational and selfish characteristics of the servers, the servers and their own sensor nodes may falsely feedback to manipulate the BS's node activation if doing so increases their own performance. The overall

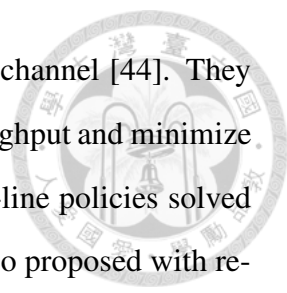
system performance may become inefficient. To this end, we propose an incentive-based node activation mechanism to guarantee truthful feedback from the servers and the sensor nodes. The detailed contributions are stated as follows:



1. We provide the theoretic foundation for the node activation decision problem in the energy-harvesting IoT, considering spatial-temporal data correlations and incomplete information on the data statistics and the energy states.
2. The proposed node activation mechanism ensures the servers and the sensor nodes to feedback the true data statistics and energy states. The system then operates at the truth-revealing equilibrium (incentive compatibility).
3. The proposed node activation mechanism maximizes the system data fidelity, i.e., the meaning and quality of data.
4. The proposed node activation mechanism also ensures that the payment is always made from the servers to the BS (budget balance). In other words, the BS does not need to pay the servers to guarantee truthful feedback.
5. The servers will join the proposed node activation mechanism to obtain higher utility than without joining (individual rationality).

4.2 Related Works

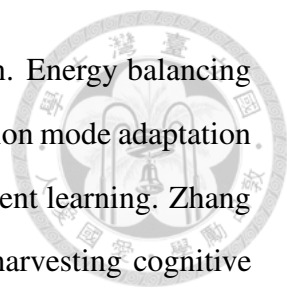
We first survey some previous works about transmission scheduling of sensor nodes with renewable energy. Sharma et al. studied a sensor node with an energy harvesting source [71]. They proposed energy management policies that are throughput optimal and mean delay optimal. Comparisons with other energy management policies were also made to justify their proposed policies. Michelusi et al. also considered a wireless sensor powered by an energy harvesting device [72]. By classifying data into different importance, they proposed transmission policies to achieve near-optimal performance in terms of the average long-term data importance. Heuristic policies were also proposed based on the analysis of a system with a deterministic and periodic energy supply. Ozel et al. considered



data transmission of an energy harvesting node in a wireless fading channel [44]. They studied optimal off-line transmission policies that maximize the throughput and minimize the transmission completion time. They also considered optimal on-line policies solved via stochastic dynamic programming. Near-optimal policies were also proposed with reduced complexity.

Correlated data gathering is also a mature topic. Vuran et al. developed a theoretical framework to model the spatial and temporal correlations in wireless sensor networks [73]. Their framework enabled the designs of efficient communication protocols which exploit intrinsic features of the spatial and temporal correlations. Liu et al. developed a framework to exploit spatial and temporal correlations to partition sensors into clusters and to restore the data in the sink with high fidelity [74]. An empirical study was also conducted to test their method using both a real test bed system and a large-scale synthetic data set. Yoon and Shahabi proposed a clustered aggregation algorithm that forms clusters based on sensing values [75]. One sensed data per cluster was transmitted to achieve a predefined error threshold. Another approach to exploit data correlations was given in [76]. Luo et al. applied compressive sampling theory to propose compressive data gathering that reduces global scale communication cost and extends the lifetime the entire sensor network. They also tested their proposed method on real sensor data to show the efficiency and robustness.

Combining transmission scheduling and data gathering, several existing research papers also proposed sensor node activation schemes to achieve different design goals. Since these papers are the most related to this chapter, we also show our differences below. Roy et al. defined application fidelity and studied the fidelity maximization problem in the application layer of wireless sensor networks [77]. They proposed a utility-based algorithm to select the optimal subset of applications to deploy given the available resources. However, the work of [77] was focused on one-shot optimization where energy variations were not considered. Zheng et al. studied the node activation control problem in energy-harvesting wireless sensor networks with a dynamic and unknown environment [78]. They decomposed the problem into energy balancing among sensors in the spatial



dimension and activation mode adaptation in the temporal dimension. Energy balancing was optimized with game theory in a distributed way, whereas activation mode adaptation in the dynamic and unknown environment was solved via reinforcement learning. Zhang et al. investigated resource management and allocation in energy-harvesting cognitive radio sensor networks [79]. They developed an aggregate network utility optimization framework and proposed an on-line algorithm to achieve energy balancing and licensed spectrum utilization of unlicensed sensors. Both [78] and [79] did not consider spatial-temporal data correlations. In other words, even if the node activation policies were designed to maximize the system utility/throughput, the system data fidelity may not be optimal. Also, the fully distributed optimization in [78] may not work when considering spatial-temporal data correlations. Moreover, the work of [79] did not consider the rational and selfish characteristics of sensors. As their proposed method consisted of distributed optimization in each sensor and global optimization in the BS, information feedback from the sensors to the BS is required. Intentionally false feedback may occur if doing so increases an individual sensor's performance.

We also introduced some of our previous works in energy harvesting. Shih et al. investigated two fundamental push-based and pull-based random access channel (RACH) procedures in Long Term Evolution (LTE) for energy-harvesting devices [80]. A hybrid scheme was proposed to manage different traffic loads, avoiding severe RACH collisions in the push-based scheme and the long delay in the pull-based scheme. Lin et al. proposed a deep sleeping mechanism that is a median Medium Access Control (MAC) enhancement scheme on IEEE 802.11 power saving mode (PSM) for energy-harvesting devices [81]. By properly considering the energy levels and contention windows of the energy-harvesting devices, their proposed deep sleeping mechanism is shown to reduce the overall outage probability and collision probability and thus improve energy efficiency. Kuan et al. proposed an erasure-based broadcast scheme to guarantee reliable broadcast transmission in energy-harvesting networks [52]. They proposed three policies to determine the broadcast period for different performance requirements, balancing the tradeoff between reliability and throughput. Compared with [80, 81, 52] that assumed full

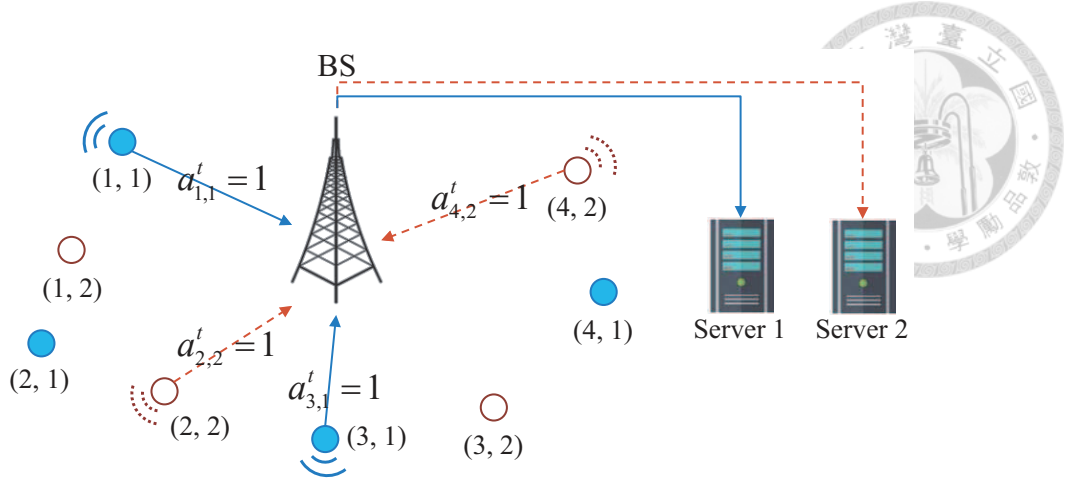


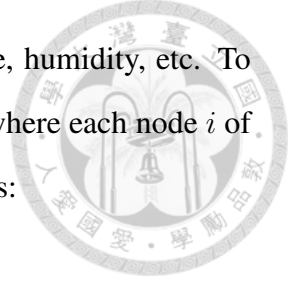
Figure 4.1: A model of the energy-harvesting IoT. There are one BS and multiple sensor nodes owned by different servers. Sensor node i owned by server g is denoted by node (i, g) . The nodes can harvest energy from the environment. The BS decides to activate nodes to sense and transmit data back through the BS to their servers. The node activation $a_{i,g}^t = 1$ means that the BS activates node (i, g) in time slot t .

knowledge on the network environment, this chapter investigates a totally different node activation decision problem with incomplete information of the network environment.

This chapter studies the node activation decision problem in energy-harvesting IoT with energy variations and limited radio resources. Considering spatial-temporal data correlations, we aim to maximize the system data fidelity. Unlike most of the previous works, we assume that the data statistics and the energy states are only known to the servers and the sensor nodes. We further assume that the servers are rational and selfish. Thus, the servers and their own sensor nodes may feedback the false information to increase their own performance. We then propose an incentive-based node activation mechanism that can elicit truthful feedback and also achieve several desirable properties.

4.3 System Model

We consider the time-slotted IoT consisting of three different groups of entities: a BS, servers, and sensor nodes. A simple illustration of the proposed energy-harvesting IoT is given in Fig. 4.1. The BS operates the network starting from time slot 0. It manages and gives activation to nodes to sense data. It also provides R radio resource blocks in each time slot for nodes to transmit the sensed data. A set of servers $\mathcal{G} = \{1, 2, \dots, G\}$ aims



to collect different environmental data such as temperature, pressure, humidity, etc. To sense data, each server g deploys a set of nodes $\mathcal{I}_g = \{1, 2, \dots, I_g\}$ where each node i of server g is denoted by node (i, g) . Each node has the simple functions:

1. It harvests energy from the environment.
2. It senses and transmits data to the server through the BS when being activated.

As the BS has R resource blocks, it can decide to activate up to R nodes to sense and transmit data. Sensing and transmitting data is assumed to consume one unit of energy. The activation status of node (i, g) in time slot t is denoted by $a_{i,g}^t = \{0, 1\}$ where 1 means activation. The notations $\mathbf{a}^t = (a_{i,g}^t)_{i \in \mathcal{I}_g, g \in \mathcal{G}}$, $\mathbf{a}_g^t = (a_{i,g}^t)_{i \in \mathcal{I}_g}$, and $\mathbf{a}_{-g}^t = (a_{i,k}^t)_{i \in \mathcal{I}_k, k \in \mathcal{G} \setminus g}$ are used to denote the activation profiles of all nodes in the system, all nodes of server g , and all nodes other than those of server g , in time slot t , respectively. The notation $\mathbf{a}^{(t)}$ and $\mathbf{a}^{(q \geq t)}$ are used to denote the activation profiles in each time slot t and each time slot $q \geq t$, respectively. Without special mention, the uses of g and $-g$ in the subscript and $\langle \cdot \rangle$ in the superscript have the same meaning to other notations throughout the paper.

4.3.1 Data Statistics and Entropy

We model the data of each server g in the network area by a discrete-space discrete-time Gaussian random field

$$\mathbf{X}_g^{(t)} \sim N(\mu_g, \Sigma_g). \quad (4.1)$$

where $X_{i,g}^t$ represents the data at node (i, g) in time slot t [82, 83]. The notation μ_g is the mean vector of the data at all nodes in all time slots, and Σ_g is the covariance matrix that models the spatio-temporal data correlations. We assume that the Gaussian random field is stationary and Markov in time.¹ The data statistics μ_g and Σ_g are assumed to be only known to each server g .

¹Such an assumption is reasonable since the duration of a resource block is usually on the order of millisecond, while the environmental remains constant for a much longer duration.

We further consider the data entropy of the proposed Gaussian data model. Suppose that various nodes of server g are activated in different time slots to sense data. The set of the data is denoted by \mathcal{K} with the mean vector $\mu_{\mathcal{K},g}$ and the covariance matrix $\Sigma_{\mathcal{K},g}$, where $\mu_{\mathcal{K},g}$ and $\Sigma_{\mathcal{K},g}$ are sub-vector and sub-matrix of μ_g and Σ_g , respectively. The entropy is

$$H(\mathcal{K}) = \frac{1}{2} \log [(2\pi e)^{|\mathcal{K}|} |\Sigma_{\mathcal{K},g}|], \quad (4.2)$$

which is only related to the covariance matrix $\Sigma_{\mathcal{K},g}$. Therefore, in the rest of the paper, when referring to the data statistics, we refer to the covariance matrix Σ_g . The entropy means the expected value of the information obtained in the data. It is regarded as the data fidelity that will be used as the optimization metric.

4.3.2 Energy States and Activation Intervals

In each time slot t , each node (i, g) is assumed to have independent and identically distributed (i.i.d.) energy arrivals denoted by $e_{i,g}$ [53, 45]. The i.i.d. assumption can be generalized to stationary and Markov energy arrivals as will be shown in Chapter 4.7.3. The energy arrivals in time slot t will be ready for use in the next time slot $(t + 1)$. The energy arrivals of different nodes can be different and correlated, which may be related to each device's energy-harvesting environment such as the physical location. At the beginning of each time slot t , the energy stored in each node (i, g) is defined as the energy state $es_{i,g}^t \in \mathcal{ES}_{i,g} = \{0, 1, \dots, EC_{i,g}\}$ where $EC_{i,g}$ is the energy capacity. As a node consumes one unit of energy to sense and transmit data when being activated, the energy state transition is given as follows:

$$es_{i,g}^{t+1} = \min(es_{i,g}^t - \min(es_{i,g}^t, a_{i,g}^t) + e_{i,g}, EC_{i,g}), \quad (4.3)$$

where $a_{i,g}^t$ is the activation status of node (i, g) in time slot t . One can note that the energy states have the stochastic Markov transition due to the i.i.d. energy arrivals in different time slots. The energy state transition function of each node (i, g) , which can be derived



from (4.3), is denoted by

$$E_{i,g}(es_{i,g}^{t+1}|es_{i,g}^t, a_{i,g}^t). \quad (4.4)$$

Also, the energy state transition function of all nodes in the system is denoted by $E(es^{t+1}|es^t, \mathbf{a}^t)$, the energy state transition function of all nodes other than those of server g is denoted by $E_{-g}(es_{-g}^{t+1}|es_{-g}^t, \mathbf{a}_{-g}^t)$.

We also introduce an activation interval variable $\tau_{i,g}^t$ to show how many time slots ago the last activation of node (i, g) was. For instance, $\tau_{i,g}^t = q$ means that the last activation of node (i, g) was in time slot $(t - q)$. The initial activation interval is set $\tau_{i,g}^0 = \infty$ which means there is no previous activation. It can be shown that the activation interval has the deterministic Markov transition:

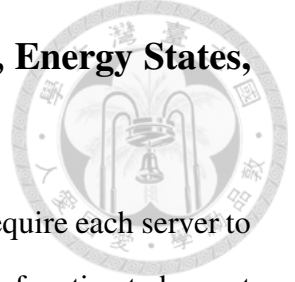
$$\tau_{i,g}^{t+1} = \begin{cases} \tau_{i,g}^t + 1, & a_{i,g}^t = 0 \\ 1, & a_{i,g}^t = 1 \end{cases}. \quad (4.5)$$

Derived from (4.5), we can also denote the activation interval transition function by $T_{i,g}(\tau_{i,g}^{t+1}|\tau_{i,g}^t, a_{i,g}^t)$. Similarly, we can also show the activation interval transition functions of all nodes in the system, and all nodes other than those of server g , respectively, as follows:

$$T(\tau^{t+1}|\tau^t, \mathbf{a}^t) = \prod_{i \in \mathcal{I}_g, g \in \mathcal{G}} T_{i,g}(\tau_{i,g}^{t+1}|\tau_{i,g}^t, a_{i,g}^t), \quad (4.6)$$

$$T_{-g}(\tau_{-g}^{t+1}|\tau_{-g}^t, \mathbf{a}_{-g}^t) = \prod_{i \in \mathcal{I}_k, k \in \mathcal{G} \setminus g} T_{i,k}(\tau_{i,k}^{t+1}|\tau_{i,k}^t, a_{i,k}^t). \quad (4.7)$$

In addition to the Markov energy states and activation intervals, we do not consider channel fluctuations to simplify the model and analysis. The case of time-varying channel conditions will be discussed in Chapter 4.7.3.



4.3.3 Information Assumption on the Data Statistics, Energy States, and Activation Intervals

Data statistics Σ_g is only known to each server g itself. The BS will require each server to feedback the data statistics. Also note that each node only has a simple function to harvest energy from the environment. It does not have to predict or measure how much energy it can harvest. We assume that the measurement is done by the BS.² However, even if the BS can measure the energy harvesting dynamics, the exact energy state $es_{i,g}^t$ in each time slot t is only known to each node (i, g) itself. The BS will also require each node to feedback the energy state. On the other hand, the activation intervals are always known to the BS since they are deterministic and fully controlled by the BS's activation decision.

4.3.4 Data Fidelity

Data fidelity is defined in the sense that when more nodes are activated to get more data samples, the server will obtain more information and thus more precise knowledge on the environmental data. Data fidelity then represents how precise the knowledge we have on the environmental data. However, as the data has spatio-temporal correlations, different data samples may contain different information. This means the data fidelity achieved may be different. We define the new information obtained in each time slot as the one-shot data fidelity. For server g , given the activation status profile \mathbf{a}_g^t , the energy state profile es_g^t and the activation interval profile τ_g^t in time slot t , we denote the set of data sensed by the nodes with $a_{i,g}^t = 1$ in time slot t by $\mathcal{K}_1(\mathbf{a}_g^t) = \{X_{i,g}^t | a_{i,g}^t = 1\}$. We also denote the set of data sensed by the nodes with $a_{i,g}^{t-\tau_{i,g}^t} = 1$, i.e., in the most recent previous time slots, by $\mathcal{K}_2(\tau_g^t) = \{X_{i,g}^{t-\tau_{i,g}^t} | a_{i,g}^{t-\tau_{i,g}^t} = 1\}$. The new information obtained due to the activation of the nodes in time slot t is the conditional entropy $H(\mathcal{K}_1(\mathbf{a}_g^t) | \mathcal{K}_2(\tau_g^t)) = H(\mathcal{K}_1(\mathbf{a}_g^t), \mathcal{K}_2(\tau_g^t)) - H(\mathcal{K}_2(\tau_g^t))$. Because of the Markov data assumption in time, we only have to consider the data sensed by the nodes in the most recent previous time slots, instead of the data sensed in all previous time slots, to derive the new information obtained

²The BS can deploy sensor nodes in the network area to sense and measure the energy harvesting dynamics.



in time slot t . This conditional entropy is defined as the one-shot data fidelity of server g , denoted by $v_g(\mathbf{a}_g^t, \Sigma_g, \mathbf{es}_g^t, \tau_g^t)$:

Definition 4.1. [One-shot data fidelity] The one-shot data fidelity of server g in time slot t is

$$v_g(\mathbf{a}_g^t, \Sigma_g, \mathbf{es}_g^t, \tau_g^t) = H(\mathcal{K}_1(\mathbf{a}_g^t), \mathcal{K}_2(\tau_g^t)) - H(\mathcal{K}_2(\tau_g^t)). \quad (4.8)$$

We further define the (long-term) data fidelity. We introduce a time discount factor β , $0 \leq \beta \leq 1$, to consider the time value of one-shot data fidelity, emphasizing the one-shot data fidelity in the near time slots. Therefore, the (long-term) data fidelity is defined as the time-discounted sum of the one-shot data fidelity:

Definition 4.2. [Long-term data fidelity] The data fidelity of server g seen in time slot t is

$$\sum_{q=t}^{\infty} \beta^{q-t} \mathbb{E} [v_g(\mathbf{a}_g^t, \Sigma_g, \mathbf{es}_g^t, \tau_g^t) | \Sigma_g, \mathbf{es}_g^t, \tau_g^t], \quad (4.9)$$

where β , $0 \leq \beta \leq 1$, is the discount factor.

Lastly, we define the (long-term) system data fidelity:

Definition 4.3. [Long-term system data fidelity] The system data fidelity seen in time slot t is

$$\sum_{g \in \mathcal{G}} \sum_{q=t}^{\infty} \beta^{q-t} \mathbb{E} [v_g(\mathbf{a}_g^t, \Sigma_g, \mathbf{es}_g^t, \tau_g^t) | \Sigma, \mathbf{es}^t, \tau^t]. \quad (4.10)$$

Maximizing the system data fidelity will be the main design objective as will be shown in Chapter 4.4.

4.4 Node Activation Mechanism

In the proposed framework, the BS makes the node activation decision to maximize the system data fidelity. As the data statistics and the energy states are only known to the

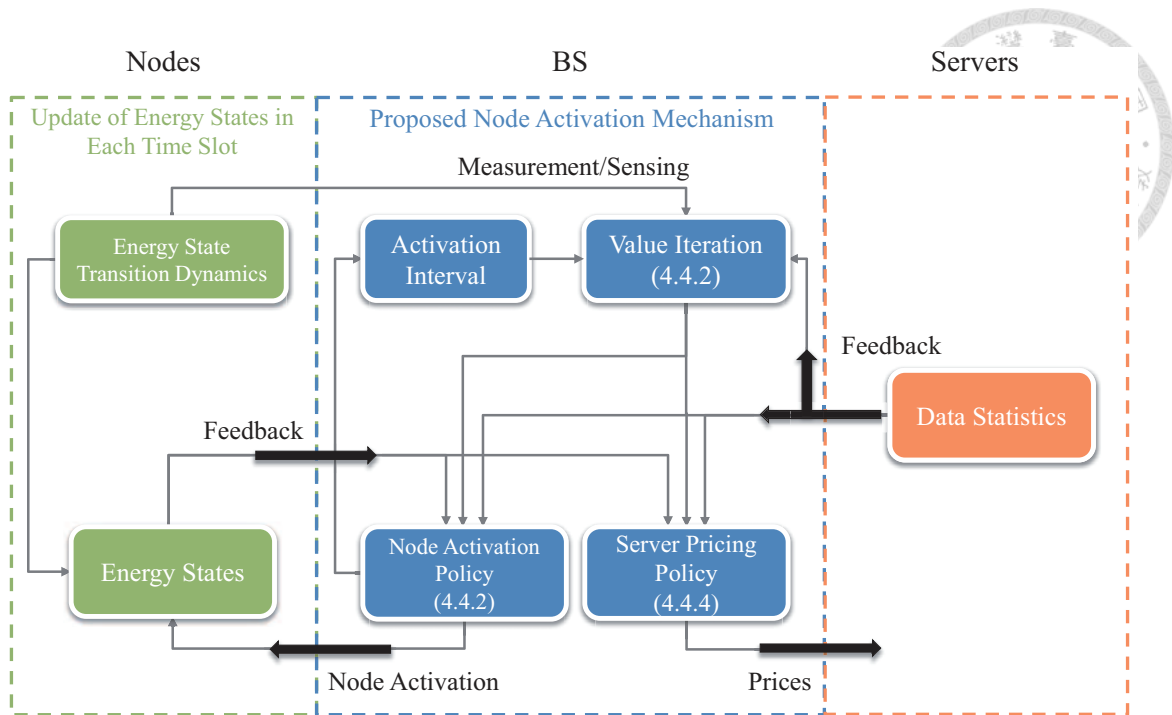
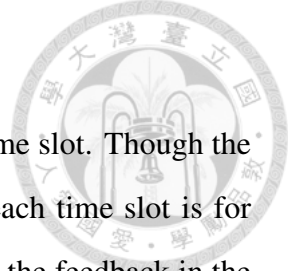


Figure 4.2: The block diagram of the proposed node activation mechanism. The servers and the nodes are required to feedback the data statistics and the energy states, respectively. The BS makes the node activation decision and also charges the servers prices.

servers and the nodes, the BS requires the feedback of the data statistics and the energy states. Since the servers and the nodes (owned by the servers) are selfish in nature, they may falsely feedback to manipulate the BS’s node activation decision if doing so increases their own performance. The overall system performance may become undesirable. Therefore, we design a node activation mechanism that can induce truthful feedback.

The proposed node activation mechanism is shown in Fig. 4.2. It consists of a node activation policy and a pricing policy. The node activation policy decides which nodes to be activated in each time slot. It is designed to maximize the system data fidelity. The pricing policy decides how the BS charges each server in each time time slot. It is designed to ensure truthful feedback and achieve several desirable properties. Also, a value iteration algorithm is proposed to derive the optimal solutions of the resource allocation policy and the pricing policy. The details are specified as below.



4.4.1 Feedback Strategies of the Servers

Each server g is required to feedback the data statistics Σ_g in each time slot. Though the data statistics will not vary with time, we require the feedback in each time slot is for the following reasons: Once the feedback is untruthful in a time slot, the feedback in the future time slots can still be truthful. As we will propose a node activation policy and a pricing policy both based on the current feedback, the untruthful current feedback will not affect the future node activation and pricing. On the other hand, each node (i, g) is required to feedback the energy state $es_{i,g}^t$ in each time slot. We assume that each server makes a feedback strategy that decides how itself and its nodes feedback the data statistics and the energy states. To be specific, when the mechanism starts, each server g decides a feedback strategy $s_g = (\hat{\Sigma}_g^{(t)}, \hat{\mathbf{e}}\mathbf{s}_g^{(t)})$ upon which server g feedbacks the data statistics $\hat{\Sigma}_g^t$ and each node (i, g) feedbacks the energy state $\hat{e}s_{i,g}^t$ in each time slot t . A truthful feedback strategy means $s_g^* = (\Sigma_g^{(t)}, \mathbf{e}\mathbf{s}_g^{(t)})$ where $\Sigma_g^t = \Sigma_g \forall t$. The collection of the feedback and the activation intervals $\tau^{(q \leq t-1)}$ (no feedback is required as fully controlled by the BS) up to time slot $(t-1)$ is called the history in time slot t and denoted by $h^t = (\hat{\Sigma}^{(q \leq t-1)}, \hat{\mathbf{e}}\mathbf{s}^{(q \leq t-1)}, \tau^{(q \leq t-1)})$. The feedback data statistics $\hat{\Sigma}_g^t$ and energy state $\hat{e}s_{i,g}^t$ should be functions of the history h^t , the true data statistics Σ_g , and true energy state $es_{i,g}^t$. However, we omit the complex notations and just use $\hat{\Sigma}_g^t$ and $\hat{e}s_{i,g}^t$ for short.

4.4.2 Node Activation Policy and Value Iteration

The system is Markov due to the Markov energy state and activation interval transitions. The BS's node activation decision can be modelled as a Markov decision process. Note that the data statistics also affect the node activation decision. Therefore, we propose a node activation policy under which the node activation in each time slot depends on the feedback of the current data statistics and energy states. To be specific, the proposed node activation policy is denoted by $\pi^* = (\pi_g^*)_{g \in \mathcal{G}} = (\pi_{i,g}^*)_{i \in \mathcal{I}_g, g \in \mathcal{G}}$. The node activation in time slot t is $\mathbf{a}^t = \pi^*(\hat{\Sigma}^t, \hat{\mathbf{e}}\mathbf{s}^t, \tau^t)$, given the current feedback data statistics $\hat{\Sigma}^t$, energy state $\hat{\mathbf{e}}\mathbf{s}^t$, and activation interval τ^t . The proposed node activation policy π^* is designed

to maximize the system data fidelity.³

Design 4.1. [Node activation policy] The node activation policy π^* is designed to maximize the system data fidelity with any initial data statistics $\tilde{\Sigma}$, energy state $\tilde{\mathbf{e}}\mathbf{s}^0$, and activation interval $\tilde{\tau}^0$:

$$\pi^* = \arg \max_{\mathbf{a}^{(t)}} \sum_{g \in \mathcal{G}} \sum_{t=0}^{\infty} \beta^t \mathbb{E} \left[v_g(\mathbf{a}_g^t, \tilde{\Sigma}_g, \tilde{\mathbf{e}}\mathbf{s}_g^t, \tilde{\tau}_g^t) | \tilde{\Sigma}, \tilde{\mathbf{e}}\mathbf{s}^0, \tilde{\tau}^0 \right] \quad (4.11)$$

$$s.t. \quad \sum_{i \in \mathcal{I}_g, g \in \mathcal{G}} \pi_{i,g}^* \leq R,$$

where the energy state $\tilde{\mathbf{e}}\mathbf{s}^t$ and the activation interval $\tilde{\tau}^t$ satisfy the transition functions E and T with $\mathbf{a}^t = \pi^*(\tilde{\Sigma}, \tilde{\mathbf{e}}\mathbf{s}^t, \tilde{\tau}^t)$, respectively.

Given the feedback data statistics $\hat{\Sigma}^t$, energy state $\hat{\mathbf{e}}\mathbf{s}^t$, and activation interval τ^t in each time slot t , the node activation is $\mathbf{a}^t = \pi^*(\hat{\Sigma}^t, \hat{\mathbf{e}}\mathbf{s}^t, \tau^t)$.

From (4.11), we can also show the maximum system data fidelity denoted by a value function V^* in a recursive form as follows:

$$V^*(\Sigma, \mathbf{e}\mathbf{s}, \tau) = \max_{\mathbf{a}} \left[\sum_{g \in \mathcal{G}} v_g(\mathbf{a}_g, \Sigma_g, \mathbf{e}\mathbf{s}_g, \tau_g) + \beta \sum_{\mathbf{e}\mathbf{s}', \tau'} E(\mathbf{e}\mathbf{s}' | \mathbf{e}\mathbf{s}, \mathbf{a}) T(\tau' | \tau, \mathbf{a}) V^*(\Sigma, \mathbf{e}\mathbf{s}', \tau') \right]. \quad (4.12)$$

Equation (4.12) is usually referred to as the Bellman equation. There are several algorithms for solving the Bellman equation. One of the most widely used is value iteration due to its many advantages, such as quick convergence and easy implementation, especially when the state space is very large [65]. The value iteration algorithm for deriving the node activation policy π^* and the value function V^* is given in Algorithm 4.1. It involves the arbitrary initialization of the value function V^* (line 1) and the iterative update of the value function according to the Bellman equation in (4.12) (lines 2 to 8). The update process repeats until the convergence criterion is met, i.e., the update error δ is less than the specified error tolerance ϵ (line 9). Lastly, the value iteration algorithm outputs

³Because of the stationary and Markov properties of the system, the optimal policy is indeed stationary and a function of the current data statistics, energy state and activation interval.

the optimal value function V^* and node activation policy π^* (line 10).



Algorithm 4.1: Value iteration algorithm for node activation

- 1: Given Σ , initialize $V^*(\Sigma, \mathbf{es}, \tau)$ for each \mathbf{es} and τ .
 - 2: Repeat
 - 3: $\delta \leftarrow 0$.
 - 4: For each \mathbf{es} and τ .
 - 5: $v \leftarrow V^*(\Sigma, \mathbf{es}, \tau)$.
 - 6: $V^*(\Sigma, \mathbf{es}, \tau) \leftarrow$
 - 7: $\max_{\mathbf{a}} \left[\sum_{g \in \mathcal{G}} v_g(\mathbf{a}_g, \Sigma_g, \mathbf{es}_g, \tau_g) + \beta \sum_{\mathbf{es}', \tau'} E(\mathbf{es}' | \mathbf{es}, \mathbf{a}) T(\tau' | \tau, \mathbf{a}) V^*(\Sigma, \mathbf{es}', \tau') \right]$.
 - 8: $\delta \leftarrow \max(\delta, |v - V^*(\Sigma, \mathbf{es}, \tau)|)$.
 - 9: Until $\delta < \epsilon$ (a small positive number).
 - 10: Output the value function V^* and the policy π^* .
-

Lastly, it is useful to denote the system data fidelity other than server g (and its nodes) by the value function V_{-g}^* . For the use in the pricing policy in 4.4.4, we can also design a node activation policy π^{-g} that maximizes the system data fidelity with server g excluded from the system. The system data fidelity with server g excluded is denoted by V^{-g} .

4.4.3 Update of the Energy State Information

We discuss how the BS and the servers update the probability mass function (pmf) $\Delta(\mathbf{es}^t)$ of the energy state after the feedback in each time slot t .⁴ The time instant after the feedback is called the ex-post stage of the time slot. In fact, we can define the other two stages: the ex-ante stage and the interim stage [57]. However, since any properties that are ex-post must be interim and ex-ante, we focus on the ex-post stage. So without special mention, the system data fidelity in Definition 4.3 and everything else that will be defined or designed later are all in the ex-post manner. Also note that there is no need to update the information of the data statistics and the activation intervals since the former is not time-varying and the latter is fully controlled by the BS.

After each node feedbacks the energy state, the BS updates the pmf $\Delta(\mathbf{es}^t | h^{t+1})$ by

⁴Since each node's feedback is based on the server's feedback strategy, we keep the functions of the node as simple as possible and assume that each node needs not update the system energy state information.

the Bayes' rule as follows:

$$\Delta(\mathbf{es}^t|h^{t+1}) = \frac{\Delta(\mathbf{es}^t|h^t)\Delta(\hat{\mathbf{es}}^t|\mathbf{es}^t, h^t)}{\sum_{\mathbf{es}^t} \Delta(\mathbf{es}^t|h^t)\Delta(\hat{\mathbf{es}}^t|\mathbf{es}^t, h^t)}, \quad (4.13)$$



where $\Delta(\mathbf{es}^t|h^t)$ is derived via the energy state transition function E as follows:

$$\Delta(\mathbf{es}^t|h^t) = \sum_{\mathbf{es}^{t-1}} \Delta(\mathbf{es}^{t-1}|h^t)E(\mathbf{es}^t|\mathbf{es}^{t-1}, \pi^*(\hat{\Sigma}^{t-1}, \hat{\mathbf{es}}^{t-1}, \tau^{t-1})). \quad (4.14)$$

On the other hand, though the feedback may not be truthful, we assume that each server g can transform untruthful feedback to the real energy states of its nodes (an inverse transform from its feedback strategy). Thus, each server g knows the energy state \mathbf{es}_g^t and updates the pmf $\Delta(\mathbf{es}^t|\mathbf{es}_g^t, h^{t+1})$ as follows:

$$\Delta(\mathbf{es}^t|\mathbf{es}_g^t, h^{t+1}) = \frac{\Delta(\mathbf{es}^t|\mathbf{es}_g^t, h^t)\Delta(\hat{\mathbf{es}}^t|\mathbf{es}^t, h^t)}{\sum_{\mathbf{es}_{-g}^t} \Delta(\mathbf{es}^t|\mathbf{es}_{-g}^t, h^t)\Delta(\hat{\mathbf{es}}^t|\mathbf{es}^t, h^t)}, \quad (4.15)$$

where $\Delta(\mathbf{es}^t|\mathbf{es}_g^t, h^t)$ is derived via the energy state transition function E_{-g} as follows:

$$\Delta(\mathbf{es}^t|\mathbf{es}_g^t, h^t) = \sum_{\mathbf{es}_{-g}^{t-1}} \Delta(\mathbf{es}^{t-1}|\mathbf{es}_g^{t-1}, h^t)E_{-g}(\mathbf{es}_{-g}^t|\mathbf{es}_{-g}^{t-1}, \pi_{-g}^*(\hat{\Sigma}^{t-1}, \hat{\mathbf{es}}^{t-1}, \tau^{t-1})). \quad (4.16)$$

4.4.4 Server Pricing Policy

We propose a pricing policy by which the BS charges each server for not only using the network service but also ensuring truthful feedback. Several desirable properties can also be achieved with the proposed pricing policy. The basic idea of the proposed pricing policy comes from the Vickrey-Clarke-Groves (VCG) mechanism [58, 59, 60]. Since the proposed node activation mechanism have multiple time slots, we extend the design idea from one shot to multiple time slots. Specifically, after the feedback in each time slot t , the BS pays each server g $\sum_{k \in \mathcal{G} \setminus g} v_k(\pi_k^*, \hat{\Sigma}_k^t, \hat{\mathbf{es}}_k^t, \tau_k^t)$, i.e., the one-shot system data fidelity other than server g . To balance the payment, the BS also charges each server g the



one-shot price

$$\kappa_g^t(h^t, \hat{\Sigma}^t, \hat{\mathbf{e}}\mathbf{s}^t) = V^{-g}(\hat{\Sigma}_{-g}^t, \hat{\mathbf{e}}\mathbf{s}_{-g}^t, \tau_{-g}^t) - \beta \mathbb{E} \left[V^{-g}(\hat{\Sigma}_{-g}^t, \mathbf{e}\mathbf{s}_{-g}^{t+1}, \tau_{-g}^{t+1}) | h^{t+1} \right], \quad (4.17)$$

where $h^{t+1} = (h^t, \hat{\Sigma}^t, \hat{\mathbf{e}}\mathbf{s}^t, \tau^t)$. Just as in the VCG mechanism, we want the time discounted sum of κ_g^t to be V^{-g} , i.e., the system data fidelity with server g excluded from the system. However, directly using the VCG mechanism to charge $\sum_{k \in \mathcal{G} \setminus g} v_k(\pi_k^{-g}, \hat{\Sigma}_{-g}^t, \hat{\mathbf{e}}\mathbf{s}_{-g}^t, \tau_{-g}^t)$, i.e., the one-shot system data fidelity with server g excluded from the system, cannot make the time discounted sum equal to V^{-g} . Therefore, we find another way to decompose V^{-g} in time into κ_g^t in (4.17). The proposed pricing policy denoted by $\rho^{(t)} = (\rho_g^{(t)})_{g \in \mathcal{G}}$ is then designed as follows:

Design 4.2. [Pricing policy] *The one-shot price the BS charges each server g in time slot t is*

$$\rho_g^t(h^t, \hat{\Sigma}^t, \hat{\mathbf{e}}\mathbf{s}^t) = - \sum_{k \in \mathcal{G} \setminus g} v_k(\pi_k^*(\hat{\Sigma}^t, \hat{\mathbf{e}}\mathbf{s}^t, \tau^t), \hat{\Sigma}_k^t, \hat{\mathbf{e}}\mathbf{s}_k^t, \tau_k^t) + \kappa_g^t(h^t, \hat{\Sigma}^t, \hat{\mathbf{e}}\mathbf{s}^t), \quad (4.18)$$

where κ_g^t is given in (4.17).

4.4.5 Utility of the Servers

With the proposed node activation policy π^* and pricing policy $\rho^{(t)}$, we define the ex-post utility of each server g , denoted by $u_g(\mathbf{s} | t, \Sigma_g, \mathbf{e}\mathbf{s}_g^t, h^{t+1})$, as the data fidelity minus the price:

Definition 4.4. [Ex-post utility] *The utility of server g seen in time slot t is*

$$u_g(\mathbf{s} | \Sigma_g, \mathbf{e}\mathbf{s}_g^t, h^{t+1}) = \sum_{q=t}^{\infty} \beta^{q-t} \mathbb{E} \left[v_g(\pi_g^*(\hat{\Sigma}^q, \hat{\mathbf{e}}\mathbf{s}^q, \tau^q), \Sigma_g, \mathbf{e}\mathbf{s}_g^q, \tau_g^q) - \rho_g^q(h^q, \hat{\Sigma}^q, \hat{\mathbf{e}}\mathbf{s}^q) | \Sigma_g, \mathbf{e}\mathbf{s}_g^t, h^{t+1} \right] \quad (4.19)$$

Each server g maximizes its own utility by choosing the feedback strategy s_g . As will be proved in Chapter 4.6, the proposed node activation mechanism can induce the truthful

feedback strategy s_g^* from each server g .



4.5 Node Activation Game and Solution Concept

The data statistics and the energy states in each time slot are only known to the servers and the nodes, respectively. Since the energy state transition, the node activation transition, and the node activation policy are all Markov, the servers' feedback decisions under the proposed node activation mechanism can be formulated as a stochastic game with incomplete information. The induced node activation game is denoted by $G = (\mathcal{G}, \Sigma, \text{es}^{(t)}, \tau^{(t)}, \mathbf{s}, E, T, \mathbf{u})$ where each component is specified as below:

- Player set \mathcal{G} : Each server $g \in \mathcal{G}$ is a player in the game.
- Data statistics profile Σ , energy state profile $\text{es}^{(t)}$, and activation interval profile $\tau^{(t)}$: Each server g knows the data statistics Σ_g and the energy state es_g^t in each time slot t . The activation interval τ^t in each time slot t is fully controlled by and known to the BS.
- Strategy profile \mathbf{s} : Each server g has a strategy $s_g = (\hat{\Sigma}_g^{(t)}, \hat{\text{es}}_g^{(t)})$ to feedback the data statistics and the energy states in each time slot. The strategy profile is $\mathbf{s} = (\hat{\Sigma}^{(t)}, \hat{\text{es}}^{(t)})$.
- Energy state transition function E and activation interval transition function T : The energy state transition function is $E(\text{es}^{t+1} | \text{es}^t, \pi^*(\hat{\Sigma}^t, \hat{\text{es}}^t, \tau^t))$, and the activation interval transition function is $T(\tau^{t+1} | \tau^t, \pi^*(\hat{\Sigma}^t, \hat{\text{es}}^t, \tau^t))$. The energy state transition function and the activation interval transition function are both known to the BS and the servers.
- Utility profile \mathbf{u} : Each server g has the ex-post utility u_g as shown in Definition 4.4. The utility profile is $\mathbf{u} = (u_g)_{g \in \mathcal{G}}$.

The solution concept "perfect ex-post equilibrium" will be used to analyze the proposed node activation game. A perfect ex-post equilibrium is a refinement of a subgame

perfect equilibrium [62] where the strategies form an ex-post equilibrium in any subgame. It is a stronger solution concept than Bayesian equilibrium and Nash equilibrium that require Bayesian and complete information, respectively. The formal definition of a perfect ex-post equilibrium is given as follows:

Definition 4.5. [*Perfect ex-post equilibrium*] *The strategy profile s is a perfect ex-post equilibrium if*

$$u_g(s|\Sigma_g, \mathbf{es}_g^t, h^{t+1}) \geq u_g(s'_g, \mathbf{s}_{-g}|\Sigma_g, \mathbf{es}_g^t, h^{t+1}) \quad \forall t, g, \Sigma_g, \mathbf{es}_g^t, h^t, s'_g \neq s_g. \quad (4.20)$$

It is well-known that a strategy profile is a subgame perfect equilibrium if and only if there are no profitable one-shot deviations. The definitions of one-shot deviation strategy and the one-shot deviation principle [63, 64] for the proposed node activation game are given as follows:

Definition 4.6. [*One-shot deviation strategy*] *A strategy $s'_g = (\Sigma_g^{t, \langle q \rangle}, \mathbf{es}_g^{t, \langle q \rangle})$ is a one-shot deviation from another strategy $s_g = (\hat{\Sigma}_g^{\langle q \rangle}, \hat{\mathbf{es}}_g^{\langle q \rangle})$ after some history h^t in time slot t if*

$$(\Sigma_g^{t, \langle q \rangle}, \mathbf{es}_g^{t, \langle q \rangle}) \neq (\hat{\Sigma}_g^{\langle q \rangle}, \hat{\mathbf{es}}_g^{\langle q \rangle}) \text{ and } (\Sigma_g^{t, \langle q \rangle}, \mathbf{es}_g^{t, \langle q \rangle}) = (\hat{\Sigma}_g^{\langle q \rangle}, \hat{\mathbf{es}}_g^{\langle q \rangle}). \quad (4.21)$$

Definition 4.7. [*One-shot deviation principle*] *The strategy profile s is a perfect ex-post equilibrium if and only if*

$$u_g(s|\Sigma_g, \mathbf{es}_g^t, h^{t+1}) \geq u_g(s'_{i,g}, \mathbf{s}_{-g}|\Sigma_g, \mathbf{es}_g^t, h^{t+1}) \quad \forall t, g, \Sigma_g, \mathbf{es}_g^t, h^t, s'_g \quad (4.22)$$

where s'_g is any one-shot deviation strategy from s_g after history h^t .

4.6 Truth-Revealing Equilibrium and Desirable Properties

In the following, we prove that the proposed node activation game reaches the truth-revealing perfect ex-post equilibrium $s^* = (\Sigma^{q \geq t}, \mathbf{es}^{q \geq t})$ where $\Sigma^t = \Sigma$. The proposed

node activation mechanism is then called *ex-post incentive compatible*. Before that we first show the following lemma about κ_g^t that will be used in the proof for Theorem 4.1.

Lemma 4.1. *Given any strategy $s_g = (\hat{\Sigma}_g^{(q \geq t)}, \hat{\mathbf{e}}_g^{(q \geq t)})$ of server g and the truthful feedback strategies $\mathbf{s}_{-g}^* = (\Sigma_{-g}^{(q \geq t)}, \mathbf{e}_{-g}^{(q \geq t)})$ of the other servers after any history h^t , the time discounted sum of κ_g^t is*

$$\sum_{q=t}^{\infty} \beta^{q-t} \mathbb{E} \left[\kappa_g^q(h^q, \hat{\Sigma}_g^q, \Sigma_{-g}^q, \hat{\mathbf{e}}_g^q, \mathbf{e}_{-g}^q) | h^{t+1} \right] = V^{-g}(\Sigma_{-g}^t, \mathbf{e}_{-g}^t, \tau_{-g}^t), \quad (4.23)$$

where $h^{q+1} = (h^q, \hat{\Sigma}_g^q, \Sigma_{-g}^q, \hat{\mathbf{e}}_g^q, \mathbf{e}_{-g}^q) \forall q \geq t$.

Proof. From (4.17), we know $\forall q \geq t$

$$\begin{aligned} \beta^{q-t} \mathbb{E} \left[\kappa_g^q(h^q, \hat{\Sigma}_g^q, \Sigma_{-g}^q, \hat{\mathbf{e}}_g^q, \mathbf{e}_{-g}^q) | h^{t+1} \right] &= \beta^{q-t} \mathbb{E} \left[V^{-g}(\Sigma_{-g}^q, \mathbf{e}_{-g}^q, \tau_{-g}^q) | h^{t+1} \right] \\ &\quad - \beta^{q+1-t} \mathbb{E} \left[V^{-g}(\Sigma_{-g}^{q+1}, \mathbf{e}_{-g}^{q+1}, \tau_{-g}^{q+1}) | h^{t+1} \right], \end{aligned} \quad (4.24)$$

where $\mathbb{E} \left[V^{-g}(\Sigma_{-g}^t, \mathbf{e}_{-g}^t, \tau_{-g}^t) | h^{t+1} \right] = V^{-g}(\Sigma_{-g}^t, \mathbf{e}_{-g}^t, \tau_{-g}^t)$. Therefore, (4.23) can be easily derived by summing (4.24) $\forall q \geq t$. \square

Theorem 4.1. [*Ex-post incentive compatibility*] *The proposed node activation mechanism is ex-post incentive compatible. The proposed game reaches the truth-revealing perfect ex-post equilibrium $\mathbf{s}^* = (\Sigma^{(t)}, \mathbf{e}_{-g}^{(t)})$ where $\Sigma^t = \Sigma$.*

Proof. The proof follows the one-shot deviation principle. We consider the truthful feedback strategy profile $\mathbf{s}^* = (\Sigma^{(q \geq t)}, \mathbf{e}_{-g}^{(q \geq t)})$ and another feedback strategy profile (s_g, \mathbf{s}_{-g}^*) where server g plays a one-shot deviation strategy s_g with $(\hat{\Sigma}_g^t, \hat{\mathbf{e}}_g^t)$ after some history h^t in time slot t .

From (4.19), given \mathbf{s}^* , we can derive server g 's utility after history h^t :



$$\begin{aligned}
u_g(\mathbf{s}^*|\Sigma_g, \mathbf{es}_g^t, h^{t+1}) &= \sum_{k \in \mathcal{G}} \sum_{q=t}^{\infty} \beta^{q-t} \mathbb{E} [v_k(\pi_k^*(\Sigma, \mathbf{es}^q, \tau^q), \Sigma_k, \mathbf{es}_k^q, \tau_k^q) | \Sigma_g, \mathbf{es}_g^t, h^{*,t+1}] \\
&\quad - \sum_{q=t}^{\infty} \beta^{q-t} \mathbb{E} [\kappa_g^q(h^q, \Sigma^q, \mathbf{es}^q) | \Sigma_g, \mathbf{es}_g^t, h^{t+1}] \\
&= V^*(\Sigma, \mathbf{es}^t, \tau^t) - V^{-g}(\Sigma_{-g}, \mathbf{es}_{-g}^t, \tau_{-g}^t), \tag{4.25}
\end{aligned}$$

where the first and the second terms in the last equality come from Design 4.1 and Lemma 4.1, respectively.

Given (s_g, \mathbf{s}_{-g}^*) , we can also derive server g 's utility after history h^t :

$$u_g(s_g, \mathbf{s}_{-g}^* | \Sigma_g, \mathbf{es}_g^t, h^{t+1}) = V'(\Sigma, \mathbf{es}^t, \tau^t) - V^{-g}(\Sigma_{-g}, \mathbf{es}_{-g}^t, \tau_{-g}^t), \tag{4.26}$$

where

$$\begin{aligned}
V'(\Sigma, \mathbf{es}^t, \tau^t) &= \mathbb{E} \left[v_g(\pi_g^*(\hat{\Sigma}_g^t, \Sigma_{-g}, \hat{\mathbf{es}}_g^t, \mathbf{es}_{-g}^t, \tau^t), \Sigma_g, \mathbf{es}_g^t, \tau_g^t) | \Sigma_g, \mathbf{es}_g^t, h^{t+1} \right] \\
&\quad + \sum_{k \in \mathcal{G} \setminus g} \mathbb{E} \left[v_k(\pi_k^*(\hat{\Sigma}_g^t, \Sigma_{-g}, \hat{\mathbf{es}}_g^t, \mathbf{es}_{-g}^t, \tau^t), \Sigma_k^t, \mathbf{es}_k^t, \tau_k^t) | \Sigma_g, \mathbf{es}_g^t, h^{t+1} \right] \\
&\quad + \sum_{k \in \mathcal{G}} \sum_{q=t+1}^{\infty} \beta^{q-t} \mathbb{E} [v_k(\pi_k^*(\Sigma, \mathbf{es}^q, \tau^q), \Sigma_k, \mathbf{es}_k^q, \tau_k^q) | \Sigma_g, \mathbf{es}_g^t, h^{t+1}]. \tag{4.27}
\end{aligned}$$

According to Design 4.1, since $\mathbf{a}^q = \pi^*(\Sigma, \mathbf{es}^q, \tau^q)$ maximizes the system data throughput, we know $V^*(\Sigma, \mathbf{es}^t, \tau^t) \geq V'(\Sigma, \mathbf{es}^t, \tau^t)$. Therefore, we have $u_g(\mathbf{s}^* | \Sigma_g, \mathbf{es}_g^t, h^{t+1}) \geq u_g(s_g, \mathbf{s}_{-g}^* | \Sigma_g, \mathbf{es}_g^t, h^{t+1})$. In other words, for each server g , the truthful feedback strategy \mathbf{s}_g^* always brings higher ex-post utility than any one-shot deviation strategy s_g after any history h^t . The game then has the truth-revealing perfect ex-post equilibrium \mathbf{s}^* . The proposed node activation mechanism is ex-post incentive compatible. \square

Theorem 4.1 means that the proposed node activation mechanism reaches the equilibrium point where the BS always collects the true data statistics and energy states from the servers and the nodes. The equilibrium is perfect in that if each server is allowed to

change a feedback strategy in each time slot, each server still always truthfully feedbacks. The equilibrium is also ex-post in that after the true data statistics and energy states are revealed in each time slot, each device will not regret the strategy it has made before the proposed node activation mechanism starts. In the following propositions, we show the node activation, the history, and the energy state information at the truth-revealing equilibrium.

Proposition 4.1. [*Equilibrium node activation*] *The equilibrium node activation in each time slot t is*

$$\mathbf{a}^{*,t} = \pi^*(\Sigma, \mathbf{es}^t, \tau^t). \quad (4.28)$$

Proposition 4.2. [*Equilibrium history and energy state information*] *The equilibrium history in time slot t is*

$$h^{*,t} = (\Sigma^{\langle q \leq t-1 \rangle}, \mathbf{es}^{\langle q \leq t-1 \rangle}, \tau^{\langle q \leq t-1 \rangle}). \quad (4.29)$$

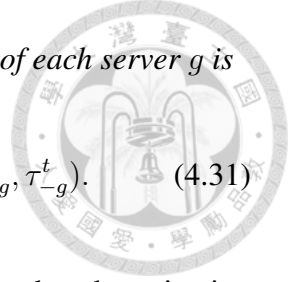
In the ex-post stage of time slot t , the BS and each server knows the exact energy state \mathbf{es}^t .

Since the energy states have the Markov transition, Proposition 4.2 implies that once the true energy state \mathbf{es}^t is revealed in each time slot t , the BS and each server do not need to memorize the history $h^{*,t}$. At the truth-revealing equilibrium, the BS and each device can also easily compute the prices and the utility given in Propositions 4.3 and 4.4, respectively.

Proposition 4.3. [*Equilibrium price*] *The (long-term) equilibrium price seen in time slot t is*

$$\sum_{q=t}^{\infty} \beta^{q-t} \mathbb{E} [\rho_g^{*,q} | \Sigma_g, \mathbf{es}_g^t, h^{*,t+1}] = -V_{-g}^*(\Sigma, \mathbf{es}^t, \tau^t) + V^{-g}(\Sigma_{-g}, \mathbf{es}_{-g}^t, \tau_{-g}^t), \quad (4.30)$$

where $\rho_g^{*,q} = \rho_g^q(h^{*,q}, \Sigma^q, \mathbf{es}^q)$.



Proposition 4.4. [Ex-post equilibrium utility] *The equilibrium utility of each server g is*

$$u_g(\mathbf{s}^* | \Sigma_g, \mathbf{es}_g^t, h^{*,t+1}) = V^*(\Sigma, \mathbf{es}^t, \tau^t) - V^{-g}(\Sigma_{-g}, \mathbf{es}_{-g}^t, \tau_{-g}^t). \quad (4.31)$$

In addition to the property of incentive compatibility, the proposed node activation mechanism also achieves several desirable properties, including maximum system data fidelity, budget balance, and individual rationality, all in the ex-post manner [34]. Maximum system data fidelity means that the node activation is the most efficient since no other node activation can achieve greater system data fidelity.

Theorem 4.2. [Maximum ex-post system data fidelity] *The proposed node activation mechanism achieves maximum ex-post system data fidelity. Mathematically, the equilibrium node activation $\mathbf{a}^{*,\langle q \geq t \rangle}$ maximizes the ex-post system data fidelity:*

$$\mathbf{a}^{*,\langle q \geq t \rangle} = \arg \max_{\mathbf{a}^{\langle q \geq t \rangle}} \sum_{g \in \mathcal{G}} \sum_{t=0}^{\infty} \beta^t \mathbb{E} [v_g(\mathbf{a}_g^q, \Sigma_g^q, \mathbf{es}_g^q, \tau_g^q) | \Sigma, \mathbf{es}^t, \tau^t]. \quad (4.32)$$

Proof. The proposed node activation policy is designed to maximize the system data fidelity as shown in Design 4.1. Therefore, the proof follows Design 4.1 and Theorem 4.1. □

Budget balance means that the payment is always made from the servers to the BS. This is desirable as the BS does not need to pay the servers to ensure truthful feedback [34]. We show that the proposed node activation mechanism achieves ex-post budget balance.

Theorem 4.3. [Ex-post budget balance] *The proposed node activation mechanism is ex-post budget-balanced.*

$$\sum_{g \in \mathcal{G}} \sum_{q=t}^{\infty} \beta^{q-t} \mathbb{E} [\rho_g^{*,q} | \Sigma_g, \mathbf{es}_g^t, h^{*,t+1}] \geq 0. \quad (4.33)$$

Proof. Since π^{-g} maximizes the system data fidelity with server g excluded from the

system, we know

$$V^{-g}(\Sigma_{-g}, \mathbf{es}_{-g}^t, \tau_{-g}^t) \geq V^*(\Sigma, \mathbf{es}^t, \tau^t). \quad (4.34)$$



Therefore, (4.33) can be derived from (4.30) and (4.34). \square

Lastly, individual rationality means that all servers will join the proposed node activation mechanism since they can obtain as much utility as without joining.

Theorem 4.4. [*Ex-post individual rationality*] *The proposed node activation mechanism is ex-post individual rational.*

$$u_g(\mathbf{s}^* | \Sigma_g, \mathbf{es}_g^t, h^{*,t+1}) \geq 0 \quad \forall g \in \mathcal{G}. \quad (4.35)$$

Proof. Since π^* maximizes the ex-post system data fidelity, we know

$$V^*(\Sigma, \mathbf{es}^t, \tau^t) \geq V^{-g}(\Sigma_{-g}, \mathbf{es}_{-g}^t, \tau_{-g}^t). \quad (4.36)$$

From (4.31) and (4.36), we have (4.35). \square

To sum up, the proposed node activation mechanism is ex-post incentive compatible that reaches the perfect ex-post equilibrium where the server and the nodes feedback the true data statistics and energy states in each time slot, respectively. At the truth-revealing equilibrium, the system achieves the maximum ex-post system data fidelity. The BS charges the servers for node activation from the concept of user pays. There will be no net payment from the BS to the servers to ensure truthful feedback (ex-post budget balance). Also, the servers will join the proposed node activation mechanism as they can obtain as much utility as without joining (ex-post individual rationality).

4.7 Further Discussions

We first show the complexity of the value iteration algorithm. Since the data statistics are not time-varying and the activation intervals are deterministic that do not need to

be feedbacked, we focus on the energy states $\mathbf{es}^{(t)}$ in the following analysis. To derive the value function V^* and the node activation policy π^* , the number of iterations is $\text{Poly}(|\mathcal{ES}|^{\sum_{g \in \mathcal{G}} |\mathcal{I}_g|}, |\mathcal{A}|, \frac{1}{1-\beta})$ and the worst-case computational complexity per iteration is $O(|\mathcal{ES}|^{2 \sum_{g \in \mathcal{G}} |\mathcal{I}_g|} |\mathcal{A}|)$ where $|\mathcal{A}|$ is the number of possible node activation [66]. As the proposed node activation mechanism requires feedback in each time slot, to reduce the signalling overhead, we propose two methods – one with synchronous feedback and the other with asynchronous feedback – in Chapters 4.7.1 and 4.7.2, respectively. We also show the trade-off between the complexity and signalling overhead. In addition, recall in Chapter 4.3.2 that each node's energy arrivals are assumed to be i.i.d. in each time slot. We discuss how this assumption can be generalized to stationary and Markov energy arrivals in Chapter 4.7.3. Lastly, channels are assumed to be perfect throughout the paper. We also discuss how the proposed node activation mechanism can work in time-varying channels in Chapter 4.7.3.

4.7.1 Synchronous Feedback per n Time Slots

To reduce the signalling overhead to $1/n$, we can allow each node to feedback the energy state per n time slots. In this case, the node activation policy is $\psi^{*, \langle 0 \leq q \leq n-1 \rangle}$ that decides the node activation in time slot $(nl + q)$ based on the feedback energy state in time slot nl , i.e., $\mathbf{a}^{nl+q} = \psi^{*,q}(\hat{\mathbf{e}}\mathbf{s}^{nl})$. The node activation policy is designed to maximize the system data fidelity seen in each time slot nl where the value function is denoted by Ψ^* . To simplify the notation, we also denote $v(\mathbf{a}^t, \mathbf{es}^t) = \sum_{g \in \mathcal{G}} v_g(\mathbf{a}_g^t, \mathbf{es}_g^t)$.

Design 4.3. [Node activation policy and value function for synchronous feedback per n time slots] The node activation policy $\psi^{*, \langle 0 \leq q \leq n-1 \rangle}$ and the value function Ψ^* are derived as follows:

$$\psi^{*, \langle 0 \leq q \leq n-1 \rangle}(\mathbf{es}^0) = \arg \max_{\mathbf{a}^{\langle 0 \leq q \leq n-1 \rangle}} \Psi(\mathbf{a}^{\langle 0 \leq q \leq n-1 \rangle}, \mathbf{es}^0), \quad (4.37)$$

$$\Psi^*(\mathbf{es}^0) = \Psi(\psi^{*, \langle 0 \leq q \leq n-1 \rangle}, \mathbf{es}^0), \quad (4.38)$$



where

$$\begin{aligned} \Psi(\mathbf{a}^{(0 \leq q \leq n-1)}, \mathbf{es}^0) = & v(\mathbf{a}^0, \mathbf{es}^0) + \sum_{q=1}^{n-1} \beta^q \sum_{\mathbf{es}^q} E^q(\mathbf{es}^q | \mathbf{es}^0, \mathbf{a}^{(0 \leq l \leq q-1)}) v(\mathbf{a}^q, \mathbf{es}^q) \\ & + \beta^n \sum_{\mathbf{es}^n} E^n(\mathbf{es}^n | \mathbf{es}^0, \mathbf{a}^{(0 \leq l \leq n-1)}) \Psi^*(\mathbf{es}^n), \end{aligned} \quad (4.39)$$

and $E^q(\mathbf{es}^q | \mathbf{es}^0, \mathbf{a}^{(0 \leq l \leq q-1)})$ for $1 \leq q \leq n$ is the q -step transition function satisfying

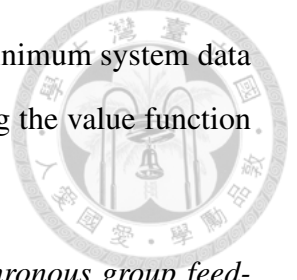
$$E^q(\mathbf{es}^q | \mathbf{es}^0, \mathbf{a}^{(0 \leq l \leq q-1)}) = \sum_{\mathbf{es}^1, \dots, \mathbf{es}^{q-1}} \prod_{l=1}^q E(\mathbf{es}^l | \mathbf{es}^{l-1}, \mathbf{a}^{l-1}). \quad (4.40)$$

Comparing (4.12) and (4.38), we know $V^* \geq \Psi^*$. To solve (4.38) via the value iteration algorithm, the number of iterations becomes $\text{Poly}(|\mathcal{ES}|^{\sum_{g \in \mathcal{G}} |\mathcal{I}_g|}, |\mathcal{A}|^n, \frac{1}{1-\beta^n})$ but each iteration becomes more costly with the time complexity $O(|\mathcal{ES}|^{2 \sum_{g \in \mathcal{G}} |\mathcal{I}_g|} |\mathcal{A}|^n)$. Therefore, reducing the signalling overhead by synchronous feedback per n time slots brings lower system data fidelity and higher time complexity. To further reduce the time complexity, we can add a constraint that the node activations are the same in the n time slots, i.e., $\psi^{*,0} = \psi^{*,1} = \dots = \psi^{*,n-1}$. In this way, the system data fidelity should be even lower but the number of iterations and the time complexity of each iteration both decrease to $\text{Poly}(|\mathcal{ES}|^{\sum_{g \in \mathcal{G}} |\mathcal{I}_g|}, |\mathcal{A}|, \frac{1}{1-\beta^n})$ and $O(|\mathcal{ES}|^{2 \sum_{g \in \mathcal{G}} |\mathcal{I}_g|} |\mathcal{A}|)$, respectively.

4.7.2 Asynchronous Group Feedback

To reduce the signalling overhead to $1/n$, another method is partition the servers into n groups where each group is denoted by \mathcal{C}_q for $q = 0, 1, \dots, n-1$. (Note that a group can be empty. Also note that the nodes of the same server must be in the same group; otherwise, the property of truth-revelation will not hold.) We allow each group \mathcal{C}_q to feedback the energy state $\hat{\mathbf{es}}_{\mathcal{C}_q}^{nl+q}$ in each time slot $(nl+q)$. In this case, the node activation policy is $\phi^{*,(0 \leq q \leq n-1)}$ that decides the node activation in time slot $(nl+q)$ based on group \mathcal{C}_q 's feedback energy states, i.e., $\mathbf{a}^{nl+q} = \phi^{*,q}(\hat{\mathbf{es}}_{\mathcal{C}_q}^{nl+q})$. Note that the BS only has the feedback energy state from group \mathcal{C}_q in each time slot $(nl+q)$. As we want to prevent the BS from memorizing the feedback energy states of the other groups in the previous

time slots, the node activation policy is designed to maximize the minimum system data fidelity given all possible energy states of the other groups. Denoting the value function in each time slot $(nl + q)$ by $\Phi^{*,q}$, we have the following designs:



Design 4.4. [Node activation policy and value functions for asynchronous group feedback] The node activation policy $\phi^{*,\langle 0 \leq q \leq n-1 \rangle}$ and the value functions $\Phi^{*,\langle 0 \leq q \leq n-1 \rangle}$ are derived as follows:

$$\phi^{*,q}(\mathbf{es}_{C_q}^q) = \arg \max_{\mathbf{a}^q} \left[\min_{\mathbf{es}_{-C_q}^q} \Phi^q(\mathbf{a}^q, \mathbf{es}^q) \right], \quad (4.41)$$

$$\Phi^{*,q}(\mathbf{es}^q) = \Phi^q(\phi^{*,q}, \mathbf{es}^q), \quad (4.42)$$

for $q = 0, 1, \dots, n - 1$, where

$$\Phi^q(\mathbf{a}^q, \mathbf{es}^q) = v(\mathbf{a}^q, \mathbf{es}^q) + \beta \sum_{\mathbf{es}^{q+1}} E(\mathbf{es}^{q+1} | \mathbf{es}^q, \mathbf{a}^q) \Phi^{*,(q+1)_n}(\mathbf{es}^{q+1}), \quad (4.43)$$

and $(\cdot)_n$ means modulus of n .

We know $V^* \geq \Phi^{*,q}$ by comparing (3.42) and (4.42). The number of iterations for solving each equation in (4.42) is $\text{Poly}(|\mathcal{ES}|^{\sum_{g \in \mathcal{G}} |I_g|}, |\mathcal{A}|, \frac{1}{1-\beta})$ and the time complexity of each iteration is $O(|\mathcal{ES}|^2 \sum_{g \in \mathcal{G}} |I_g| |\mathcal{A}|)$. Since there are n equations in (4.42), the total number of iterations is n times. Therefore, reducing the signalling overhead by asynchronous group feedback brings lower system data fidelity and more iterations with the same time complexity.

4.7.3 Stationary, Markov Energy Arrivals and Time-Varying Channels

We consider a more general case that each node has stationary and Markov energy arrivals. In the following analysis, we still omit the data statistics and node activations for simplicity. Specifically, the energy arrivals in time slot t , denoted by \mathbf{e}^t , are assumed to be

stationary and Markov. Then, according to (4.3) with $e_{i,g}$ replaced by $e_{i,g}^{t+1}$, we can derive the stationary and Markov energy state transition function as $E(\mathbf{es}^{t+1}, \mathbf{e}^{t+1} | \mathbf{es}^t, \mathbf{e}^t, \mathbf{a}^t)$. Just as in Chapter 4.3.3, we assume that the BS knows the energy state transition E . The BS does not know the exact energy state \mathbf{es}^t and energy arrivals \mathbf{e}^t and thus requires the feedback of them. The Bellman equation for the value function becomes

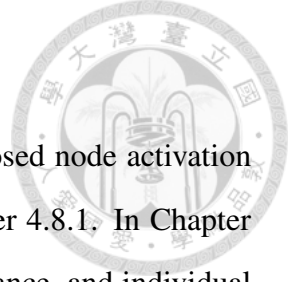
$$V^*(\mathbf{es}^t, \mathbf{e}^t) = \max_{\mathbf{a}^t} \left[v(\mathbf{a}^t, \mathbf{es}^t) + \beta \sum_{\mathbf{es}^{t+1}, \mathbf{e}^{t+1}} E(\mathbf{es}^{t+1}, \mathbf{e}^{t+1} | \mathbf{es}^t, \mathbf{e}^t, \mathbf{a}^t) V^*(\mathbf{es}^{t+1}, \mathbf{e}^{t+1}) \right]. \quad (4.44)$$

One can note that if the energy arrivals are i.i.d., (4.44) reduces to (3.42).

On the other hand, we have assumed perfect channels so far in this chapter. However, we can also model the time-varying channels by assuming that each node experiences the constant channel quality in a time slot, and the channel quality has the Markov transition over time slots [54, 55]. To be specific, each node (i, g) has the packet success probability, i.e., the channel state, $cs_{i,g}^t \in \mathcal{CS}_{i,g}$ in each time slot t where $\mathcal{CS}_{i,g}$ is the set of possible channel states. The system channel state is denoted by $\mathbf{cs}^t = (cs_{i,g}^t)_{i \in \mathcal{N}_g, g \in \mathcal{G}}$ with the Markov transition function $C(\mathbf{cs}^{t+1} | \mathbf{cs}^t)$. Since the channels are uplink from the nodes to the BS, the BS is assumed to know the channel states and no feedback is required. The system data fidelity should be a function of the energy states and channel states, i.e., $v(\mathbf{a}^t, \mathbf{es}^t, \mathbf{cs}^t)$. The Bellman equation for the value function becomes

$$V^*(\mathbf{es}^t, \mathbf{cs}^t) = \max_{\mathbf{a}^t} \left[v(\mathbf{a}^t, \mathbf{es}^t, \mathbf{cs}^t) + \beta \sum_{\mathbf{es}^{t+1}, \mathbf{cs}^{t+1}} E(\mathbf{es}^{t+1} | \mathbf{es}^t, \mathbf{a}^t) C(\mathbf{cs}^{t+1} | \mathbf{cs}^t) V^*(\mathbf{es}^{t+1}, \mathbf{cs}^{t+1}) \right]. \quad (4.45)$$

With the assumptions of stationary and Markov energy arrivals and time-varying channels, our proposed node activation mechanism can still work to have the same desirable properties of ex-post incentive compatibility, maximum system data fidelity, budget balance, and individual rationality.



4.8 Numerical Results

In this section, numerical results are presented to evaluate the proposed node activation mechanism. The general set-up of the parameters is given in Chapter 4.8.1. In Chapter 4.8.2, we verify the properties of incentive compatibility, budget balance, and individual rationality. In Chapter 4.8.3, we change various parameters to show their impacts on the system data fidelity. Lastly, the comparison of the synchronous feedback per n time slots and asynchronous group feedback in the system data fidelity and the complexity is given in Chapter 4.8.4.

4.8.1 Parameter Setting

The number of servers is $\mathcal{G} = \{1, 2\}$. Each server has 3 nodes, $\mathcal{I}_g = \{1, 2, 3\}$. The 6 nodes are uniformly deployed in a rectangular area where the BS is in the center. The BS has the number of resource blocks $R = 2$ in each time slot. The energy capacity of each node (i, g) is $EC_{i,g} = 1$. Each node has i.i.d. Bernoulli energy arrivals in each time slot with mean uniformly generated from $[0, 1]$. For each server g , the spatial-temporal covariance of any two data points whose locations are x_1 and x_2 and whose time are t_1 and t_2 is given as $\sigma^2 \exp\left(-\frac{\|x_1 - x_2\|}{l_x}\right) \exp\left(-\frac{|t_1 - t_2|}{l_t}\right)$, with the variance $\sigma^2 = 1$, the spatial kernel $l_x = 5$, and the temporal kernel $l_t = 1$. The discount factor is $\beta = 0.9$ and the threshold for the value iteration algorithm is $\epsilon = 10^{-6}$. The results are plotted for a single network instance if not specially mentioned.

4.8.2 Verification of Incentive Compatibility, Budget Balance, and Individual Rationality

We first verify the property of incentive compatibility, i.e., truth-revelation. Each server has 8 possible feedback energy states (2 possible energy states of 3 nodes). We also assume that each server can feedback 3 different values of the spatial kernel $l_x = 0, 5, 10$ and 3 different values of the temporal kernel $l_t = 0, 1, 2$. Fig. 4.3(a) shows that each server always achieves the highest utility when feedbacking the true energy states and the

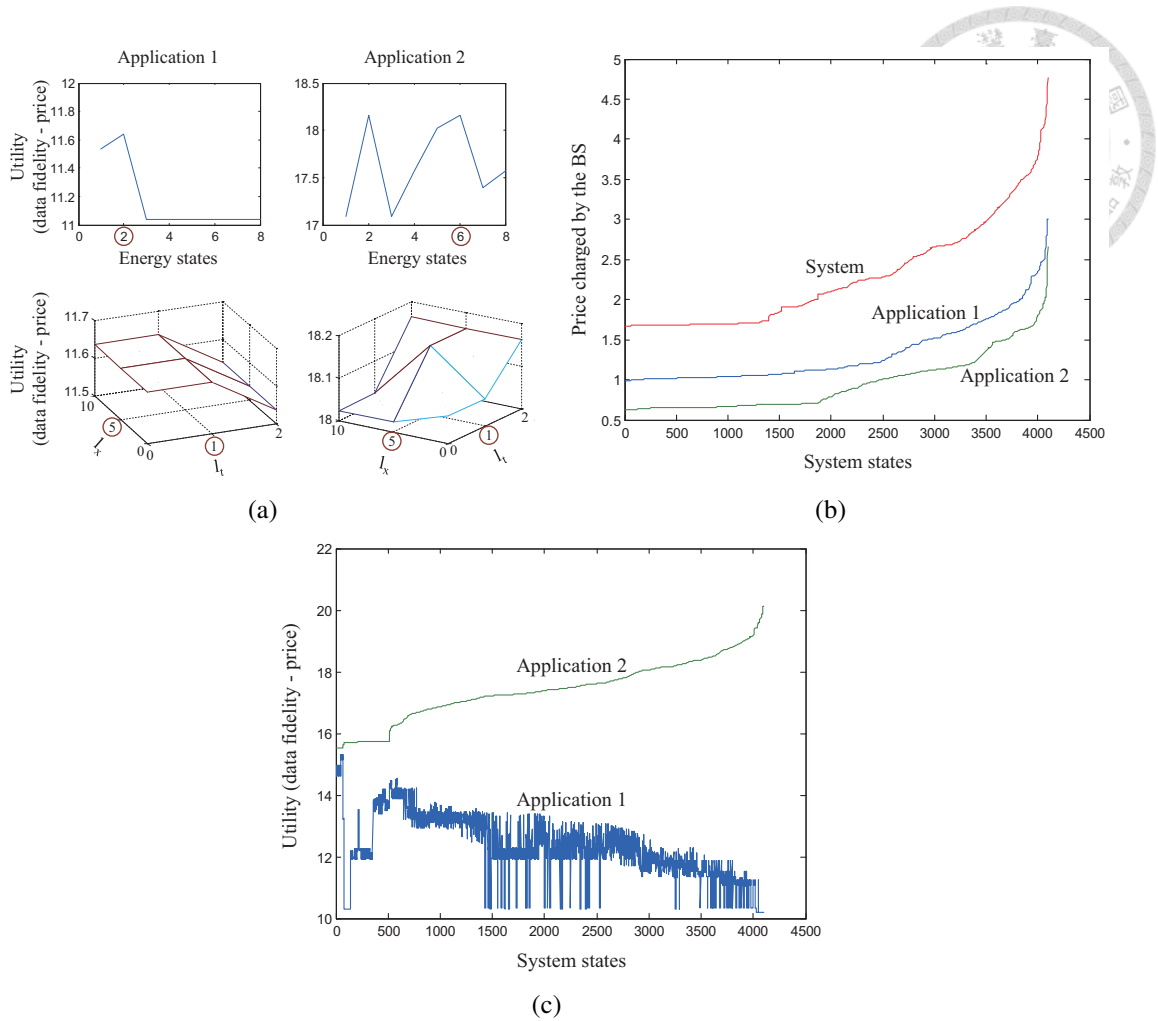


Figure 4.3: Incentive compatibility, budget balance, and individual rationality: (a) The utility of each server under all possible one-shot deviation strategies in time slot 0. (b) The price charged by the BS in all system states. (c) The utility of each server in all system states.

true spatial-temporal kernel values (the true values are circled). Therefore, each server will feedback the true energy state and data statistics, which then ensures incentive compatibility. In the following figures, we sort the curve with the highest value in ascending order for better presentation. Fig. 4.3(b) shows the price charged by the BS in all system states, where a system state means the collection of the energy state and activation interval of each node. It can be seen that the price charged to each server and the overall price are always greater than zero in all system states. Therefore, the payment is always made to the BS (budget balance). Fig. 4.3(c) shows that the utility of each server is always greater than zero in all system states. This then verifies individual rationality: each server will join the proposed node activation mechanism as it always obtains utility greater than or

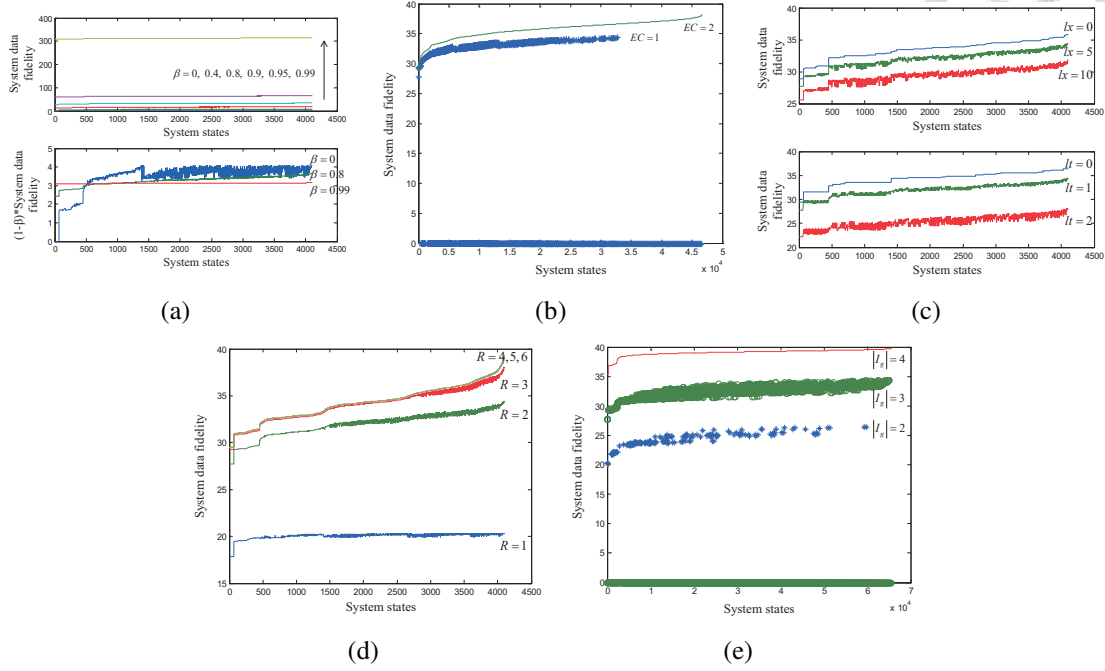
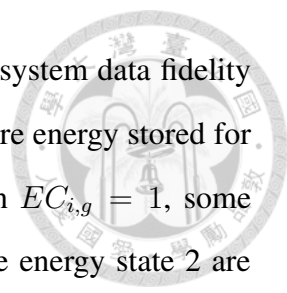


Figure 4.4: Impacts of the parameter change on the system data fidelity: (a) The discount factor $\beta = 0, 0.4, 0.8, 0.9, 0.95, .099$. (b) The energy capacity $EC_{i,g} = 1, 2$. (c) The spatial kernel $l_x = 0, 5, 10$ and the temporal kernel $l_t = 0, 1, 2$. (d) The number of resource blocks $R = 1, 2, 3, 4, 5, 6$. (e) The number of nodes $|I_g| = 2, 3, 4$.

equal to zero. Due to the resource constraint, when the utility of server 1 goes up, the utility of server 2 goes down.

4.8.3 Impacts of Parameter Change

We change the values of different parameters to show their impacts on the system data fidelity. Given different values of the discount factor $\beta = 0, 0.4, 0.8, 0.9, 0.95, 0.99$, the upper plot of Fig. 4.4(a) shows that the system data fidelity is higher when the discount factor is higher since more future data fidelity is taken into account. Another way is to see the normalized system data fidelity, i.e., the system data fidelity times $(1 - \beta)$. As shown in the lower plot of Fig. 4.4(a), when $\beta = 0$, the normalized system data fidelity, i.e., the one-shot system data fidelity, varies from zero to 4 in different system states. However, when $\beta = 0.99$, the normalized system data fidelity is quite stable above 3 in all system states. This is because even if the one-shot system data fidelity may be high or low ($\beta = 0$), the long-term performance of the system data fidelity is more stable by averaging the system data fidelity in more future time slots. In Fig. 4.4(b),



by varying the energy capacity $EC_{i,g}$ of each node from 1 to 2, the system data fidelity becomes higher. The reason is that higher energy capacity means more energy stored for future activation and thus higher future system data fidelity. (When $EC_{i,g} = 1$, some points have zero value since the system states where nodes have the energy state 2 are not feasible.) We also vary the values of the spatial kernel $l_x = 0, 5, 10$ and the temporal kernel $l_t = 0, 1, 2$ in Fig. 4.4(c) and find that the system data fidelity is higher when the values of the kernels are smaller. In fact, smaller values of kernels mean the data are less correlated. Therefore, each node activation should obtain more new information and thus higher system data fidelity. Revealed in Fig. 4.4(d), by varying the number of resource blocks $R = 1, 2, 3, 4, 5, 6$, the system data fidelity becomes higher. However, there is no significant increase in the system data fidelity when $R = 4, 5, 6$ as the probability that more than 5 or 6 nodes have energy to be activated in a time slot is relatively small. Lastly, we vary the number of the nodes of each server $|\mathcal{I}_g| = 2, 3, 4$. Fig. 4.4(e) reveals that the system data fidelity is higher when each server has more nodes to sense the data. (When $|\mathcal{I}_g| = 2, 3$, some points have zero value since the system states where the fourth node of each server has non-zero energy state are not feasible.)

4.8.4 Performance Comparison of Synchronous and Asynchronous Feedback Designs

In Chapters 4.7.1 and 4.7.2, we propose two schemes to reduce the signaling overhead. Here we show their trade-offs in the system data fidelity and the complexity. As shown in Figs. 4.5(a) and 4.5(b), we have the highest system data fidelity and the lowest complexity under feedback per time slot. When reducing the signaling overhead to $1/2$ and $1/3$ by synchronous feedback per 2 and 3 time slots, the system data fidelity reduces to 93% and 88% and the complexity becomes 13 times and 199 times, respectively. On the other hand, When reducing the signaling overhead to $1/2$ by asynchronous 2-group feedback, the system data fidelity reduces to 82%. This is the lowest among all schemes since we use the "max min" optimization criterion to prevent the BS from memorizing the feedback energy states in the previous time slots. However, the complexity is only 2.5 times that is

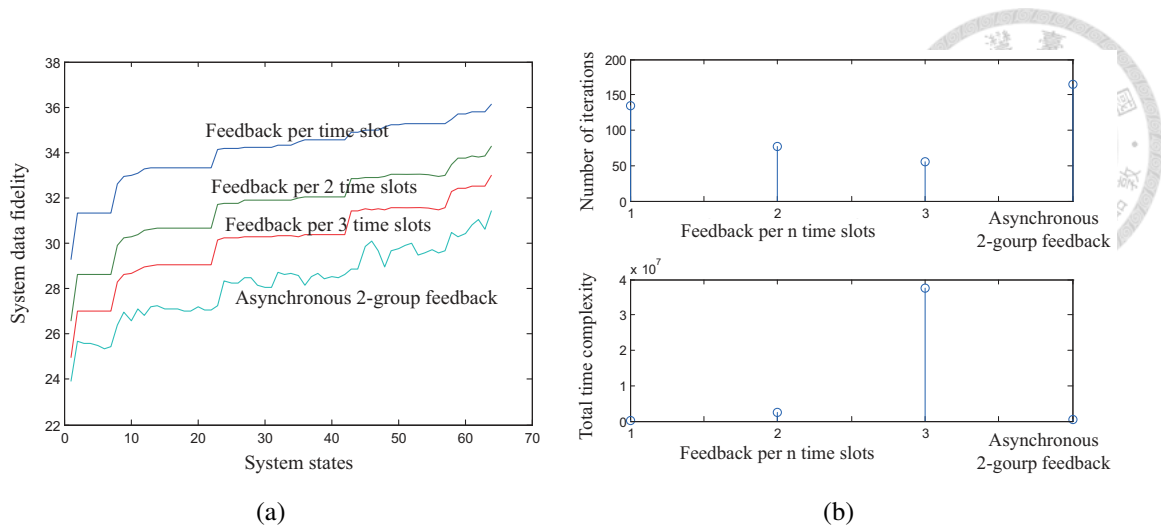


Figure 4.5: Comparison of the synchronous and the asynchronous feedback designs: (a) The system data fidelity. (b) The complexity.

quite lower than that of feedback per 2 and 3 time slots.

4.9 Summary

In this chapter, we investigate the node activation decision problem in the energy-harvesting IoT. We model time-varying harvested energy, limited radio resources and spatial-temporal data correlations. From the viewpoint of incentive mechanism design, we also consider the rational and selfish characteristics of servers and incomplete information on the data statistics and the energy states. Our theoretic analysis shows that the proposed node activation mechanism is incentive compatible. That is, the network operates at the truth-revealing equilibrium where each server and each node feedback the true data statistics and energy states, respectively. With truthful feedback, the network operation also achieves the desirable properties of maximum system data fidelity, budget balance, and individual rationality. From the algorithmic viewpoint, the value iteration algorithm is proposed to solve the optimal node activation policy. The numerical results also verify our theoretical findings.



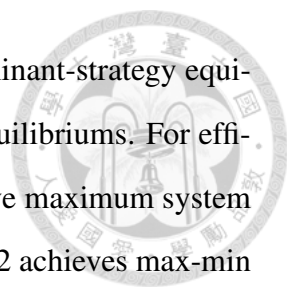
Chapter 5

Conclusions

Table 5.1: Summary of the significant results

	Time horizon	Truthful equilibrium	Efficiency	Fairness	Budget balance	Individual rationality
Multimedia multicast (Chapter 2)	One-shot	Dominant-strategy	Pareto	Max-min and proportional	Yes	Access control
Small data multicast (Chapter 3)	Infinite	Perfect ex-post	Max system throughput		Yes	Yes
Correlated data gathering (Chapter 4)	Infinite	Perfect ex-post	Max system data fidelity		Yes	Yes

In this dissertation, we first indicate the importance of radio resource allocation in the IoT. We also consider selfishness of IoT devices and incomplete information of the network environment. This dissertation then takes a mechanism design approach to addressing the resource allocation problems for IoT information gathering and multicast distribution. In Chapter 2, the multi-flow multimedia multicast is studied. The users' private CQI are also considered. Chapter 3 addresses multi-flow multicast for common data transmissions over time-varying channels for energy-harvesting devices. We also consider the incomplete state information of the devices. Chapter 4 solves the activation decision for energy-harvesting sensors to gather information and transmit to servers. We model time-varying harvested energy, limited radio resources and spatial-temporal data correlations. We also consider the incomplete information on the data statistics and the energy states. Traditional solutions may not work as they did not consider selfishness of the devices and incomplete information of the network environment. This dissertation then has significant contributions in proposing the novel resource allocation mechanisms to induce truthful feedback of the incomplete information and to achieve desirable prop-



erties in the equilibria. Specifically, Chapter 2 achieves truthful dominant-strategy equilibrium whereas Chapters 3 and 4 achieve truthful perfect ex-post equilibria. For efficiency, Chapter 2 achieves Pareto efficiency. Chapters 3 and 4 achieve maximum system throughput and maximum system data fidelity, respectively. Chapter 2 achieves max-min fairness and proportional fairness. Though Chapter 3 does not achieve specific fairness metrics, the proposed weight design brings fairness resource allocation to some extent as justified in the numerical result. Budget balance is guaranteed in all chapters as the proposed mechanisms ensures that the BS does not need to pay to ensure truth-revelation. Lastly, Chapter 2 achieves access control. Only devices with channel quality higher than the system-defined threshold will join the proposed mechanism to gain non-negative utility. Individual rationality is achieved in both Chapters 3 and 4. All devices and servers will join the proposed mechanisms to gain non-negative utility. We summarize the significant results in Table 5.1.

For future research, multimedia sensing and multimedia data processing may be one direction. How to model the characteristics of multimedia data and to provide efficient resource allocation are worth investigating. This also completes the multimedia data flow from gathering to distribution in the IoT. On the other hand, the value iteration algorithms are used to derive resource allocation policies in this dissertation. We have discussed some methods in Chapters 3.8.1, 4.7.1, and 4.7.2. We may investigate faster and more efficient algorithms to derive the optimal or sub-optimal solutions. With our current research results and future endeavors, our long-term goal is to complete resource allocation mechanism design for the IoT, solving the issues of selfishness and incomplete information of devices, enhancing network performance, and ultimately achieving greater user utility.



Appendix A

Proofs for Lemmas 2.1, 2.3, and 2.4

A.1 Lemma 2.1

Proof. We only prove the case of the loss-tolerant flows. The proof for the loss-sensitive flows is quite similar, so we skip it for simplicity. For the loss-tolerant flows, we prove that $v_g(e_{i,g}, A_g)$ is strictly decreasing with respect to $e_{i,g}$ by showing that $\frac{\partial v_g(e_{i,g}, A_g)}{\partial e_{i,g}} \leq 0$ for $0 \leq e_{i,g} \leq 1$.



$$\begin{aligned}
& \frac{\partial v_g(e_{i,g}, A_g)}{\partial e_{i,g}} \\
&= \sum_{j=0}^{A_g} \min \left\{ 1, \frac{j}{M_g} \right\} \binom{A_g}{j} \left[-j(1 - e_{i,g})^{j-1} e_{i,g}^{A_g-j} + (A_g - j)(1 - e_{i,g})^j e_{i,g}^{A_g-j-1} \right] \\
&= \sum_{j=0}^{A_g} \min \left\{ 1, \frac{j}{M_g} \right\} \binom{A_g}{j} (1 - e_{i,g})^{j-1} e_{i,g}^{A_g-j-1} [-j e_{i,g} + (A_g - j)(1 - e_{i,g})] \\
&= \sum_{j=0}^{A_g} \min \left\{ 1, \frac{j}{M_g} \right\} \binom{A_g}{j} (1 - e_{i,g})^{j-1} e_{i,g}^{A_g-j-1} [A_g(1 - e_{i,g}) - j] \\
&= \sum_{j=0}^{A_g} \min \left\{ 1, \frac{j}{M_g} \right\} \binom{A_g}{j} A_g (1 - e_{i,g})^j e_{i,g}^{A_g-j-1} \\
&\quad - \sum_{j=0}^{A_g} \min \left\{ 1, \frac{j}{M_g} \right\} \binom{A_g}{j} j (1 - e_{i,g})^{j-1} e_{i,g}^{A_g-j-1} \\
&= \sum_{j=0}^{A_g} \min \left\{ 1, \frac{j}{M_g} \right\} \binom{A_g}{j} A_g (1 - e_{i,g})^j e_{i,g}^{A_g-j-1} \\
&\quad - \sum_{j=1}^{A_g} \min \left\{ 1, \frac{j}{M_g} \right\} \binom{A_g - 1}{j - 1} A_g (1 - e_{i,g})^{j-1} e_{i,g}^{A_g-j-1} \\
&\stackrel{(a)}{=} \sum_{j=0}^{A_g-1} \min \left\{ 1, \frac{j}{M_g} \right\} \binom{A_g - 1}{j} A_g (1 - e_{i,g})^j e_{i,g}^{A_g-j-1} \\
&\quad + \sum_{j=1}^{A_g} \min \left\{ 1, \frac{j}{M_g} \right\} \binom{A_g - 1}{j - 1} A_g (1 - e_{i,g})^j e_{i,g}^{A_g-j-1} \\
&\quad - \sum_{j=1}^{A_g} \min \left\{ 1, \frac{j}{M_g} \right\} \binom{A_g - 1}{j - 1} A_g (1 - e_{i,g})^{j-1} e_{i,g}^{A_g-j-1} \\
&= \sum_{j=0}^{A_g-1} \min \left\{ 1, \frac{j}{M_g} \right\} \binom{A_g - 1}{j} A_g (1 - e_{i,g})^j e_{i,g}^{A_g-j-1} \\
&\quad - \sum_{j=1}^{A_g} \min \left\{ 1, \frac{j}{M_g} \right\} \binom{A_g - 1}{j - 1} A_g (1 - e_{i,g})^{j-1} e_{i,g}^{A_g-j} \\
&= \sum_{j=0}^{A_g-1} \min \left\{ 1, \frac{j}{M_g} \right\} \binom{A_g - 1}{j} A_g (1 - e_{i,g})^j e_{i,g}^{A_g-j-1} \\
&\quad - \sum_{j'=0}^{A_g-1} \min \left\{ 1, \frac{j'+1}{M_g} \right\} \binom{A_g - 1}{j'} A_g (1 - e_{i,g})^{j'} e_{i,g}^{A_g-j'-1} \\
&= - \sum_{j=0}^{M_g-1} \frac{A_g}{M_g} \binom{A_g - 1}{j} (1 - e_{i,g})^j e_{i,g}^{A_g-j-1} \leq 0. \tag{A.1}
\end{aligned}$$

where (a) uses the combinatorial equality $\binom{A_g}{j} = \binom{A_g-1}{j} + \binom{A_g-1}{j-1}$ for $0 \leq j \leq A_g$. Note that the equality of (A.1) holds if and only if $e_{i,g} = 0$ and 1. Therefore, $v_g(e_{i,g}, A_g)$ is strictly decreasing with respect to $e_{i,g}$. We also prove that $v_g(e_{i,g}, A_g)$ is strictly increasing with respect to A_g by showing that $v_g(e_{i,g}, A_g + 1) - v_g(e_{i,g}, A_g) \geq 0 \forall A_g \geq 0$.

$$\begin{aligned}
v_g(e_{i,g}, A_g + 1) &= \sum_{j=0}^{A_g+1} \min \left\{ 1, \frac{j}{M_g} \right\} \binom{A_g+1}{j} (1 - e_{i,g})^j e_{i,g}^{A_g+1-j} \\
&\stackrel{(b)}{=} \sum_{j=0}^{A_g} \min \left\{ 1, \frac{j}{M_g} \right\} \binom{A_g}{j} (1 - e_{i,g})^j e_{i,g}^{A_g+1-j} \\
&\quad + \sum_{j=1}^{A_g+1} \min \left\{ 1, \frac{j}{M_g} \right\} \binom{A_g}{j-1} (1 - e_{i,g})^j e_{i,g}^{A_g+1-j}, \quad (A.2)
\end{aligned}$$

where (b) uses the combinatorial equality $\binom{A_g}{j} = \binom{A_g-1}{j} + \binom{A_g-1}{j-1}$ for $0 \leq j \leq A_g$.

$$v_g(e_{i,g}, A_g) = \sum_{j=0}^{A_g} \min \left\{ 1, \frac{j}{M_g} \right\} \binom{A_g}{j} (1 - e_{i,g})^j e_{i,g}^{A_g-j}, \quad (A.3)$$

$$\begin{aligned}
v_g(e_{i,g}, A_g + 1) - v_g(e_{i,g}, A_g) &= - \sum_{j=0}^{A_g} \min \left\{ 1, \frac{j}{M_g} \right\} \binom{A_g}{j} (1 - e_{i,g})^{j+1} e_{i,g}^{A_g-j} \\
&\quad + \sum_{j=1}^{A_g+1} \min \left\{ 1, \frac{j}{M_g} \right\} \binom{A_g}{j-1} (1 - e_{i,g})^j e_{i,g}^{A_g+1-j} \\
&= - \sum_{j=0}^{A_g} \min \left\{ 1, \frac{j}{M_g} \right\} \binom{A_g}{j} (1 - e_{i,g})^{j+1} e_{i,g}^{A_g-j} \\
&\quad + \sum_{j'=0}^{A_g} \min \left\{ 1, \frac{j'+1}{M_g} \right\} \binom{A_g}{j'} (1 - e_{i,g})^{j'+1} e_{i,g}^{A_g-j'} \\
&= \sum_{j=0}^{M_g-1} \frac{1}{M_g} \binom{A_g}{j} (1 - e_{i,g})^{j+1} e_{i,g}^{A_g-j} \geq 0. \quad (A.4)
\end{aligned}$$

Also note that the equality of (A.4) holds if and only if $e_{i,g} = 0$ and 1. Therefore, $v_g(e_{i,g}, A_g)$ is strictly increasing with respect to A_g \square

A.2 Lemma 2.3

Proof. We only prove the loss-tolerant case. The proof for the loss-sensitive case is quite similar and thus skipped. We first prove that the gradient function is single-peaked with respect to $e_{i,g}$. Note that the gradient function

$$\Delta v_g(e_{i,g}, A_g) = v_g(e_{i,g}, A_g + 1) - v_g(e_{i,g}, A_g) = \sum_{j=0}^{M_g-1} \frac{1}{M_g} \binom{A_g}{j} (1 - e_{i,g})^{j+1} e_{i,g}^{A_g-j} \quad (\text{A.5})$$

Differentiating $\Delta v_g(e_{i,g}, A_g)$ with respect to $e_{i,g}$, we have

$$\begin{aligned} \frac{\partial \Delta v_g(e_{i,g}, A_g)}{\partial e_{i,g}} &= \binom{A_g}{M_g} (1 - e_{i,g})^{M_g} e_{i,g}^{A_g - M_g} - \frac{1}{M_g} \sum_{j=0}^{M_g-1} \binom{A_g}{j} (1 - e_{i,g})^j e_{i,g}^{A_g-j} \\ &= e_{i,g}^{A_g} \left[\binom{A_g}{M_g} \left(\frac{1 - e_{i,g}}{e_{i,g}} \right)^{M_g} - \frac{1}{M_g} \sum_{j=0}^{M_g-1} \binom{A_g}{j} \left(\frac{1 - e_{i,g}}{e_{i,g}} \right)^j \right] \end{aligned} \quad (\text{A.6})$$

Let $x = (1 - e_{i,g})/e_{i,g}$, and equivalently $e_{i,g} = 1/(1+x)$. Note that $e_{i,g}$ and x is one-to-one mapping. Also note that $e_{i,g}$ increases when x decreases, and vice versa. Substituting x into (A.6) and using $f(x, A_g)$ to denote $\frac{\partial \Delta v_g(e_{i,g}, A_g)}{\partial e_{i,g}}$ for short, we have

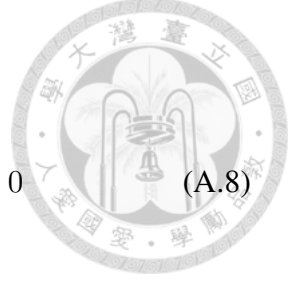
$$f(x, A_g) = \frac{\partial \Delta v_g(e_{i,g}, A_g)}{\partial e_{i,g}} = \left(\frac{1}{1+x} \right)^{A_g} \left[\binom{A_g}{M_g} x^{M_g} - \frac{1}{M_g} \sum_{j=0}^{M_g-1} \binom{A_g}{j} x^j \right] \quad (\text{A.7})$$

The term inside the square brackets is increasing with respect to x , from negative to positive (can be easily proved by the first-order differentiation). We denote the point that makes the term inside the square brackets equal to zero by $x^*(A_g)$. Besides, the term $\left(\frac{1}{1+x} \right)^{A_g}$ is always positive. Therefore, the function $f(x, A_g)$ is negative on $[0, x^*(A_g))$, zero at $x^*(A_g)$, and positive on $(x^*(A_g), \infty)$. In other words, the function $\frac{\partial \Delta v_g(e_{i,g}, A_g)}{\partial e_{i,g}}$, with respect to $e_{i,g}$, is positive on $[0, e_g^*(A_g))$, zero at $e_g^*(A_g)$, and negative on $(e_g^*(A_g), 1]$, where $e_g^*(A_g) = 1/(1 + x^*(A_g))$. That is, the gradient function $\Delta v_g(e_{i,g}, A_g)$ is single-peaked with respect to $e_{i,g}$, and is maximized at $e_g^*(A_g)$.

We continue to prove that the function $e_g^*(A_g)$ is strictly increasing with respect to A_g .

From (A.7), we know $x^*(A_g)$ satisfies

$$\binom{A_g}{M_g} (x^*(A_g))^{M_g} - \frac{1}{M_g} \sum_{j=0}^{M_g-1} \binom{A_g}{j} (x^*(A_g))^j = 0 \quad (\text{A.8})$$



Consider the function $f(x, A_g + 1)$

$$\begin{aligned} f(x, A_g + 1) &= \frac{\partial \Delta v_g(e_{i,g}, A_g + 1)}{\partial e_{i,g}} \\ &= \left(\frac{1}{1+x} \right)^{A_g+1} \left[\binom{A_g+1}{M_g} x^{M_g} - \frac{1}{M_g} \sum_{j=0}^{M_g-1} \binom{A_g+1}{j} x^j \right] \end{aligned} \quad (\text{A.9})$$

We prove the following to be true

$$\begin{aligned} &\binom{A_g+1}{M_g} (x^*(A_g))^{M_g} - \frac{1}{M_g} \sum_{j=0}^{M_g-1} \binom{A_g+1}{j} (x^*(A_g))^j \\ &\stackrel{(a)}{=} \binom{A_g}{M_g} (x^*(A_g))^{M_g} + \binom{A_g}{M_g-1} (x^*(A_g))^{M_g} - \frac{1}{M_g} \sum_{j=0}^{M_g-1} \binom{A_g}{j} (x^*(A_g))^j \\ &\quad - \frac{1}{M_g} \sum_{j=1}^{M_g-1} \binom{A_g}{j-1} (x^*(A_g))^j \\ &= \binom{A_g}{M_g-1} (x^*(A_g))^{M_g} - \frac{1}{M_g} \sum_{j=1}^{M_g-1} \binom{A_g}{j-1} (x^*(A_g))^j \\ &= \frac{M_g}{A_g - M_g + 1} \binom{A_g}{M_g} (x^*(A_g))^{M_g} - \frac{1}{M_g} \sum_{j=1}^{M_g-1} \binom{A_g}{j-1} (x^*(A_g))^j \\ &= \frac{1}{A_g - M_g + 1} \sum_{j=0}^{M_g-1} \binom{A_g}{j} (x^*(A_g))^j - \frac{1}{M_g} \sum_{j=1}^{M_g-1} \binom{A_g}{j-1} (x^*(A_g))^j \\ &= \frac{1}{A_g - M_g + 1} + \sum_{j=1}^{M_g-1} \left[\frac{1}{A_g - M_g + 1} \binom{A_g}{j} - \frac{1}{M_g} \binom{A_g}{j-1} \right] (x^*(A_g))^j > 0 \end{aligned} \quad (\text{A.10})$$

where (a) uses (A.8) and the combinatorial equality $\binom{A_g+1}{j} = \binom{A_g}{j} + \binom{A_g}{j-1}$ for $0 \leq j \leq M_g$. The last inequality of (A.10) holds since $\binom{A_g}{j}/(A_g - M_g + 1) - \binom{A_g}{j-1}/M_g > 0$ for

$j = 1, 2, \dots, M_g - 1$. From (A.9) and (A.10), we know

$$\left(\frac{1}{1+x^*(A_g)}\right)^{A_g+1} \left[\binom{A_g+1}{M_g} (x^*(A_g))^{M_g} - \frac{1}{M_g} \sum_{j=0}^{M_g-1} \binom{A_g+1}{j} (x^*(A_g))^j \right] > 0 \quad (\text{A.11})$$

Lastly, we know $x^*(A_g + 1) < x^*(A_g)$ according to (A.11) and the fact that the function $f(x, A_g + 1)$ is negative on $[0, x^*(A_g + 1))$, zero at $x^*(A_g + 1)$, and positive on $(x^*(A_g + 1), \infty)$. That is $x^*(A_g)$ is strictly decreasing with respect to A_g . In other words, $e_g^*(A_g)$ is strictly increasing with respect to A_g . \square

A.3 Lemma 2.4

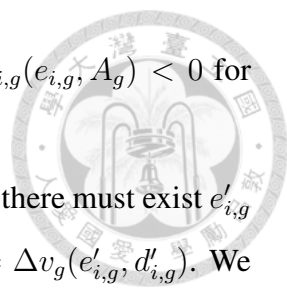
Proof. As we increase A_g , three possible relationships among $e_g^*(A_g)$, $e_{i,g}$, and $e_{c,g}$ will be as follows:

1. $e_g^*(A_g) \leq e_{i,g} < e_{c,g}$.
2. $e_{i,g} < e_g^*(A_g) \leq e_{c,g}$.
3. $e_{i,g} < e_{c,g} < e_g^*(A_g)$.

According Lemma 2.3, we know that the utility gradient function is positive in the first case and negative in the last case, shown as follows:

$$\begin{cases} \Delta u_{i,g}(e_{i,g}, A_g) > 0, & e_g^*(A_g) \leq e_{i,g} < e_{c,g} \\ \Delta u_{i,g}(e_{i,g}, A_g) < 0, & e_{i,g} < e_{c,g} < e_g^*(A_g) \end{cases} \quad (\text{A.12})$$

We also know that there must exist the smallest-value A_g , denoted by $d_{i,g}$, such that $\Delta u_{i,g}(e_{i,g}, d_{i,g}) \geq 0$ and $\Delta u_{i,g}(e_{i,g}, d_{i,g} + 1) < 0$. In the following, we derive the last inequality of (2.11), $\Delta u_{i,g}(e_{i,g}, A_g) < 0$ for $A_g > d_{i,g}$, from $\Delta u_{i,g}(e_{i,g}, d_{i,g} + 1) < 0$. We denote $(d_{i,g} + 1)$ by $d'_{i,g}$ for short. There are two possible relationships among $e_g^*(d'_{i,g})$, $e_{i,g}$, and $e_{c,g}$. If $e_{i,g} < e_{c,g} < e_g^*(d'_{i,g})$, as $e_g^*(A_g)$ is increasing with A_g , we know $e_{i,g} <$



$e_{c,g} < e_g^*(A_g)$ for $A_g > d_{i,g}$. According to (A.12), this implies $\Delta u_{i,g}(e_{i,g}, A_g) < 0$ for $A_g > d_{i,g}$.

If $e_{i,g} < e_g^*(d'_{i,g}) \leq e_{c,g}$, since $\Delta v_g(e_{i,g}, d'_{i,g})$ is continuous on $e_{i,g}$, there must exist $e'_{i,g}$ satisfying $e_{i,g} < e_g^*(d_{i,g}) \leq e_{c,g} < e'_{i,g}$ and such that $\Delta v_g(e_{i,g}, d'_{i,g}) = \Delta v_g(e'_{i,g}, d'_{i,g})$. We show $\Delta v_g(e_{i,g}, d'_{i,g} + 1) < \Delta v_g(e'_{i,g}, d'_{i,g} + 1)$ as below.

$$\begin{aligned}
 & \Delta v_g(e_{i,g}, d'_{i,g} + 1) < \Delta v_g(e'_{i,g}, d'_{i,g} + 1) \\
 \Leftrightarrow & \frac{1}{M_g} \sum_{j=0}^{M_g-1} \binom{d'_{i,g} + 1}{j} (1 - e_{i,g})^{j+1} e_{i,g}^{d'_{i,g}+1-j} \\
 & < \frac{1}{M_g} \sum_{j=0}^{M_g-1} \binom{d'_{i,g} + 1}{j} (1 - e'_{i,g})^{j+1} (e'_{i,g})^{d'_{i,g}+1-j} \\
 \Leftrightarrow & \sum_{j=0}^{M_g-1} \binom{d'_{i,g}}{j} (1 - e_{i,g})^{j+1} e_{i,g}^{d'_{i,g}+1-j} + \sum_{j=1}^{M_g-1} \binom{d'_{i,g}}{j-1} (1 - e_{i,g})^{j+1} e_{i,g}^{d'_{i,g}+1-j} \\
 & < \sum_{j=0}^{M_g-1} \binom{d'_{i,g}}{j} (1 - e'_{i,g})^{j+1} (e'_{i,g})^{d'_{i,g}+1-j} + \sum_{j=1}^{M_g-1} \binom{d'_{i,g}}{j-1} (1 - e'_{i,g})^{j+1} (e'_{i,g})^{d'_{i,g}+1-j} \\
 \Leftrightarrow & \sum_{j=0}^{M_g-2} \binom{d'_{i,g}}{j} (1 - e_{i,g})^{j+1} e_{i,g}^{d'_{i,g}-j} + \binom{d'_{i,g}}{M_g-1} (1 - e_{i,g})^{M_g} e_{i,g}^{d'_{i,g}-M_g+2} \\
 & < \sum_{j=0}^{M_g-2} \binom{d'_{i,g}}{j} (1 - e'_{i,g})^{j+1} (e'_{i,g})^{d'_{i,g}-j} + \binom{d'_{i,g}}{M_g-1} (1 - e'_{i,g})^{M_g} (e'_{i,g})^{d'_{i,g}-M_g+2} \\
 \Leftrightarrow & (1 - e'_{i,g}) \binom{d'_{i,g}}{M_g-1} (1 - e'_{i,g})^{M_g} (e'_{i,g})^{d'_{i,g}-M_g+1} \\
 & < (1 - e_{i,g}) \binom{d'_{i,g}}{M_g-1} (1 - e_{i,g})^{M_g} e_{i,g}^{d'_{i,g}-M_g+1} \tag{A.13}
 \end{aligned}$$

Let $x = (1 - e_{i,g})/e_{i,g}$ and $x' = (1 - e'_{i,g})/e'_{i,g}$. We know $x > x'$. Also, from $\Delta v_g(e_{i,g}, d'_{i,g}) = \Delta v_g(e'_{i,g}, d'_{i,g})$, we know

$$\frac{x}{1+x} \left(\frac{1}{1+x} \right)^{d'_{i,g}} \sum_{j=0}^{M_g-1} \binom{d'_{i,g}}{j} x^j = \frac{x'}{1+x'} \left(\frac{1}{1+x'} \right)^{d'_{i,g}} \sum_{j=0}^{M_g-1} \binom{d'_{i,g}}{j} (x')^j \tag{A.14}$$

With the substitution of x and x' and the use of (A.14), the last inequality in (A.13)

becomes

$$\begin{aligned}
 & (1 - e'_{i,g}) \binom{d'_{i,g}}{M_g - 1} (1 - e'_{i,g})^{M_g} (e'_{i,g})^{d'_{i,g} - M_g + 1} \\
 & < (1 - e_{i,g}) \binom{d'_{i,g}}{M_g - 1} (1 - e_{i,g})^{M_g} e_{i,g}^{d'_{i,g} - M_g + 1} \\
 \Leftrightarrow & \left(\frac{x'}{1 + x'} \right)^2 \left(\frac{1}{1 + x'} \right)^{d'_{i,g}} \binom{d'_{i,g}}{M_g - 1} (x')^{M_g - 1} \\
 & < \left(\frac{x}{1 + x} \right)^2 \left(\frac{1}{1 + x} \right)^{d'_{i,g}} \binom{d'_{i,g}}{M_g - 1} x^{M_g - 1} \\
 \Leftrightarrow & \frac{x' \binom{d'_{i,g}}{M_g - 1} (x')^{M_g - 1}}{1 + x' \sum_{j=0}^{M_g - 1} \binom{d'_{i,g}}{j} (x')^j} < \frac{x \binom{d'_{i,g}}{M_g - 1} x^{M_g - 1}}{1 + x \sum_{j=0}^{M_g - 1} \binom{d'_{i,g}}{j} x^j} \tag{A.15}
 \end{aligned}$$



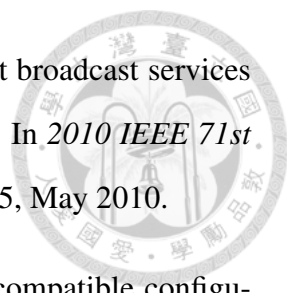
The last inequality can be proved easily from the first-order differentiation. Therefore, if $e_{i,g} < e_g^*(d_{i,g} + 1) \leq e_{c,g}$, $\Delta u_{i,g}(e_{i,g}, d_{i,g} + 1) < 0$ implies $\Delta u_{i,g}(e_{i,g}, d_{i,g} + 2) < 0$. We may continue to consider the possible relationships among $e_g^*(d_{i,g} + 2)$, $e_{i,g}$, and $e_{c,g}$, and apply the same proof procedure. Finally, we get $\Delta u_{i,g}(e_{i,g}, A_g) < 0$ for $A_g > d_{i,g}$. The first inequality of (2.11), $\Delta u_{i,g}(e_{i,g}, A_g) > 0$ for $A_g < d_{i,g}$, can be derived from $\Delta u_{i,g}(e_{i,g}, d_{i,g}) \geq 0$ in a similar way. So we do not repeat the proof here.

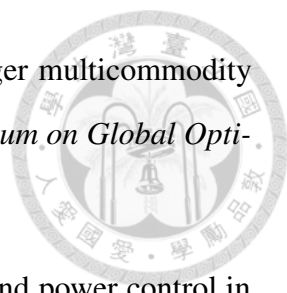
With all of the above derivations, there exists unique $d_{i,g}$ such that $u_{i,g}(e_{i,g}, A_g)$ is maximized at $A_g = d_{i,g}$, and (2.11) is satisfied. \square

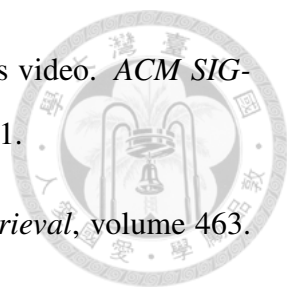



Bibliography

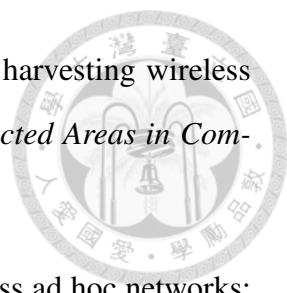
- [1] L. Atzori, A. Iera, and G. Morabito. The internet of things: A survey. *Computer networks*, 54(15):2787–2805, 2010.
- [2] A. Whitmore, A. Agarwal, and L. Da Xu. The internet of things-a survey of topics and trends. *Information Systems Frontiers*, 17(2):261–274, 2015.
- [3] S. Priya and D. J. Inman. *Energy Harvesting Technologies*, volume 21. Springer, 2009.
- [4] U. Varshney. Multicast over wireless networks. *Communications of the ACM*, 45(12):31–37, 2002.
- [5] 3GPP TS 26.346 V12.0.0 3rd Generation Partnership Project. Technical specification group services and system aspects: Multimedia broadcast/multicast service (mbms) protocols and codecs. December 2013.
- [6] IETF RFC 6330. Raptorq forward error correction scheme for object delivery. 2011.
- [7] 3GPP TR 26.848 V1.0.0 3rd Generation Partnership Project. Technical specification group services and system aspects: Multimedia broadcast/multicast service (mbms) enhanced mbms operation. March 2014.
- [8] 3GPP TR 26.849 3rd Generation Partnership Project. Technical specification group services and system aspects: Mbms improvements mbms operation on demand. March 2014.


- 
- [9] Y. Liang, C. Chou, and H. Wei. Multi-group wireless multicast broadcast services using adaptive modulation and coding: Modeling and analysis. In *2010 IEEE 71st Vehicular Technology Conference (VTC 2010-Spring)*, pages 1–5, May 2010.
- [10] F.-Y. Tsuo, J.-P. Huang, C.-H. Ko, and H.-Y. Wei. Incentive compatible configuration for wireless multicast: A game theoretic approach. *IEEE Transactions on Vehicular Technology*, 60(7):3520–3525, Sept 2011.
- [11] C.-Y. Wang, Y. Chen, H.-Y. Wei, and K. J. Ray Liu. Scalable video multicasting: A stochastic game approach with optimal pricing. *IEEE Transactions on Wireless Communications*, accepted and to appear, 2014.
- [12] W. Tu. Efficient resource utilization for multi-flow wireless multicasting transmissions. *IEEE Journal on Selected Areas in Communications*, 30(7):1246–1258, August 2012.
- [13] K. Jain, J. Padhye, V. N. Padmanabhan, and L. Qiu. Impact of interference on multi-hop wireless network performance. *ACM/Springer Wireless Networks 11:471487, 2005*.
- [14] M. Kodialam and T. Nandagopal. Characterizing achievable rates in multi-hop wireless networks: The joint routing and scheduling problem. In *ACM MobiCom*, 2003.
- [15] M. Kodialam and T. Nandagopal. Characterizing the capacity region in multi-radio multi-channel wireless mesh networks. In *ACM MobiCom*, 2005.
- [16] P. Wan. Multiflows in multihop wireless networks. In *ACM Mobihoc*, 2009.
- [17] P. Wan, Y. Cheng, Z. Wang, and F. Yao. Multiflows in multi-channel multi-radio multihop wireless networks. In *Proceedings IEEE INFOCOM*, pages 846–854, 2011.
- [18] V.S.A. Kumar, M.V. Marathe, S. Parthasarathy, and A. Srinivasan. Algorithmic aspects of capacity in wireless networks. In *SIGMETRICS Perform. Eval. Rev.* 33(1):133V144, 2005.


- 
- [19] A. E. Ozdaglar and D. P. Bertsekas. Optimal solution of integer multicommodity flow problems with application in optical networks. In *Symposium on Global Optimization*, 2003.
- [20] R. Cruz and A. Santhanam. Optimal routing, link scheduling and power control in multi-hop wireless networks. In *IEEE Infocom*, 2003.
- [21] G. B. Middleton, B. Aazhang, and J. Lilleberg. A flexible framework for polynomial time resource allocation in multiflow wireless networks. In *the 47th Allerton Conference on Communication, Control and Computing.*, September 2009.
- [22] G. B. Middleton, B. Aazhang, and J. Lilleberg. Efficient resource allocation and interference management for streaming multiflow wireless networks. In *IEEE ICC*, May 2010.
- [23] M. Baghaie, D. S. Hochbaum, and B. Krishnamachari. On hardness of multiflow transmission in delay constrained cooperative wireless networks. In *the 2011 IEEE Globecom, Houston, Texas, USA, 5-9 December 2011*.
- [24] W. Tu, C. Sreenan, C. Chou, A. Misra, and S. Jha. Resource-aware video multicasting via access gateways in wireless mesh networks. *IEEE Transactions on Mobile Computing*, 11:881–895, June 2012.
- [25] A. Gopinathan, Z. Li, and B. Li. On achieving group strategyproof information dissemination in wireless networks. In *International Conference on Game Theory for Networks, 2009. GameNets' 09.*, pages 232–240. IEEE, 2009.
- [26] A. Gopinathan, Z. Li, and B. Li. Group strategyproof multicast in wireless networks. *IEEE Transactions on Parallel and Distributed Systems*, 22(5):708–715, 2011.
- [27] S. Jakubczak and D. Katabi. A cross-layer design for scalable mobile video. In *Proceedings of the 17th annual international conference on Mobile computing and networking (MobiCom)*, pages 289–300. ACM, 2011.

- 
- [28] S. Jakubczak and D. Katabi. Softcast: one-size-fits-all wireless video. *ACM SIG-COMM Computer Communication Review*, 41(4):449–450, 2011.
- [29] R. Baeza-Yates and B. Ribeiro-Neto. *Modern Information Retrieval*, volume 463. ACM press New York, 1999.
- [30] J. Blomer, M. Kalfane, R. Karp, M. Karpinski, M. Luby, and D. Zuckerman. An xor-based erasure-resilient coding scheme, 1995.
- [31] W. K. Lin, D. M. Chiu, and Y. B. Lee. Erasure code replication revisited. In *Proceedings of the Fourth International Conference on Peer-to-Peer Computing, 2004.*, pages 90–97, 2004.
- [32] C.-H. Ko and H.-Y. Wei. On-demand resource-sharing mechanism design in two-tier ofdma femtocell networks. *IEEE Transactions on Vehicular Technology*, 60(3):1059–1071, March 2011.
- [33] J. F. Nash. Equilibrium points in n-person games. In *Proceedings of the National Academy of Sciences*, volume 36, pages 48–49, 1950.
- [34] D. C. Parkes. Combinatorial auctions. In *Iterative Combinatorial Auctions*, chapter 2. Cambridge, MA: MIT Press, 2001.
- [35] C. Courcoubetis and R. Weber. *Pricing Communication Networks: Economics, Technology and Modelling*, chapter 10. New York: Wiley, 2003.
- [36] B. Radunovic and J.-Y. Le Boudec. A unified framework for max-min and min-max fairness with applications. *ACM/IEEE Transactions on Networking*, 15(5):1073–1083, 2007.
- [37] A. Detti, G. Bianchi, W. Kellerer, et al. SVEF: an open-source experimental evaluation framework. In *In Proc. of IEEE MediaWIN 2009, Sousse, Tunisia, 2009*.
- [38] Joint scalable video model software.


- 
- [39] Foreman yuv video. <ftp://ftp.tnt.uni-hannover.de/pub/svc/testsequences/>.
- [40] 3GPP. TR 36.814, evolved universal terrestrial radio access (e-utra); further advancements for e-utra physical layer aspects, Mar. 2010.
- [41] S. Schwarz, J.C. Ikuno, M. Simko, M. Taranetz, Q. Wang, and M. Rupp. Pushing the limits of LTE: A survey on research enhancing the standard. *IEEE Access*, 1:51–62, 2013.
- [42] M. Condoluci, G. Araniti, T. Mahmoodi, and M. Dohler. Enabling the iot machine age with 5g: Machine-type multicast services for innovative real-time applications. *IEEE Access*, 4:5555–5569, 2016.
- [43] C.-H. Ko, C.-C. Chou, H.-Y. Meng, and H.-Y. Wei. Strategy-proof resource allocation mechanism for multi-flow wireless multicast. *IEEE Transactions on Wireless Communications*, 14(6):3143–3156, 2015.
- [44] O. Ozel, K. Tutuncuoglu, J. Yang, S. Ulukus, and A. Yener. Transmission with energy harvesting nodes in fading wireless channels: Optimal policies. *IEEE Journal on Selected Areas in Communications*, 29(8):1732–1743, 2011.
- [45] C. Keong Ho and R. Zhang. Optimal energy allocation for wireless communications with energy harvesting constraints. *IEEE Transactions on Signal Processing*, 60(9):4808–4818, 2012.
- [46] H. Ju and R. Zhang. Throughput maximization in wireless powered communication networks. *IEEE Transactions on Wireless Communications*, 13(1):418–428, 2014.
- [47] J. Yang, O. Ozel, and S. Ulukus. Broadcasting with an energy harvesting rechargeable transmitter. *IEEE Transactions on Wireless Communications*, 11(2):571–583, 2012.

- 
- [48] J. Xu and R. Zhang. Throughput optimal policies for energy harvesting wireless transmitters with non-ideal circuit power. *IEEE Journal on Selected Areas in Communications*, 32(2):322–332, 2014.
- [49] S. Guo and O. WW Yang. Energy-aware multicasting in wireless ad hoc networks: A survey and discussion. *Computer Communications*, 30(9):2129–2148, 2007.
- [50] S.-P. Chuah, Z. Chen, and Y.-P. Tan. Energy-efficient resource allocation and scheduling for multicast of scalable video over wireless networks. *IEEE Transactions on Multimedia*, 14(4):1324–1336, 2012.
- [51] L. Al-Kanj and Z. Dawy. Energy-aware resource allocation in ofdma wireless multicasting networks. In *2012 19th International Conference on Telecommunications (ICT)*, pages 1–5. IEEE, 2012.
- [52] C.-C. Kuan, G.-Y. Lin, H.-Y. Wei, and R. Vannithamby. Reliable multicast and broadcast mechanisms for energy-harvesting devices. *IEEE Transactions on Vehicular Technology*, 63(4):1813–1826, 2014.
- [53] C. K. Ho, P. D. Khoa, and P. C. Ming. Markovian models for harvested energy in wireless communications. In *2010 IEEE International Conference on Communication Systems (ICCS)*, pages 311–315. IEEE, 2010.
- [54] H. S. Wang and N. Moayeri. Finite-state markov channel—a useful model for radio communication channels. *IEEE Transactions on Vehicular Technology*, 44(1):163–171, 1995.
- [55] Q. Zhang and S. A. Kassam. Finite-state markov model for rayleigh fading channels. *IEEE Transactions on Communications*, 47(11):1688–1692, 1999.
- [56] M. A. Alsheikh, D. T. Hoang, D. Niyato, H.-P. Tan, and S. Lin. Markov decision processes with applications in wireless sensor networks: A survey. *IEEE Communications Surveys & Tutorials*, 17(3):1239–1267, 2015.

- 
- [57] T. R. Palfrey and S. Srivastava. On bayesian implementable allocations. *The Review of Economic Studies*, 54(2):193–208, 1987.
- [58] W. Vickrey. Counterspeculation, auctions, and competitive sealed tenders. *The Journal of Finance*, 16(1):8–37, 1961.
- [59] E. H. Clarke. Multipart pricing of public goods. *Public Choice*, 11(1):17–33, 1971.
- [60] T. Groves. Incentives in teams. *Econometrica: Journal of the Econometric Society*, pages 617–631, 1973.
- [61] D. Gillette. Stochastic games with zero stop probabilities. *Contributions to the Theory of Games*, 3:179–187, 1957.
- [62] D. Fudenberg and D. Levine. Subgame-perfect equilibria of finite-and infinite-horizon games. *Journal of Economic Theory*, 31(2):251–268, 1983.
- [63] D. Abreu. On the theory of infinitely repeated games with discounting. *Econometrica: Journal of the Econometric Society*, pages 383–396, 1988.
- [64] E. Hendon, H. J. Jacobsen, and B. Sloth. The one-shot-deviation principle for sequential rationality. *Games and Economic Behavior*, 12(2):274–282, 1996.
- [65] J. Pineau, G. Gordon, S. Thrun, et al. Point-based value iteration: An anytime algorithm for pomdps. In *IJCAI*, volume 3, pages 1025–1032, 2003.
- [66] M. L. Littman, T. L. Dean, and L. P. Kaelbling. On the complexity of solving markov decision problems. In *Proceedings of the Eleventh conference on Uncertainty in artificial intelligence*, pages 394–402. Morgan Kaufmann Publishers Inc., 1995.
- [67] J. Wu, C. Yuen, M. Wang, and J. Chen. Content-aware concurrent multipath transfer for high-definition video streaming over heterogeneous wireless networks. *IEEE Transactions on Parallel and Distributed Systems*, 27(3):710–723, 2016.
- [68] L. Mainetti, L. Patrono, and A. Vilei. Evolution of wireless sensor networks towards the internet of things: A survey. In *2011 19th International Conference on Software, Telecommunications and Computer Networks (SoftCOM)*, pages 1–6. IEEE, 2011.

- 
- [69] W. KG Seah, Z. A. Eu, and H.-P. Tan. Wireless sensor networks powered by ambient energy harvesting (wsn-heap)-survey and challenges. In *1st International Conference on Wireless Communication, Vehicular Technology, Information Theory and Aerospace & Electronic Systems Technology, 2009. Wireless VITAE 2009.*, pages 1–5. Ieee, 2009.
- [70] F. K. Shaikh and S. Zeadally. Energy harvesting in wireless sensor networks: A comprehensive review. *Renewable and Sustainable Energy Reviews*, 55:1041–1054, 2016.
- [71] V. Sharma, U. Mukherji, V. Joseph, and S. Gupta. Optimal energy management policies for energy harvesting sensor nodes. *IEEE Transactions on Wireless Communications*, 9(4):1326–1336, 2010.
- [72] N. Michelusi, K. Stamatiou, and M. Zorzi. Transmission policies for energy harvesting sensors with time-correlated energy supply. *IEEE Transactions on Communications*, 61(7):2988–3001, 2013.
- [73] M. Vuran, Ö. Akan, and I. Akyildiz. Spatio-temporal correlation: Theory and applications for wireless sensor networks. *Computer Networks*, 45(3):245–259, 2004.
- [74] C. Liu, K. Wu, and J. Pei. An energy-efficient data collection framework for wireless sensor networks by exploiting spatiotemporal correlation. *IEEE Transactions on Parallel and Distributed Systems*, 18(7), 2007.
- [75] S. Yoon and C. Shahabi. The clustered aggregation (cag) technique leveraging spatial and temporal correlations in wireless sensor networks. *ACM Transactions on Sensor Networks (TOSN)*, 3(1):3, 2007.
- [76] C. Luo, F. Wu, J. Sun, and C. W. Chen. Compressive data gathering for large-scale wireless sensor networks. In *Proceedings of the 15th Annual International Conference on Mobile Computing and Networking*, pages 145–156. ACM, 2009.
- [77] N. Roy, V. Rajamani, and C. Julien. Supporting multi-fidelity-aware concurrent applications in dynamic sensor networks. In *2010 8th IEEE International Conference*

on *Pervasive Computing and Communications Workshops (PERCOM Workshops)*, pages 43–49. IEEE, 2010.

- 
- [78] J. Zheng, Y. Cai, X. Shen, Z. Zheng, and W. Yang. Green energy optimization in energy harvesting wireless sensor networks. *IEEE Communications Magazine*, 53(11):150–157, 2015.
- [79] D. Zhang, Z. Chen, M. K. Awad, N. Zhang, H. Zhou, and X. S. Shen. Utility-optimal resource management and allocation algorithm for energy harvesting cognitive radio sensor networks. *IEEE Journal on Selected Areas in Communications*, 34(12):3552–3565, 2016.
- [80] M.-J. Shih, G.-Y. Lin, and H.-Y. Wei. Two paradigms in cellular internet-of-things access for energy-harvesting machine-to-machine devices: push-based versus pull-based. *IET Wireless Sensor Systems*, 6(4):121–129, 2016.
- [81] H.-H. Lin, M.-J. Shih, H.-Y. Wei, and R. Vannithamby. Deepsleep: Ieee 802.11 enhancement for energy-harvesting machine-to-machine communications. *Wireless Networks*, 21(2):357–370, 2015.
- [82] N. Cressie. *Statistics for Spatial Data*. John Wiley & Sons, 2015.
- [83] A. Deshpande, C. Guestrin, S. R. Madden, J. M. Hellerstein, and W. Hong. Model-driven data acquisition in sensor networks. In *Proceedings of the Thirtieth International Conference on Very Large Data Bases-Volume 30*, pages 588–599. VLDB Endowment, 2004.